

See discussions, stats, and author profiles for this publication at: <https://www.researchgate.net/publication/261173987>

# Design of Material Structures Using Topology Optimization

Thesis · January 1994

---

CITATIONS

197

READS

1,590

1 author:



Ole Sigmund

Technical University of Denmark

260 PUBLICATIONS 12,286 CITATIONS

SEE PROFILE

Some of the authors of this publication are also working on these related projects:



Inverse Design Engineering - Toplogy Optimization [View project](#)



Optically Designed Anodised Aluminium Surfaces [View project](#)

All content following this page was uploaded by [Ole Sigmund](#) on 26 August 2015.

The user has requested enhancement of the downloaded file. All in-text references [underlined in blue](#) are added to the original document and are linked to publications on ResearchGate, letting you access and read them immediately.

# **Design of Material Structures using Topology Optimization**

**Ole Sigmund  
December, 1994**

**Department of Solid Mechanics  
(now: Department of Mechanical Engineering/Solid Mechanics)  
Technical University of Denmark  
Lyngby, Denmark**

**DCAMM, Special report, S69**

Note added December 7th, 2005:

Please note that almost all the contents of this thesis have been published in various journal papers, thus reference to the work should preferably be given to the journal papers and not to this thesis.

---

## Preface

The work presented in this thesis for the Ph.D. degree has been carried out at the Department of Solid Mechanics, Technical University of Denmark (DTU) and has been supervised by Docent Pauli Pedersen (Dept. of Solid Mech., DTU), and co-supervised by Docent Martin P. Bendsøe (Institute of Mathematics, DTU) and Lektor Jon J. Thomsen (Dept. of Solid Mech., DTU). I would like to express my sincere thanks to my supervisors for inspiring me to do this work, and for their helpful advice, suggestions, support, encouragement and patience when I needed it.

I would also like to thank Robert B. Zetterlund and Kurt Fries Weihe (both Dept. of Solid Mech., DTU) for their valuable ideas and help in producing working models of the material microstructures.

The work was supported by Denmarks Technical Research Council through the Program on Computer Aided Design. This support is gratefully acknowledged.

The introductory part of this Ph.D. work (October 1991 to December 1992) was performed under supervision of Professor George I.N. Rozvany, University of Essen, Germany. The stay in Essen was sponsored by the Deutsche Forschungsgemeinshaft whose support is gratefully acknowledged. I would like to express my sincere thanks to G.I.N. Rozvany for giving me a valuable introduction to optimality criteria methods and to him and his staff for a professionally and personally instructive and memorable period.

Part of this work (Appendix 1), was done together with Professor Alejandro R. Díaz, Michigan State University (MSU). I would like to thank A. R. Díaz for our co-operation and also Professors Noboru Kikuchi and John E. Taylor, University of Michigan (UofM) for many inspiring research discussions during my stay in Michigan in the spring of 1994.

Last but not least, I would like to thank my fellow students at the Department of Solid Mechanics, DTU for great support and many social activities through the years.

Lyngby, December 1994

Ole Sigmund

## **Abstrakt (in Danish)**

En numerisk metode er udviklet til design af materialer med foreskrevne termoelastiske parametre. Materiale design problemet er formuleret som en optimering af topologien for en periodisk mikrostruktur repræsenteret ved en enhedscelle. Materialets vægt er valgt som objektfunktion, men funktionen er modificeret for at kunne tage hensyn til produktionsbegrænsninger. Mikrostrukturen er diskretiseret med stang, ramme eller kontinuum finite elementer, hvor respektivt tværstiksareal, bredde og densitet af de individuelle elementer indgår som design variable. De effektive elastiske parametre for den diskretiserede mikrostruktur er fundet ved hjælp af en numerisk homogeniseringsmetode og materiale design problemet kan derved defineres som et inverst homogeniseringsproblem.

Numeriske eksperimenter, i hvilke den foreslæde metode er anvendt til design af gitter- (i to og tre dimensioner) og rammeagtige mikrostrukturer, indikerer, at det er muligt at designe nye mikrostrukturer med alle termodynamisk tilladelige elastiske parametre og som kun har en længdeskala.

Anvendelse af metoden på kontinuumagtige mikrostrukturer var vanskelig på grund af problemer med skakternede områder i de resulterende topologier. Skakternede områder er et velkendt problem indenfor generel topologi optimering af strukturer, og problemet er derfor undersøgt i detaljer og er forklaret ved, at lavere ordens finite elementer modellerer stivheden af en skakternet mikrostruktur dårligt. Der foreslæs en procedure til at eliminere problemet uden at forøge beregningstiden. Den foreslæde procedure kan samtidig mindske net-afhængighed af de optimale løsninger. Selvom metoden er heuristisk baseret, opnåes lovende resultater ved dens anvendelse i topologi optimering af strukturer og materialer.

Brug af den foreslæde net-afhængigheds procedure gør design af kontinuumagtige mikrostrukturer simplere, og eksempler viser, at materialer med ekstreme termoelastiske parametre også kan designes i kontinuum formuleringen.

Af produktionstekniske årsager foretrækkes de kontinuumagtige mikrostrukturer fremfor de gitter- og rammeagtige materialer, men det kan konkluderes, at enhver topologisk begrænsning indskrænker de opnåelige termoelastiske parametre.

---

## Abstract

A numerical method for the design of linear elastic materials with prescribed thermoelastic properties is proposed. The material design problem is formulated as a topology optimization problem of a periodic material microstructure represented by a base cell. The objective function is a measure of weight, modified to take manufacturability constraints into account. The microstructure is discretized by truss-, frame- or continuum-type finite elements where cross-sectional areas, widths and densities of individual elements respectively are taken as design variables. Effective properties of the discretized microstructure are found by a numerical homogenization method which leads to the definition of the material design problem as an inverse homogenization problem.

Numerical experiments with the proposed method applied to the design of truss- (2-d and 3-d) and frame-like microstructures indicate that it possible to design novel microstructures on one length scale that attain any elastic properties admissible by thermodynamics.

Applying the method to continuum-like microstructures was difficult due to occurrence of checkerboard patterns in the solutions. The reason for the occurrence of checkerboard patterns which is a well known problem in general topology optimization of continuum structures is studied in detail and explained by poor modelling of the stiffness of checkerboards by lower order finite elements. A procedure is proposed to eliminate the problem without increasing computational complexity and at the same time preventing the mesh-dependency problem which refers to the non-convergence of solutions with mesh refinement. Although based on heuristics, the method shows promising results applied to topology optimization of structures and materials.

Taking advantage of the proposed mesh-independency algorithm, design of continuum-like materials was facilitated and examples show that materials with extreme thermoelastic properties can be designed by the continuum formulation as well.

Due to manufacturability constraints, the continuum type microstructures are preferred to the truss- and frame-like materials but it is concluded that any topological constraint on the material microstructure damps out attainable elastic properties.

---

# Table of Contents

<b>Preface .....</b>	<b>I</b>
<b>Abstrakt (in Danish) .....</b>	<b>II</b>
<b>Abstract .....</b>	<b>III</b>
<b>Table of Contents .....</b>	<b>IV</b>
<b>Introduction .....</b>	<b>1</b>
Hierarchical materials and structures .....	1
Negative Poisson's ratio materials .....	2
Approaches to material design .....	4
Topology optimization .....	5
Problem formulation .....	6
About this thesis .....	7
<b>1. Numerical homogenization procedures .....</b>	<b>9</b>
1.1 Homogenization of elastic properties .....	10
1.2 Homogenization of thermal properties .....	12
1.3 Finite element discretization .....	13
1.4 Solution procedures for the finite element problem .....	15
1.5 Discretizations of microstructure .....	17
1.6 Examples .....	22
1.7 Summary .....	25
<b>2. Design of materials .....</b>	<b>26</b>
2.1 The inverse homogenization problem .....	29
2.2 Solving the optimization problem .....	33
2.3 Truss-like materials .....	37
2.4 Frame-like materials .....	44
2.5 Continuum-like materials .....	46
2.6 Continuum-like materials with prescribed thermoelastic properties ..	53
2.7 Practical considerations .....	55
2.8 Summary and discussion .....	59
<b>3. The checkerboard and mesh-dependency problems     in layout optimization .....</b>	<b>61</b>
3.1 Design of structures by compliance optimization .....	62
3.2 Checkerboard prevention scheme using image processing .....	70
3.3 Implementation of the checkerboard prevention scheme .....	72
3.4 Elimination of mesh-dependency .....	76
3.5 Summary .....	86
<b>Conclusions .....</b>	<b>87</b>
<b>List of publications .....</b>	<b>90</b>
<b>References .....</b>	<b>91</b>

## Appendices

<b>Appendix 1</b> .....	<b>A1</b>
Checkerboard patterns in layout optimization .....	A1
<b>Appendix 2</b> .....	<b>A2</b>
Notations for the constitutive tensor .....	A2
<b>Appendix 3</b> .....	<b>A4</b>
The Element-by-Element Preconditioned Conjugate Gradient Method ..	A4
<b>Appendix 4</b> .....	<b>A6</b>
Continuum equivalence of bar elements and equivalent nodal loads .....	A6

# **Introduction**

Optimization of material properties play an important role in the design of structures. Using the right material for a specific application can give great payoffs such as lower weight, higher stiffness or strength or improvement of thermal or dynamic response.

Looking at any material through a microscope, a microstructure is seen if the magnification is strong enough. If the microstructure itself has a microstructure, the material can be called a hierarchical material. The topologies and compositions of the individual microstructural levels are crucial for the effective properties of the material.

A microstructure can be regarded as a small structure and therefore, techniques developed for the optimization of general structures can be used in the optimization of materials. Using this idea, the present thesis suggests that a numerical method based on topology optimization of structures can be used in the design of new material microstructures with prescribed thermoelastic properties.

In the following sections, an introduction to matters important for microstructural design is given together with references to literature. First the benefits obtained from designing hierarchical materials and structures are summarized. Then examples of approaches to material design are given together with a description of the important subproblem of designing materials with negative Poisson's ratios. Finally, approaches to topology optimization of structures are listed together with their possible applications to material design.

## **Hierarchical materials and structures**

The usual engineering practice in the design of elastic structures has been to take an existing material and try to utilize it in the best possible way by varying structural dimensions or shape. After the introduction of fiber based composites a few decades ago, ways were opened for the design of more efficient structures taking advantage of the high stiffness to weight ratio and anisotropy of such materials. Recently, a new approach to the design of structures has been suggested by different authors. Instead of trying to utilize an *existing* material the best possible way, the approach suggests that the material microstructure itself should be tailored to the specific application. Ideally, the material at each point of a structure should be specifically designed for the local loading condition. The idea of tailoring material microstructures for specific needs has been presented by Ashby, (1991), who suggests that efficient structures can be constructed by combining the design of structural shape with the design of material microstructure; by Lakes, (1993)<sup>2</sup>, who discusses the benefits of using hierarchical materials; by Ashley, (1994)<sup>1</sup>, who predicts big property payoffs from design of materials on the atomic (nano-) scale and finally by

Bendsøe *et al.*, (1993)<sup>1,2</sup> and Ringertz, (1993), who suggest that weight optimal structures subject to simple and multiple loading cases are obtained by a free parametrization of the elasticity tensor and the former conclude, that a lower bound on compliance can be reached under the condition that materials with properties that are only restricted to be thermodynamically admissible can be made.

As a result of evolution, nature has tailored many hierarchical and highly specialized materials. One of the most structurally efficient materials that exists is wood, as pointed out by Ashby, (1991). Wood has a porous microstructure where the solid part is distributed as prismatic cells. In this way, material is moved away from the bending axis, making the tree stronger in bending per unit weight than the solid it is made of. Human bone structure is another example of naturally occurring hierarchical materials. Bone material has two hierarchical levels [e.g. Hollister and Riemer, (1993)], the first is the architectural level on a scale ranging from 100 to 500 microns, the second is the tissue microstructural level which contains structure ranging in size from 3 to 50 microns. During life time the microstructure of bone constantly adapts to outer stimuli. As pointed out in a review paper by Huiskes and Hollister, (1993), it is not yet fully understood how bone structure adapts to mechanical stimuli but it is generally believed that the microstructure remodels to support given loads in some optimal way.

Apart from the direct structural benefits discussed above, designing materials with specific properties has many other applications. For example, it is rewarding to design materials that mimic naturally occurring materials as seen in the next two examples. Human bone structure is known to exhibit extreme elastic properties, and Evans, (1990) points out that it is important to mimic replaced tissue as closely as possible, in order to make the best artificial replacements of human bone structure in surgery. The other example is the interesting task of constructing an "artificial" Stradivarius. In Ashby and Jones, (1986) a desire is expressed of being able to design a synthetic material that reproduces the acoustic properties of wood as closely as possible, in order to construct great sounding violins.

## Negative Poisson's ratio materials

The design of a material with a very special form of elastic properties has been the goal of many researchers for the last few years. The existence of materials with negative Poisson's ratios, or in other words, the existence of materials that expand transversely subject to an applied tensile load has been questioned by researchers and engineers for a long time and many basic books on elasticity limit the possible value of the Poisson's ratio to the interval  $[0, 0.5]$ . However, thermodynamics or the requirement that the constitutive tensor be positive semi-definite allow the Poisson's ratio of an isotropic material to approach  $-1$ . Particular microstructures of materials with negative Poisson's ratios were reported by Almgren, (1985) who suggested a mechanism like

---

structure with hinges, springs and sliding collars and Kolpakov, (1985) and Gibson and Ashby, (1988) who suggested an inverted honeycomb. Later, Evans, (1989) proposed microstructures composed of rotating disks connected by inextensible strings and Rothenburg, [Berlin and Bathurst, \(1991\)](#) proposed a triangular truss structure with telescopic bars. Many of these solutions are not isotropic or can not be characterized as elastic continua because they have internal sliding surfaces. This lead Milton, (1991) to ask the question: is it possible to produce isotropic materials with negative Poisson's ratios within the framework of linear continuum elasticity? Milton answered the question himself in the affirmative, by introducing a two-phase composite based on layerings at different length scales and made a mathematically rigorous proof that the composite has Poisson's ratio close to  $-1$  and has no sliding surfaces.

Two approaches have been made to produce negative Poisson's ratio materials in practice. The first is by [Lakes \(1987\)](#) (and several following papers by the same author) who modifies open walled foam materials by subjecting them to heat and compression, to get Poisson's ratios as low as  $-0.7$ . The second is by Caddock and Evans, (1989) who obtained an expanded polytetrafluoroethylene microporous material with negative Poisson's ratio. However, the latter is strongly anisotropic and therefore many of the positive features reported for isotropic negative Poisson's ratio materials might not exist for this material.

Applications and benefits of negative Poisson's ratio materials are numerous. Lakes, (1993)<sup>1</sup> has investigated several applications and reports that negative Poisson's ratio materials are good as core materials for convex sandwich plates because they can be easily bent into a convex shape as opposed to a core material with positive Poisson's ratio. Lakes also investigates the implications of having a negative Poisson's ratio on stress concentration at holes or cracks and concludes, that stress concentration factors are reduced in some cases and unchanged or increased in others. [Lakes and Elms, \(1993\)](#) have investigated indentability of negative Poisson's ratio foams and calculated energy absorption rates that were considerably higher than for conventional foams. Another application of negative Poisson's ratio materials are as fasteners, investigated in [Choi and Lakes, \(1991\)](#), where insertion of the fastener is facilitated due to the transverse contraction of the fastener when pressed into the hole while removal is resisted due to the transverse expansion of the fastener when pulled. The fastener can therefore be seen as a sort of "raw-plug". An open but interesting question is whether fibre pull-out would be resisted if the fiber is made of a negative Poisson's ratio material? Finally, an application due to the change in bulk modulus of a negative Poisson's ratio material shall be mentioned. The bulk modulus of a material is defined as  $K=E/(3(1-\nu))$ , where  $E$  is Young's modulus and  $\nu$  is Poisson's ratio. A low bulk modulus makes a material more sensitive to hydrostatic pressure. The sensitivity to hydrostatic pressure is increased with a factor of three for a Poisson's ratio  $-1$  material compared to one with Poisson's ratio  $0.33$  and it is expected that the high sensitivity of Poisson's ratio  $-1$  materials can

---

be utilized in the design of micro–hydrophones or in sensors and actuators for use in smart materials and structures.

## Approaches to material design

The problem of designing materials with specific properties is being attacked by researchers from many different areas, ranging from theoretically developed composite materials by applied mathematicians over lamination and braiding of existing composite materials to the manipulation of individual atoms by nano–technologies.

In Milton and Cherkaev, (1993) materials with elastic parameters ranging over the entire scale compatible with thermodynamics are constructed by a multi scale layering of isotropic soft and strong material. From bounds obtained by [Cherkaev and Gibiansky, \(1993\)](#), it is known that the stiffness ratio between the strong and the soft material should be large in order to be able to design materials with extreme elastic properties. A layered material with Poisson’s ratio close to –1 was constructed from rigid and infinitely weak material by Milton, (1992). These materials are usually regarded as mathematical tools rather than practical composites due to their widely differing length scales [Lakes, (1993)<sup>2</sup>].

Stiffness, strength and other material properties can be tailored to a certain extent by varying layer directions, layer thicknesses, types, etc. in fibre/matrix materials [e.g. Autio, Laitinen and Pramilla, (1993)] and by varying yarn orientations and fiber densities in braided composites [e.g. Kostar and Chou, (1994)]. Dvorak, (1993) tailored conduction properties of a periodic 2–phase material by varying the shape of the inclusion phase. All three papers produce solid materials which are more or less readily manufacturable, but the attainable material properties are limited by the choice of fibre/matrix material.

Considering design of materials at a smaller scale, Moore, (1993) lists different attempts to chemically synthesize hinged molecular crystals which apart from exhibiting negative Poisson’s ratio behaviour can be tailored to have special mechano–coupled optical and electrical properties.

Designing materials on the atomic scale is the subject of the rapidly expanding research field of nanostructures where techniques are developed to manipulate microstructures atom by atom. Great efforts are invested on producing materials with a variety of properties such as strength, hardness, toughness, thermal expansion, conductivity, corrosion–resistance, optical and magnetic properties and many others as listed in Ashley, (1994)<sup>1</sup>.

---

Material design can roughly be divided into three different length scales, namely nano-, meso- and micro-scale. The nano-scale includes design at atomic and molecular levels, the meso- or submicron-scale goes up to approximately one micron and micro-scale is here defined as everything above one micrometer. Usual continuum elasticity laws hold for the micro-scale and with some caution for the meso-scale [e.g. Nkansah, Evans and Hutchinson, (1994)] but the nano-scale requires other non-linear analysis tools.

## Topology optimization

Topology optimization of structures is a rapidly growing field of particular interest to the automotive and aerospace industries. Topology optimization, as opposed to shape optimization, allows the introduction of holes or cavities in structures which usually results in great savings in weight or improvement of structural behaviour such as stiffness, strength or dynamic response.

Topology optimization has received revived interest since the introduction of the "homogenization approach to topology optimization" by [Bendsøe and Kikuchi, \(1988\)](#) but has its origins back to the minimum weight structures of Michell, (1904).

Topology optimization has in the last decades been applied to discrete structures such as trusses [e.g. Pedersen, (1970), Ringertz (1988) or Sankaranaryanan, Haftka and Kapania, (1992)] or frames [e.g. [Zhou and Rozvany, \(1993\)](#)], to continuum structures such as plates [e.g. [Cheng and Olhoff, \(1981\)](#) and Díaz, Lipton and Soto (1993)] or to membranes [e.g. [Bendsøe and Kikuchi, \(1988\)](#)]. Objective functions are most often compliance or weight but topology optimization has also been performed with other performance criteria such as dynamic behaviour [e.g. [Díaz and Kikuchi, \(1992\)](#) and [Rozvany, Zhou and Sigmund, \(1994\)](#)], thermoelastic behaviour [e.g. Rodrigues and Fernandes, (1994)]. There are several examples of topology optimization used in or inspired by medical engineering reviewed in [Huiskes and Hollister, \(1993\)](#). The author has, as a part of his Ph.D.-work, published analytical and numerical work on topology optimization of trusses, grillages and continua with single and multiple static and dynamic constraints in collaboration with G.I.N. Rozvany and his research group at University of Essen, Germany. References are given in "List of publications" at the end of this report.

Above mentioned references to applications of topology optimization methods are not complete but are selected due to their relevance to the present work. For a more exhaustive overview of the field, the reader is referred to [Bendsøe \(1994\)](#) and the references herein.

The material design problem can be formulated as a topology optimization problem. Depending on density and topology one can interpret a microstructure as a micro truss-, frame- or continuum-

---

like structure. Furthermore, desirable properties for general structures such as low weight, high stiffness or specific thermal responses are also desirable properties in material design. Therefore, assuming that material microstructure can be designed freely, the tools developed for topology optimization of general structures described above can be directly applied to the design of material microstructure.

## Problem formulation

Having realized that the design of materials ranging from atomic to millimeter scale with specific elastic, strength, optic, magnetic, thermal, electric and many other properties opens exciting perspectives, the subject of this work shall be limited to the design of materials with prescribed thermoelastic properties on a scale which makes it possible to use the rules of continuum elasticity.

Until now, many approaches to design of materials with specific properties have been based on a trial and error basis. In theoretical approaches, many solutions have been based on intuitive ideas of structures which could exhibit the wanted behaviour. Practical approaches often consist of numerous experiments trying out mixtures of different constituents and processing types and often, materials with new properties are discovered by coincidence.

As examples of systematical approaches to material design were mentioned the mathematical approach with multi-scale composites by Milton and Cherkaev, (1993) and the approach of laminating fiber/matrix materials by Autio, Laitinen and Pramilla, (1993). However, the former approach is not regarded as practical because of the differing length scales and the latter can only produce materials with a limited range of properties.

Consequently, a major goal of this thesis is to **propose a unified approach to the design of efficient linear elastic materials, with any possible prescribed elastic properties and with variation of microstructure limited to a single length scale**

To facilitate the work,

- the material microstructures will be assumed to be periodically repeated so that material properties are uniquely determined by analysis of a single representative base cell.
  - the choice of the base material of which the microstructure is built is considered unimportant for the design problem. Whether the actual microstructure is built in metal or polymer is just a matter of production method as we do not consider fatigue life, plasticity or other properties strongly related to a specific base material.
-

- manufacturability constraints such as exclusion of sliding surfaces should be taken into account in the definition of the design problem but apart from this, no further restrictions such as choice of base material, overall density or microstructural features of specific materials shall be imposed.
- actual production of the resulting microstructures is outside the scope of this thesis. The resulting microstructures can be used as inspiration for people actually involved in manufacturing of materials with novel microstructures. However, simple test models and ideas to build more practical prototypes will be discussed.

The effective properties of a periodically repeated microstructure represented by a base cell can be computed by a *homogenization method*. Homogenized or effective properties are found by subjecting the discretized base cell to different test fields and calculating the response by the finite element method. The material design problem can be seen as *an inverse homogenization problem*. In a usual homogenization problem we seek the effective properties of a given material. In the inverse problem, we seek the material that has given effective properties.

The goal of designing efficient materials with prescribed elastic properties, here termed the inverse homogenization problem, can be defined as an *optimization problem* of minimization of material weight, subject to equality constraints on the prescribed elastic properties. Minimizing weight is considered a reasonable design criteria because high stiffness to weight ratio is desirable in most cases – especially in automotive and aerospace applications. Choosing the prescribed elastic properties as equality constraints ensures that the specified properties are obtained as demanded. The *optimization problem* can be seen as a *topology optimization problem*, where the design domain is the material microstructure represented by the base cell, and the design variables are the dimensional properties of finite elements used to discretize the base cell.

## About this thesis

This thesis is divided into three self contained chapters dealing with: general numerical homogenization procedures, design of materials with prescribed thermoelastic properties and elimination of checkerboard and mesh dependency problems in topology optimization.

In chapter one, the standard numerical homogenization procedure is described. The procedure, is reformulated and extended in a way that makes it well suited for the topology optimization of material microstructure discussed in chapter two. Material microstructure is represented by groundstructures composed of truss– (two and three dimensional), frame– and continuum–like elements and it is suggested that any specific microstructure can be modelled by one of these groundstructures. The use of the groundstructure approach in homogenization is illustrated with

---

examples. Readers not interested in numerical homogenization procedures may skip chapter one and proceed directly to chapter two on material design.

An optimization algorithm is introduced in chapter two that can solve the inverse homogenization problem of finding a material with prescribed thermoelastic properties. The optimization problem is formulated in a general way, independent of the considered microstructure and the basic objective function, minimization of weight, is modified to account for manufacturability constraints as well. The optimization problem is solved by a multiple constraint optimality criteria method, based on procedures known from general topology optimization. The chapter shows numerous examples of truss-, frame- and continuum-like microstructures with a wide range of thermoelastic properties. It is shown that the proposed procedure indeed can design one-length-scale materials with any possible elastic properties by truss-like microstructures but the introduction of manufacturability constraints damps out the attainable properties as demonstrated by frame- and continuum-like microstructures.

Chapters one and two represent a compilation and extension of work published in Sigmund, (1994)<sup>1,2</sup>. Especially the part on design of continuum-like materials has been revised, and all examples have been recomputed with many more design degrees of freedom. This was partly made possible by the implementation of an iterative equation solver (appendix 3) but not least by the implementation of the mesh-independency algorithm developed in chapter three.

In chapter three a procedure to eliminate two well known problems occurring in topology optimization of continuum structures is proposed, namely the checkerboard problem and the mesh-dependency problem. The checkerboard problem refers to the formation of regions in optimized topologies with alternating solid and void elements ordered in a checkerboard like fashion. The problem is seen in many works on topology optimization of continuum structures and was one of the reasons why early results on the material design problem published in Sigmund, (1994)<sup>1</sup> only considered coarse discretizations where checkerboards were less prone to appear. The reason for the occurrence of checkerboards is discussed in Díaz and Sigmund, (1994), supplied in appendix 1, and can simply be explained by poor numerical modelling of the stiffness of checkerboards by lower order finite elements. The mesh dependency problem refers to the non-convergence of solutions with mesh refinement. Chapter three suggests a procedure that eliminates both problems and is based on ideas borrowed from image processing. Applying the procedure can be seen as applying a low-pass filter to eliminate structural variation underneath a certain length scale. Although based on heuristics, the proposed procedure shows promising results when applied to topology optimization of continuum structures.

---

## 1. Numerical homogenization procedures

In this chapter a numerical procedure to determine effective thermoelastic properties of nonhomogeneous periodic materials will be described. The material microstructure represented by a base cell is discretized in different ways, namely by micro truss-, frame- and continuum-like discretizations. The advantages and disadvantages of the different discretizations will be discussed and illustrated by examples.

Section 1.1 describes the general formulas used in homogenization of linear elastic materials and section 1.2 discusses the extension to homogenization of thermoelastic properties. In section 1.3 the homogenization problem is discretized using the finite element method. Section 1.4 describes details related to the actual implementation and advantages gained by using sparse methods to solve the finite elements problem. Characteristics and implementation issues of the different discretizations are discussed in section 1.5 and illustrated by examples in section 1.6.

Considering linear elasticity, material behaviour is governed by the generalized Hooke's law given as

$$\sigma_{ij} = E_{ijkl} \epsilon_{kl} - \Delta T E_{ijkl} \alpha_{kl} \quad (1.1)$$

where  $\sigma_{ij}$  and  $\epsilon_{kl}$  are the stress and strain tensors,  $E_{ijkl}$  is the positive semi-definite elasticity tensor,  $\alpha_{kl}$  is the coefficient tensor of thermal expansion and  $\Delta T$  is the temperature change from a reference temperature.

The generalized Hooke's law (1.1) can also be written as

$$\sigma_{ij} = E_{ijkl} \epsilon_{kl} - \Delta T \beta_{ij} \quad (1.2)$$

where  $\beta_{ij}$  is a thermal coefficient related through the elasticity tensor to the coefficient of thermal expansion  $\alpha_{kl}$ .

If we have a homogeneous material that is, a material with no microstructural variation, the material behaves according to (1.2) subjected to some strain field or temperature change. For an inhomogeneous material the elasticity and thermal coefficient tensors  $E_{ijkl}$  and  $\beta_{ij}$  will fluctuate on the microscopic scale and therefore make an accurate analysis of a structure composed of the inhomogeneous material an overwhelming computational task. We are therefore interested in determining an "average" or homogenized measure of the thermoelastic properties. The homogenized coefficients can be used for the analysis of the global structure which means, that we can ignore the microstructure in the global analysis and thereby simplify analysis considerably.

---

The "averaged" or homogenized material properties are denoted  $E_{ijkl}^H$  and  $\beta_{ij}^H$  and can be found by several different methods.

Considering simple microstructures such as honeycombs or circular inclusions in matrix materials etc., homogenized properties or good bounds can be determined analytically. The theory is developed in Bensoussan, [Lions and Papanicolaou, \(1978\)](#), Sanchez-Palencia, (1980) and Cioranescu and Saint Jean Paulin, (1986), and examples of analytical determination of effective parameters are seen in Bakhvalov and Panasenko, (1989), Aboudi, (1991) or Nemat-Nasser and Hori, (1993). Considering more complicated microstructures, analytical determination of homogenized coefficients becomes an impossible task and numerically based methods must be used. Examples of numerically based homogenization methods are the Finite Element (FE) based numerical methods described in Bourgat, (1977) and Guedes and Kikuchi, (1990), Fourier-series approaches described in Walker, Freed and Jordan (1991) and Moulinec and Suquet (1994) and boundary integral methods described in Greenbaum, Greengard and McFadden (1993).

## 1.1 Homogenization of elastic properties

The numerical homogenization method is based on analysis of a base cell together with an asymptotic expansion of the displacement field of the inhomogeneous material. A base cell is the smallest repetitive unit of a periodic material as sketched in figure 1.1.

Figure 1.1 (left) shows a periodic material in two dimensions where the microstructure consists of a matrix material with circular inclusions of another material and a three dimensional material (right) consisting of fibres embedded in a matrix material. Two coordinate systems are defined to describe the material behaviour on the macroscopic scale  $X$  and on the microscopic scale  $Y$ .

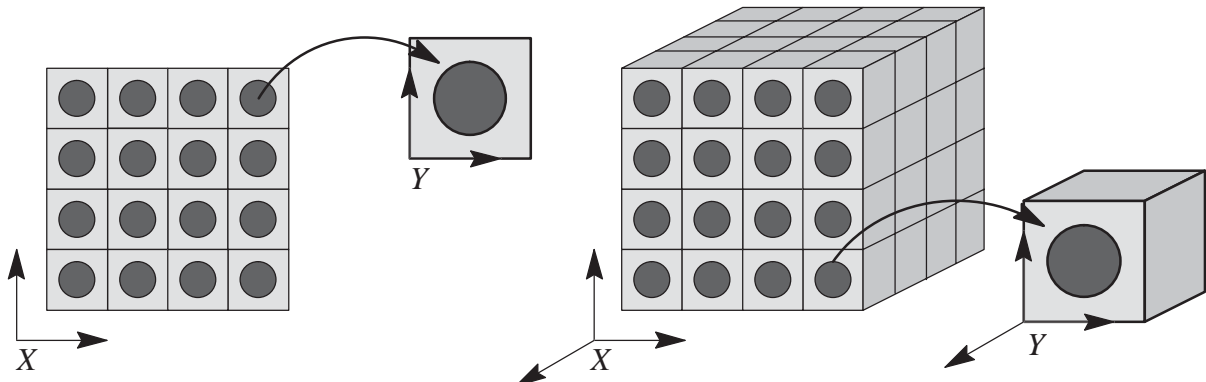


**Figure 1.1** Periodic materials in two and three dimensions represented by their base cells.

The microstructure of a two or three dimensional material is thus represented by rectangular base cells in  $\mathbb{R}^2$  or  $\mathbb{R}^3$  defined as

$$\begin{aligned} Y &= [0, y_1^0] \times [0, y_2^0] \quad (2-d) \\ Y &= [0, y_1^0] \times [0, y_2^0] \times [0, y_3^0] \quad (3-d) \end{aligned} \quad (1.3)$$

where  $y_1^0$ ,  $y_2^0$  and  $y_3^0$  is the horizontal length, vertical length and depth of the base cells respectively.

The microscopic displacement  $u$  of an inhomogeneous material can be represented by an asymptotic expansion with respect to the size of the base cell  $\eta$  and is written as

$$u = u^0(x, y) + \eta u^1(x, y) + \eta^2 u^2(x, y) + \dots, \quad y = x/\eta \quad (1.4)$$

Only considering the first order terms of the asymptotic expansion and using the notation  $\epsilon_{ij}^0 = \frac{1}{2}(\partial u_i^0 / \partial x_j + \partial u_j^0 / \partial x_i)$  and  $\epsilon_{ij}^* = \frac{1}{2}(\partial u_i^1 / \partial y_j + \partial u_j^1 / \partial y_i)$  we can write the strain  $\epsilon_{ij}$  of an inhomogeneous material as

$$\epsilon_{ij} = \epsilon_{ij}(u) \approx \epsilon_{ij}^0 + \epsilon_{ij}^* \quad (1.5)$$

The microscopic strain field  $\epsilon_{ij}$  is thus expressed as the sum of the strain field due to the average displacement over the base cell  $\epsilon_{ij}^0$  and the fluctuation strain  $\epsilon_{ij}^*$  due to the first order variation or inhomogeneity of the material.

By letting the size of the base cell  $\eta$  go to zero and by choosing four linearly independent test strain fields  $\epsilon_{ij}^0$  defined as the four unit tensors  $\epsilon_{ij}^{0(11)} = (1, 0, 0, 0)$ ,  $\epsilon_{ij}^{0(22)} = (0, 1, 0, 0)$ ,  $\epsilon_{ij}^{0(12)} = (0, 0, 1, 0)$  and  $\epsilon_{ij}^{0(21)} = (0, 0, 0, 1)$  in two dimensions and similarly with nine unit tensors in three dimensions, it can be shown that the homogenized constitutive tensor can be written as

$$E_{ijkl}^H = \frac{1}{Y} \int_Y E_{ijpq} \left( \epsilon_{pq}^{0(kl)} - \epsilon_{pq}^{*(kl)} \right) dY \quad (1.6)$$

where the fluctuation strain  $\epsilon_{ij}^*$  is the  $Y$ -periodic solution to the variational type problem

$$\int_Y E_{ijpq} \epsilon_{ij}(v) \epsilon_{pq}^{*(kl)} dY = \int_Y E_{ijpq} \epsilon_{ij}(v) \epsilon_{pq}^{0(kl)} dY \quad \forall v \in V \quad (1.7)$$

$$V = \{v : v \text{ is } Y\text{-periodic}\}$$

Finding all the coefficients in the homogenized constitutive tensor  $E_{ijkl}^H$ , requires (1.7) to be solved for the four linearly independent test strain fields  $\epsilon_{ij}^0$  and the solutions  $\epsilon_{ij}^*$  to be substituted into (1.6). Using the symmetries of the elasticity tensor, namely  $E_{ijkl} = E_{jikl} = E_{ijlk} = E_{klji}$ , the number of test fields can be reduced to three in two dimensions ( $\epsilon_{ij}^{0(12)} = \epsilon_{ij}^{0(21)}$ ) and six in three dimensions.

As mentioned in the introduction, construction of materials with prescribed constitutive parameters can conveniently be treated as a topology optimization problem. The optimality criteria methods used in topology optimization are based on energy expressions such as compliance or eigenfrequencies, so expressing the constitutive parameters in energy terms, makes it possible to use effective existing algorithms used in the topology optimization of trusses, plates, grillages, etc.

Using that (1.7) is satisfied, the homogenized constitutive tensor can be expressed in the energy bilinear form

$$E_{ijkl}^H = \frac{1}{Y} \int_Y \left( E_{pqrs} \left( \epsilon_{pq}^{0(kl)} - \epsilon_{pq}^{*(kl)} \right) \left( \epsilon_{rs}^{0(ij)} - \epsilon_{rs}^{*(ij)} \right) \right) dY \quad (1.8)$$

The homogenization formulas (1.6) and (1.7) correspond to the standard numerical homogenization formulas [e.g. Bourgat, (1977) or Guedes and Kikuchi, (1990)]. The standard equations are derived for continuum structures under the assumption that no holes intersect the boundaries of the base cell.

## 1.2 Homogenization of thermal properties

Parallel to the derivations of the homogenized elasticity tensor, it can be shown that the homogenized thermal coefficient tensor  $\beta_{ij}^H$  can be written as

$$\beta_{ij}^H = \frac{1}{Y} \int_Y E_{ijkl} \left( \alpha_{kl} - \epsilon_{kl}^C \right) dY \quad (1.9)$$

where  $\epsilon_{kl}^C$  is the  $Y$ -periodic solution to the variational type problem

$$\int_Y E_{ijkl} \epsilon_{ij}(v) \epsilon_{kl}^C dY = \int_Y E_{ijkl} \epsilon_{ij}(v) \alpha_{kl} dY \quad \forall v \in V \quad (1.10)$$

$$V = \{v : v \text{ is } Y\text{-periodic}\}$$


---

Equation (1.10) is very similar to the elasticity problem (1.7) – only difference is that the prestrain in (1.10) is not a unit prestrain but a prestrain due to the variation in the thermal expansion coefficient  $\alpha_{kl}$ . Solving equation (1.10) requires an extra analysis of the base cell. Using the Maxwell–Betti reciprocal theorem as described in Rodrigues and Fernandes, (1994), we can save this extra analysis and reuse the results from equation (1.7).

Using the Maxwell–Betti reciprocal theorem we get that

$$\int_Y E_{ijkl} \epsilon_{ij}^C dY = \int_Y \beta_{ij} \epsilon_{ij}^{*(kl)} dY \quad (1.11)$$

Using (1.11) the homogenized thermal coefficient tensor  $\beta_{ij}^H$  can be written as

$$\beta_{ij}^H = \frac{1}{Y} \int_Y \beta_{kl} \left( \epsilon_{kl}^{0(ij)} - \epsilon_{kl}^{*(ij)} \right) dY = \frac{1}{Y} \int_Y \alpha_{pq} E_{pqkl} \left( \epsilon_{kl}^{0(ij)} - \epsilon_{kl}^{*(ij)} \right) dY \quad (1.12)$$

thus saving the computation of (1.10).

### 1.3 Finite element discretization

In the following, the homogenization procedure described in the last sections will be discretized by the standard finite element method. The notations used will follow standard finite element notation as defined in Cook, Malkus and Plesha, (1989). The derivations in this section are valid for any type of element discretization. Details related to the specific finite element discretizations will be discussed in section 1.5.

The base cell is discretized by  $NE$  finite elements of various types and geometries as will be discussed later. The equation for the homogenized constitutive tensor (1.8) can then be written in discretized form as

$$E_{ijkl}^H = \frac{1}{Y} \sum_{e=1}^{NE} \int_{Y^e} \left( \{\epsilon_0^e\}_{ij} - \{\epsilon^e\}_{ij} \right)^T [E] \left( \{\epsilon_0^e\}_{kl} - \{\epsilon^e\}_{kl} \right) dY^e \quad (1.13)$$

where  $Y^e$  is the area of the  $e$ 'th element. Performing the integration over each element we get

$$E_{ijkl}^H = \frac{1}{Y} \sum_{e=1}^{NE} \left( \{d_0^e\}_{ij} - \{d^e\}_{ij} \right)^T [s^e] \left( \{d_0^e\}_{kl} - \{d^e\}_{kl} \right) \quad (1.14)$$

where the element stiffness matrix  $[s^e]$  is defined as  $[s^e] = \int_{Y^e} [B^e]^T [E^e] [B^e] dY^e$  and  $\{d^e\}$  is the local displacement vector related to the strain field  $\{\epsilon\}$  of element  $e$  by the strain–displacement matrix  $[B^e]$ .

Solving the variational type problem (1.7) corresponds to solving a finite element problem of the base cell subject to each of the test strain fields  $\{\epsilon_0\}_{ij}$ . In FE-notation this problem can be written as

$$[S]\{D\}_{ij} = \{R\}_{ij} \quad (1.15)$$

where  $[S]$  is the global stiffness matrix assembled from the local stiffness matrices  $[s^e]$ ,  $\{D\}_{ij}$  is the global displacement vector, and the load vector associated with test strain field  $\epsilon_0^{ij}$  is defined as  $\{R\}_{ij} = \sum_{e=1}^{NE} \int_{Y^e} [B^e]^T [E^e] \{\epsilon_0\}_{ij} dY^e$  where the summation implicates the usual FE-assembly procedure.

The solution of the finite element problem (1.15), the displacement vector  $\{D\}_{ij}$ , is subject to periodic boundary conditions. The boundary conditions can be imposed in different ways as will be discussed in section 1.4.

For reasons explained in the section on defining the inverse homogenization problem it is an advantage to define the homogenized properties (1.14) in terms of element mutual energy densities

$$E_{ijkl}^H = \sum_{e=1}^{NE} Q_{ijkl}^e \quad (1.16)$$

where the element mutual energy densities  $Q_{ijkl}^e$  are defined as

$$Q_{ijkl}^e = \frac{1}{Y} \left( \{d_0^e\}_{ij} - \{d^e\}_{ij} \right)^T [s^e] \left( \{d_0^e\}_{kl} - \{d^e\}_{kl} \right) \quad (1.17)$$

Design of materials in chapter 2 only considers microstructures where the elasticity tensor is linearly dependent on the design variables  $x^e$ . This feature makes the design problem well posed for the optimality criteria procedures used in topology optimization and we can conveniently write the homogenized elastic properties as

$$E_{ijkl}^H = \sum_{e=1}^{NE} q_{ijkl}^e x^e \quad (1.18)$$

where

$$q_{ijkl}^e = \frac{1}{Y} \left( \{d_0^e\}_{ij} - \{d^e\}_{ij} \right)^T [s_0^e] \left( \{d_0^e\}_{kl} - \{d^e\}_{kl} \right) \quad (1.19)$$

Here it was assumed that the element stiffness matrices are linearly dependent of the design variables such that  $[s_0^e] = [s^e]/x^e$  where  $x^e$  is the  $e$ 'th design variable.

Similar to the discretization of the computation of the homogenized elastic tensor, we can write the homogenized thermal coefficients as

$$\beta_{ij}^H = \sum_{e=1}^{NE} q_{ij}^e x^e \quad (1.20)$$

where

$$q_{ij}^e = \frac{Y^e}{Y} \left\{ \beta_0^e \right\}^T [B] \left( \{d_0^e\}_{ij} - \{d^e\}_{ij} \right) = \frac{Y^e}{Y} \left\{ \alpha_0^e \right\}^T [E_0] [B] \left( \{d_0^e\}_{ij} - \{d^e\}_{ij} \right), \quad (1.21)$$

$\{\beta_0\} = \{\beta^e\}/x^e$  and  $[E_0] = [E^e]/x^e$  and it was used that we are considering bilinear elements.

## 1.4 Solution procedures for the finite element problem

This section discusses ways to impose the periodic boundary conditions on the cell problem and shows how computer time requirements can be reduced by using an iterative element-by-element finite element solver.

The periodic boundary conditions in the FE–problem (1.15) can be imposed in different ways. The simplest way is to use a penalty method described in Cook, Malkus and Plesha, (1989). The basic idea in the penalty method is to add a very stiff (2-node) element connecting the linked degrees of freedom thus forcing the relative displacements of the two nodes to be equal. Another method is to give opposing nodes the same node number. This method has the advantage of reducing the number of degrees of freedom of the system but it also makes the housekeeping with the node numbering scheme more complicated.

Both above mentioned methods have the big disadvantage that the bandwidth of the global stiffness matrix  $[S]$  becomes almost equal to the number of Degrees Of Freedom (DOF) of the linear system. Apart from making computations time expensive and frustrating, the large bandwidth makes storage requirements huge. As an example, consider a base cell modelled by  $30 \times 30 = 900$  4-node quadrilateral finite elements. The number of DOF for this system is 1800 making the size of the stiffness matrix approximately equal to 26 Mb. The huge storage requirement for such a relatively small linear system makes the use of sparse methods promising.

One way to "overcome" the storage and computer time problem is to use a so-called skyline solver. In this approach only non-zero elements of the global stiffness matrix are stored. For a linear system with large variations in the bandwidth (as for the base cell), the skyline solver can be very efficient.

Iterative linear equation solvers belong to another class of sparse methods. Iterative methods are especially attractive for use in optimization problems. In the beginning steps of an optimization procedure we do not need an exact solution for the displacement vector. The convergence requirements for the iterative solver can therefore be relaxed. In fact, this idea was fully taken advantage of by Sankaranarayanan, Haftka and Kapania, (1992) or Ringertz, (1988), where the exact solution of the FE problem and the optimal values of the design variables only are found in the very last iteration.

In this work we will use the so-called Element–by–Element Preconditioned Conjugate Gradient solver (EBE–PCG). The general PCG method is described in Numerical Recipes, Press *et al.*, (1992). The EBE–PCG method is discussed and applied to FE analysis in Ferencz, (1989) and applied to the analysis of human bone structure discretized by up to one million finite elements in Hollister and Riemer, (1993).

The iterative algorithm of the EBE–PCG solver is described in appendix 3. Shortly summarized it solves the  $N \times N$  linear system

$$[S]\{D\} = \{R\} \quad (1.22)$$

by minimizing the function

$$f(\{D\}) = \frac{1}{2}\{D\}^T [S]\{D\} - \{R\}^T \{D\} \quad (1.23)$$

which means that we are physically back in the minimization of potential energy in the linear elastic body.

The function  $f$  (potential energy) has a stationary point when the gradient

$$\nabla f = [S]\{D\} - \{R\} \quad (1.24)$$

is zero which corresponds to (1.22).

The minimization is performed as an iterative procedure computing the search direction  $\{p\}_k$  and improved minimizers  $\{D\}_k$ . At each step  $k$  in the iteration a factor  $\alpha$  is determined such that  $f(\{D\}_k + \alpha \{p\}_k)$  is minimized. The new minimizer  $\{D\}_{k+1}$  is then set equal to the new point  $\{D\}_k + \alpha \{p\}_k$ .

---

The computationally heavy part of the EBE–PCG algorithm is the multiplication of the global stiffness matrix  $[S]$  and the search direction vector  $\{p\}$ . However, this multiplication can be done on the element level as

$$\{v\}_k = \sum_{e=1}^{NE} [s^e] \{p^e\}_k \quad (1.25)$$

using the appropriate assembly procedure from local to global coordinates. As seen in equation (1.25), the global stiffness matrix never has to be assembled – this feature makes the requirement to storage space very small in the EBE–PCG solver. Furthermore, the procedure is independent on the bandwidth of the FE–problem again because the global stiffness matrix is never assembled.

In practice, we do not require an exact solution to the FE–problem and we can therefore save considerable computational time by stopping the iterative solver when the norm of the residual vector gets below a stopping criteria  $\delta$ . In fact  $\delta$  can be chosen very gross when the EBE–PCG algorithm is used as a part of an iterative optimization procedure. Only in the final iterations of the optimization procedure we require an exact solution and then  $\delta$  can be made smaller for final convergence. Furthermore old solutions of the FE–problem can be used as starting guesses for the new iteration, making further savings in computational time possible.

Numerical experience shows that the EBE–PCG solves the FE–problems considered in this work very efficiently. Using regular continuum element discretizations, the storage space for a FE–problem with 10.000 bilinear elements is less than 1 Mb (vector of element densities, one element stiffness matrix and some work–area for the solver). In the beginning iterations, computational time is comparable to time requirements of conventional solvers (for problems without periodic boundary conditions) but as the optimization procedure converges, the computational time using the iterative FE–solver is reduced by up to a factor of 20. Further details of the computational procedure are described in appendix 3.

## 1.5 Discretizations of microstructure

Microstructures of materials can vary from very thin or porous microstructures such as sponges or foams over solid metals with no porosity, to mixtures of materials such as carbon fibers embedded in a matrix. To analyze various microstructures properly we therefore have to use different discretizations to model different material types. In this section three, different discretizations, namely truss–, frame– and continuum–like microstructures are described.

All the considered microstructures in this section are based on the "ground structure" idea. This

means that the number of elements to discretize the base cell has a fixed large number. Specific microstructures can then be built by assigning different properties such as area, Young's modulus, thickness or material type to each element in the base cell. The properties of elements which are non–important for the specific microstructures are set to small values such that they do not have significant influence on the computed properties. This procedure will be demonstrated by a simple example later in this section. Using the ground structure approach we get the following advantages

- The program can be standardized independent on the considered discretization and material topology
- Existing methods from topology optimization of structures can be applied to the material design problem
- The requirement that no holes can intersect the boundaries of the base cell will always be fulfilled because no elements are removed from the initial structure
- Regular meshes for continuum modelled microstructures allow the use of image processing techniques for pre– and post–processing of the resulting designs

The disadvantage is, that storage and computer time requirements are increased because of the large number of elements which are passively present in the structure.

### **Truss–like microstructures**

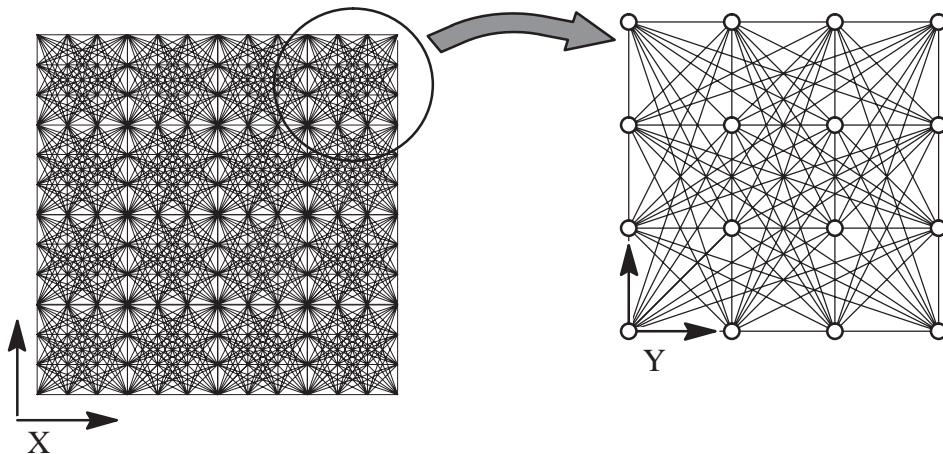
As one of the aims of this work is to design materials with extreme elastic properties and such materials are expected to show mechanism type behaviour (see chapter two), we will, as one of the discretizations of base cells, use a truss like–microstructure which can model such behaviour. *A truss structure is defined as a structure composed of bars which can only transmit longitudinal forces.* Examples of truss–like microstructures in two and three dimensions are shown in figure 1.2 and 1.3 respectively.

Figure 1.2 (right) shows a two dimensional base cell with 16 nodal points connected by bar elements – outside the nodal points, bars are allowed to cross each other without interaction.

The standard homogenization formulas discussed in section 1.1 were derived for continuum structures. Therefore, it is necessary to consider the truss structure as a continuum structure with holes which is done by treating the individual bar members as 2–node continuum elements as described in appendix 4.

As an example of how the groundstructure approach is used in the truss–like microstructure, we will show how to analyze a simple octagonal microstructure using the base cell in figure 1.2 as

---



**Figure 1.2** Composite material composed of a truss–like microstructure in two dimensions. Nodal points are illustrated by small circles.

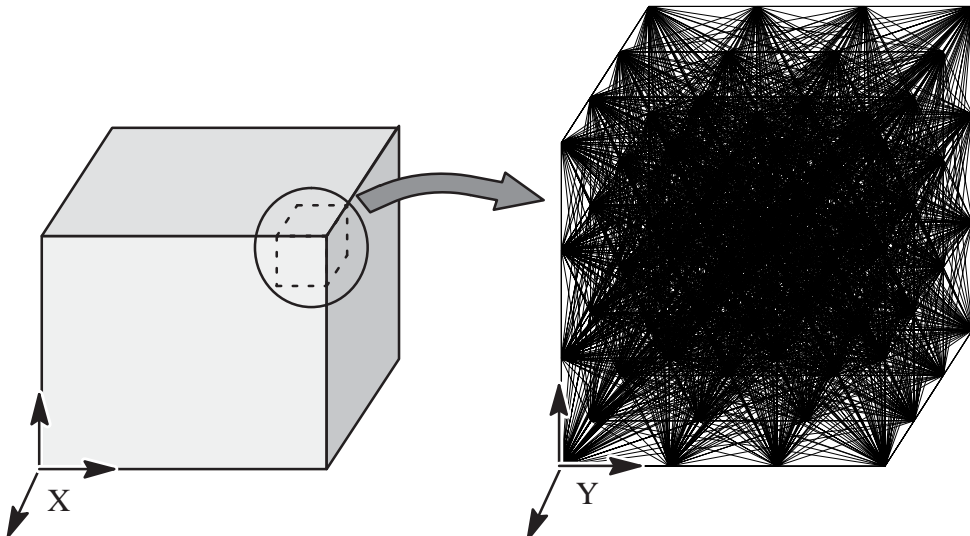


**Figure 1.3** Composite material composed of a truss–like microstructure in three dimensions. Nodal points are not shown

groundstructure. Figure 1.4 illustrates how the important members for the octagonal cell are given an area  $A_{bar}$  (thick bars) and the unimportant bar members are given a small area  $A_{min}$  (thin bars). The minimum area  $A_{min}$  is chosen such that the homogenized coefficients are unaffected by their presence (usually  $A_{min}/A_{bar} = 10^{-7}$ ).

The truss structure has two DOF per node in two dimensions and three DOF per node in three dimensions (two and three translational DOF respectively) thus the element stiffness matrix  $[s^e]$  has dimension 4x4 in two dimensions and 6x6 in three dimensions.

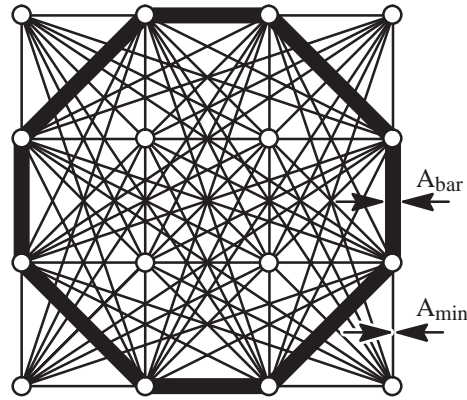


**Figure 1.4** Modelling of a simple octagonal microstructure using the groundstructure approach.

### Frame-like microstructures

Modelling porous materials as micro truss structures might be criticized in a couple of ways. First, no known naturally occurring material has moment free links in the microstructure and second, for the design of material purpose, it will be very difficult to build links at the microlevel. For these reasons we will also consider base cells discretized by frame elements. A *frame structure* is defined as a structure composed of beam elements transferring longitudinal forces and moments and connected by stiff joints. An example of a frame-like microstructure is shown in figure 1.5. The frame structure has three DOF per node (two translational and one rotational) thus the element stiffness matrix  $[s^e]$  has dimension 6x6 in two dimensions.

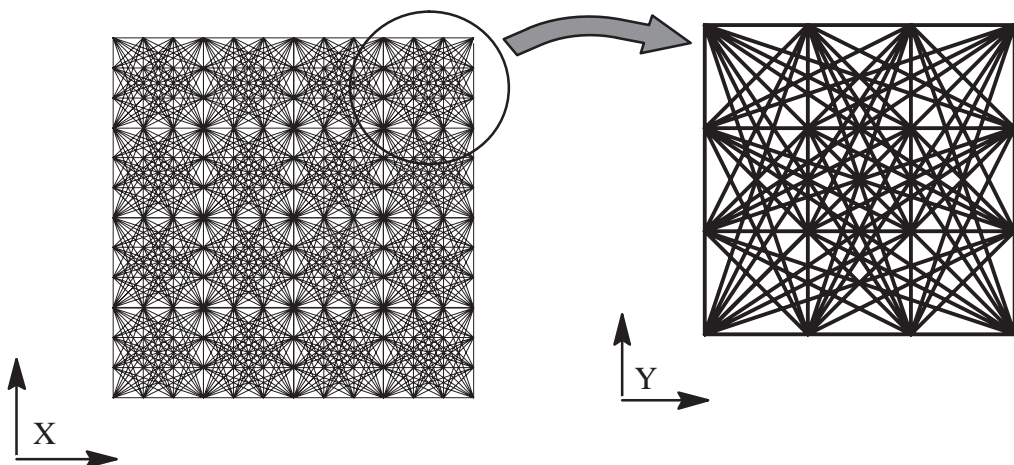


**Figure 1.5** Composite material composed of a frame-like microstructure in two dimensions.

### Continuum-like microstructures

Truss and frame-like microstructures can only be used for the modeling of porous materials. Considering materials with small voids or mixtures of different materials, a continuum-like discretization of the base cell must be used. In the continuum-like discretization the base cell is discretized by four node bilinear finite elements. The discretization can be characterized as a pixel-like microstructure where each pixel represents one finite element. Choosing a regular discretization as shown in figure 1.6, all pixels or elements will have the same geometrical properties. This feature makes the whole problem very cheap in storage space because we only have to calculate and store the element stiffness matrix  $[s^e]$  once for each material type used in modelling the microstructure. This advantage was fully utilized by Hollister and Riemer, (1993) where they calculated three dimensional human bone structure discretized by over one million 8-node brick elements.

Figure 1.6 shows a microstructure consisting of a (strong) fiber embedded in a (soft) matrix and discretized by square finite elements. The enlargement (figure 1.6 right) shows the resulting step-like boundaries between the two materials which is due to the pixel-like discretization. It might be objected that this "jagged" discretization will lead to erroneous results but examples in the next section will show that the effective properties are in fact quite insensitive to the "jagged" boundaries.

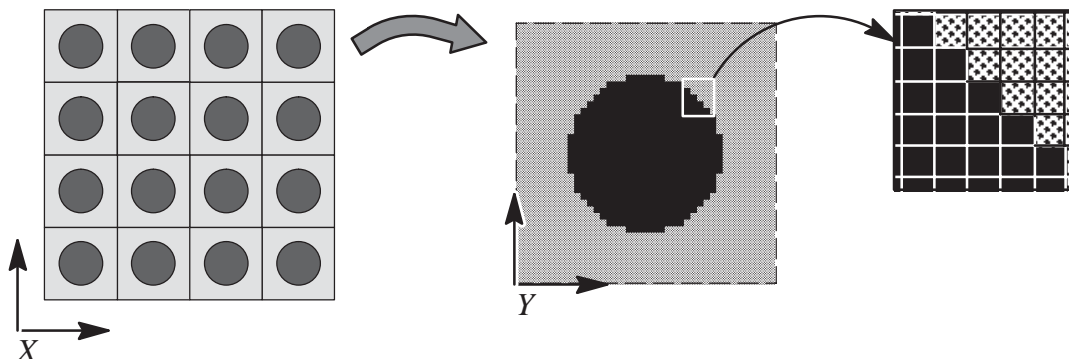


**Figure 1.6** Composite material composed of a continuum-like microstructure in two dimensions.

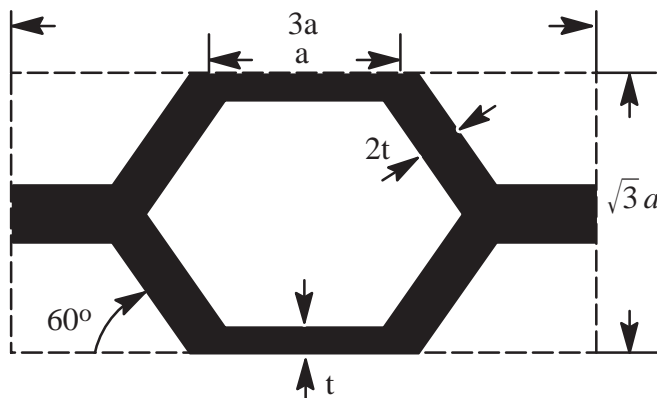
## 1.6 Examples

To illustrate the difference in modelling a porous microstructure by a frame-like or a continuum-like discretization and to discuss the consequence of modelling smooth edges by step-like edges in the continuum discretization, we will use two "famous" examples of porous microstructures, namely the honeycomb and the inverted honeycomb.

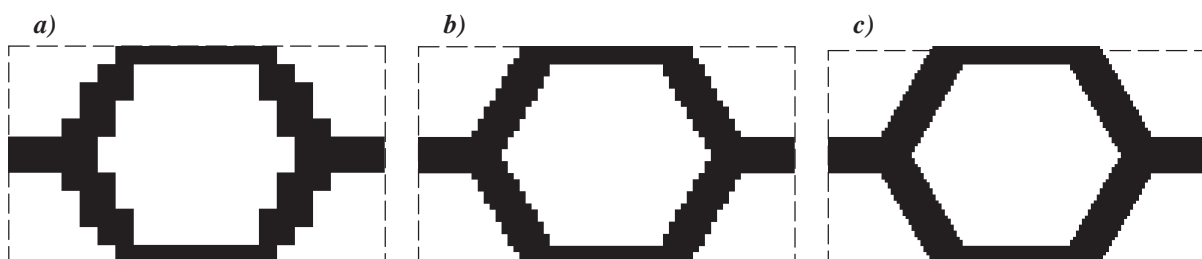
### The Perfect Honeycomb

Figure 1.7 shows the base cell and the dimensions of the perfect honeycomb. Choosing a cell with  $a=3^{-3/4}$ , the area of the base cell becomes unity. In this example the ratio of wall thickness to cell size is  $t/a=\sqrt{3}/12$ , the Youngs modulus of the isotropic base material is 0.91 and the Poisson's ratio  $\nu$  is 0.3.

Figure 1.8 shows three different continuum discretizations used to model the base cell. Areas with material are shown in black and white areas should be void. However, due to the ground structure approach, white areas actually are modelled by weak material with a very low stiffness ( $E_{void}/E_{solid}=10^{-4}$ ). The resulting homogenized elastic properties from the three discretizations are shown in table 1.1.



**Figure 1.7** Dimensions of perfect honeycomb.



**Figure 1.8** Three different discretizations of the perfect honeycomb: a)  $21 \times 12 = 252$  elements, b)  $63 \times 36 = 2268$  and c)  $126 \times 72 = 9072$  elements.

Size (elements)	CPU-time (seconds)	$\rho$	$E_{1111}$	$E_{2222}$	$E_{1212}$	$E_{1122}$	$\nu$
21x12=252	2	0.310	0.0912	0.0877	0.0121	0.0691	0.77
63x36=2268	58	0.305	0.0934	0.0940	0.0122	0.0703	0.75
126x72=9072	309	0.306	0.0958	0.0950	0.0125	0.0713	0.75
<b>PREMAT2D, 9520</b>	—	<b>0.306</b>	<b>0.0968</b>	<b>0.0968</b>	<b>0.0124</b>	<b>0.0720</b>	<b>0.74</b>
Frame model, 8	—	0.334	0.0961	0.0962	0.0129	0.0703	0.73

**Table 1.1.** Resulting homogenized properties of the perfect honeycomb calculated by continuum and frame-like microstructures and compared with results from the program PREMAT2D supplied by J.M. Guedes.

The computed effective properties for the three discretizations are compared with values obtained by running the program PREMAT2D developed and kindly supplied by José M. Guedes, Institute Superior Technico, Portugal [see Guedes and Kikuchi, (1990) and Guedes, Neves and Orlando, (1994)]. The program PREMAT2D uses the same numerical homogenization procedure as described in this chapter and uses a mesh generator which can model boundaries between solid and void (or two materials) smoothly, furthermore the program uses no elements in the void regions. PREMAT2D was used to calculate the effective properties of the perfect honeycomb discretized by 9520 4 node linear displacement finite elements.

Comparing the effective properties obtained by the pixel approach in this report with the effective properties from PREMAT2D, we notice a reasonable agreement even for the coarse mesh shown in figure 1.8a which consists of only 252 elements. The error relative to the PREMAT2D results is less than 10%. From this example we can conclude that effective properties are predicted well even for very coarse meshes with badly "jagged" edges by the proposed pixel-like discretization.

The last row in table 1.1 shows the effective properties obtained by discretizing the perfect honeycomb with frame elements. Fine agreement with the results from PREMAT2D is seen by comparing the effective stiffnesses. However, there is an error in the prediction of the density  $\rho$  for the frame case. This error can be explained by the fact that the frame modelling allows overlapping and therefore areas where two frame elements overlap are counted twice when the total material density is calculated.

It can be observed that the perfect honeycomb is an isotropic material because  $E_{1212} = (E_{1111} + E_{1122})/2$  and  $E_{1111} = E_{2222}$  but it also follows from the fact that the microstructure has  $60^\circ$  symmetry.

### The inverted honeycomb

In this example we will look at the influence of the volume fraction on the effective properties. The inverted honeycomb which has a negative Poisson's ratio was first reported by Almgren, (1985), Kolpakov, (1985) and Gibson and Ashby, (1988). Figure 1.9 shows the inverted honeycomb with three different volume fractions and using 4032 square elements for the discretizations. The microstructure was also modelled by frame elements. The resulting effective properties are shown in table 1.2.

A FE-mesh for the computation of the homogenized properties of the inverted honeycomb is not directly available in PREMAT2D (although customized FE meshes can be generated) but as in the last example, good agreement (especially for low densities) between continuum and frame-like discretization is seen in table 1.2.

Some observations can be made on the effective properties of the inverted honeycomb. The material does not fulfill the requirements for isotropy because neither is  $E_{1212} = (E_{1111} + E_{2222})/2$  nor is  $E_{1111} = E_{2222}$ . In fact the shear stiffness  $E_{1212}$  is close to zero and the inverted honeycomb is therefore a highly anisotropic material. Most of the advantages of materials with negative Poisson's ratios discussed in the introduction are lost because of the anisotropy of the inverted honeycomb.

$t/a$	$\varrho$	$E_{1111}$	$E_{2222}$	$E_{1212}$	$E_{1122}$	$\nu_{12}$	$\nu_{21}$
$\sqrt{3}/12$ (continuum)	0.397	0.0692	0.1011	0.0033	-0.0457	-0.66	-0.45
$\sqrt{3}/12$ (frame)	0.445	0.0694	0.0817	0.0021	-0.0507	-0.73	-0.62
$\sqrt{3}/24$ (continuum)	0.210	0.0299	0.0342	0.0004	-0.0274	-0.92	-0.80
$\sqrt{3}/24$ (frame)	0.222	0.0322	0.0338	0.0003	-0.0296	-0.92	-0.88
$\sqrt{3}/48$ (continuum)	0.109	0.0139	0.0144	0.0001	-0.0135	-0.97	-0.94
$\sqrt{3}/48$ (frame)	0.111	0.0157	0.0160	0.0000	-0.0154	-0.98	-0.96

**Table 1.2.** Resulting homogenized properties of the inverted honeycomb calculated by continuum and frame-like microstructures for different volume fractions of material to void.



**Figure 1.9** Three different volume fractions of the inverted honeycomb. Groundstructure is 84x48 elements.

## 1.7 Summary

A numerical homogenization procedure is described and applied to truss–, frame– and continuum–like discretizations of microstructures. The advantages gained by using sparse methods in solving the associated finite element problem is discussed and the EBE–PCG solver is chosen due to its iterative nature which can be taken fully advantage of when it is applied as solver in an iterative optimization procedure. The homogenized coefficients are expressed in a form that make them well suited for topology optimization methods. The proposed procedures and discretizations are applied to the homogenization of two practical microstructures and the results are compared with those obtained by the software PREMAT2D and show good agreement. Boundaries in the continuum formulation appear as jagged edges due to the pixel–like discretization and this could be expected to give erroneous results. However, numerical evidence shows only small errors in the homogenized properties even for very coarse meshes which is of importance when the discretization is used as groundstructure in the design of materials in chapter two.

## 2. Design of materials

In this chapter the problem of how to design a material with prescribed thermoelastic properties is considered. The design problem is formulated as an inverse homogenization problem and is solved by an optimality criteria method. The design domain is the microstructure of a periodic material represented by base cells and discretized by various types of finite elements.

The problem of how to design a material with prescribed thermoelastic properties can be approached in different ways as discussed in the introduction. We can try to utilize existing (fiber) materials the best possible way by varying lamination parameters, such as angles or thicknesses [e.g. Autio, Laitinen and Pramila, (1993)], or we can take the mathematical approach and design ranked materials consisting of laminations at several length scales [e.g. Milton and Cherkaev, (1993)]. By the former approach, we can not design materials with extreme thermoelastic properties but on the other hand the results are directly manufacturable. By the latter approach, we can design materials with any thermodynamically admissible properties. However, they will be difficult if not impossible to manufacture, because of the assumption of several length scales in the microstructure. In this chapter, we will try to design materials with extreme elastic properties but restricting the design space to microstructures with only one length scale.

The material design problem can be formulated as an *inverse homogenization problem*; figure 2.1 illustrates the problem.

As described in chapter one, the usual homogenization problem is the following: given a material with periodic inhomogeneous microstructure (figure 2.1 right), we seek the effective homogenized properties  $E_{ijkl}^H$  (figure 2.1 left). These are found by analysis of the representative base cell (figure 2.1 center). The *inverse homogenization problem* is just the opposite. Given the effective properties  $E_{ijkl}^H$  (figure 2.1 left), we seek a material (figure 2.1 right) which has these effective properties. The problem can be solved by *designing* the microstructural topology (figure 2.1 center).

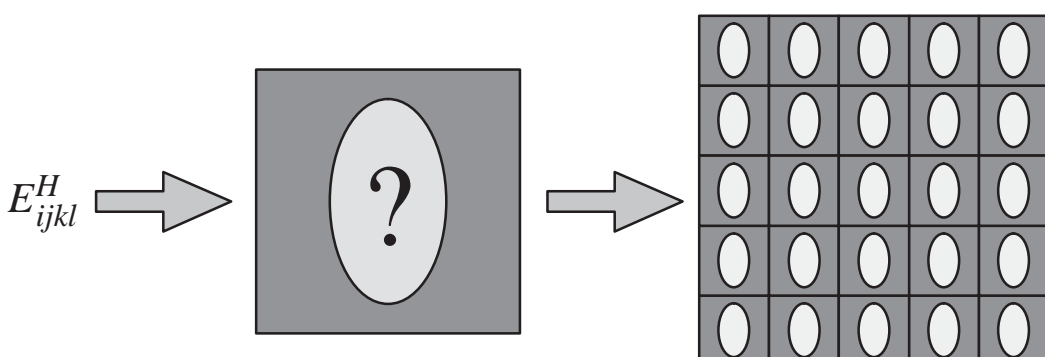


**Figure 2.1** Illustration of the inverse homogenization problem

Generally many different material microstructures can have the same constitutive properties. Consequently, we will expect the inverse homogenization problem to have several different solutions. To reduce the number of possible solutions, the inverse homogenization problem can be recast as an *optimization problem*, where the goal is to find the lightest material which has the prescribed elastic properties. The goal of minimizing weight is chosen because we are generally interested in designing materials with high stiffness-to-weight ratios as discussed in the introduction. The design domain of the optimization problem is the periodic material microstructure represented by the base cell.

The *optimization problem* can be seen as a *topology optimization problem*, where the design domain is the interior of the base cell, and the design variables are the dimensional properties of the finite elements used to discretize the base cell. By formulating the *inverse homogenization problem* as a *topology optimization problem*, we can use some of the well proven algorithms used in topology optimization of general structures; the reader is referred to [Bendsøe, \(1994\)](#), for an overview of methods.

Basically *topology optimization* consists in finding the optimal topology of a structure supported at its boundaries and subjected to some load case. The optimal topology is found within the design space defined by the *groundstructure*. The groundstructure can consist of different types of finite element discretizations, and should be chosen with so many design degrees of freedom as needed to ensure a good solution. During an iterative procedure, unimportant elements are removed from the groundstructure and the procedure is iterated until an optimum (usually consisting of only a small fraction of the elements of the original groundstructure) has been reached. For computational simplicity of this work, unimportant elements are not removed but their dimensional properties are made small such that they have no structural significance. This means, that we are actually considering a *sizing problem* because the topology is fixed, defined by the groundstructure. However, due to structural insignificance of the unimportant elements, the approach is stated as a topology optimization problem.

The best discretization type used in the groundstructure is dependent on the type of problem considered. Here, we will use truss, frame and continuum elements to model material microstructures for the following reasons:

Materials with extreme elastic behaviour are expected to show mechanism type behaviour. An example of an extreme material could be a two dimensional material with Poisson's ratio equal to one. The constitutive tensor for this material has only one non-zero eigenvalue and therefore, the material will have "zero-stress modes" where it can collapse with no structural resistance. Groundstructures consisting of *truss elements* in two or three dimensions (figures 2.2a and 2.2b

---

respectively) can model mechanism type behaviour and are therefore good choices when we want to design extreme materials.

For the design of more realistic (stable) materials, groundstructures made up of *frame elements* (figure 2.2c) can be used. Frame elements can take up bending moments and in the limit, when the thicknesses approach zero, they approach truss behaviour.

For the design of materials with high densities and only small holes, the frame element discretization is inadequate and should be replaced by a *continuum type element* discretization (figure 2.2c).

In the truss formulation the individual bar cross–sectional areas are the design variables, in the frame formulation element widths are chosen as the design variables and in the continuum formulation, the density of material in each element represents the design variables.

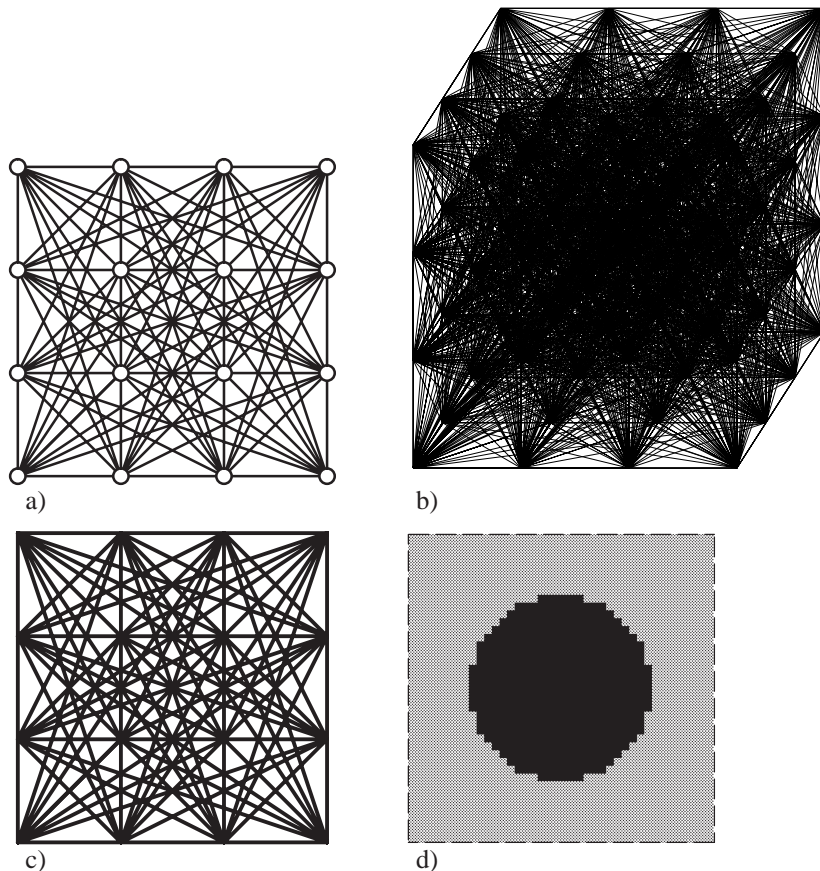


**Figure 2.2** The three different groundstructures used to model the microstructures. a) truss–like (two dimensions), b) truss–like (three dimensions), c) frame–like and d) continuum–like microstructure.

Common for the three different types of groundstructure formulations is, that the homogenized elastic properties are assumed linearly dependent on the design variables (see chapter one). The design problem can therefore be formulated in a standard way independent on the choice of microstructure.

This chapter is structured as follows. In section 2.1, the *inverse homogenization problem* is formulated as an *optimization problem*, which is common for the four different discretizations shown in figure 2.2. In section 2.2, we describe the *optimality criteria method* used to solve the optimization problem and discuss details related to the computational procedure. In sections 2.3, 2.4 and 2.5 a number of examples using the three different types of groundstructures (truss– 2d and 3d, frame– and continuum–like microstructures, respectively) are shown and discussed. In section 2.6 we design continuum–like materials with prescribed thermoelastic properties and finally, in section 2.7, we verify the numerical results by simple macro size working models.

## 2.1 The inverse homogenization problem

In this section, the inverse homogenization problem is defined as an optimization problem of minimizing the weight of the base cell subject to equality constraints on the elastic properties.

As described in chapter one, the homogenized elastic properties  $E_{ijkl}^H$  of a periodic material can be found by finite element analysis of the base cell. Under the assumption that the base cell is discretized by  $NE$  finite elements and that the homogenized properties are linearly dependent on the design variables  $x^e$ , the homogenized elastic tensor was written as

$$E_{ijkl}^H = \sum_{e=1}^{NE} q_{ijkl}^e x^e \quad (1.26)$$

where  $q_{ijkl}^e$  are the relative element mutual strain energies defined in (1.19).

Denoting the prescribed elastic tensor  $E_{ijkl}^*$ , we can write the equality constraint for the optimization problem as

$$E_{ijkl}^* - \sum_{e=1}^{NE} q_{ijkl}^e x^e = 0 \quad (2.1)$$

Equation (2.1) represents six linearly independent equality constraints in two dimensions and 21 in three dimensions. In most of the examples in this chapter we are considering symmetric (implying orthotropy) microstructures. Imposing the symmetry conditions by element linking, the number of equality constraints in (2.1) can be cut down to four and nine in two and three dimensions respectively. Definitions of notations used for the elasticity tensor and its values for specific material behaviour (isotropic, orthotropic, plane stress etc.) are given in appendix 2.

Making use of the abbreviation  $ijkl \rightarrow I$  defined by

$$\begin{aligned} 1111 &\rightarrow 1, 2222 \rightarrow 2, 1122 \rightarrow 3, 1212 \rightarrow 4 & (2-d) \\ 1111 &\rightarrow 1, 2222 \rightarrow 2, 3333 \rightarrow 3 \\ 1122 &\rightarrow 4, 1133 \rightarrow 5, 2233 \rightarrow 6 \\ 1212 &\rightarrow 7, 1313 \rightarrow 8, 2323 \rightarrow 9 \end{aligned} \quad \left. \begin{array}{l} \\ \\ \end{array} \right\} \quad (2.2) \quad \left. \begin{array}{l} \\ \\ \end{array} \right\} \quad (3-d)$$

equation (2.1) can be written in a simpler form as

$$E_I^* - \sum_{e=1}^{NE} q_I^e x^e = 0 \quad , \quad I = 1, \dots, NC \quad (2.3)$$

where  $NC$  is the number of equality constraints ( $NC=4$  in 2-d and  $NC=9$  in 3-d).

Considering porous microstructures, the material density  $\varrho$  of the homogenized material can be defined as the ratio between the volume of solid material in the base cell and the total volume of the base cell. The density  $\varrho$  is therefore bounded to the domain  $[0, 1]$ , where  $\varrho=1$  represents solid material and  $\varrho=0$  means no material at all.

Assuming that the total volume of the base cell is unity, the density of a specific microstructure can be calculated as

$$\rho = \sum_{e=1}^{NE} \gamma^e x^e \quad (2.4)$$

where  $\gamma^e$  is a "volume" factor which multiplied by the design variable  $x^e$  gives the volume of material in element  $e$ . The actual weight of a base cell can then be found by multiplying the density  $\varrho$  by the weight of a solid base cell.

As previously defined, the goal of the optimization problem is to minimize the weight of the base cell (with constraints on the elastic properties). A minimization problem with (2.4) as the objective function could now be defined. However, before we do this, we will try to incorporate some manufacturability constraints into the objective function.

It is a well known fact in the field of topology optimization, that we get complicated solutions or solutions with many intermediate values of the design variables, if we do not use some sort of penalty formulation. Choosing proper penalization factors, we can get simple and manufacturable solutions and we have the possibility to choose between solutions with different topological features as will be explained in the following.

---

A penalization of specific design variables can generally be implemented by modifying the density function (2.4) to

$$\rho = \sum_{e=1}^{NE} \kappa^e \gamma^e (x^e)^{1/p} \quad (2.5)$$

where the physical meaning of the penalty factors  $\kappa^e$  and  $p$  as well as the meaning of the "volume" factor  $\gamma^e$  is related to the considered microstructure as follows:

### Truss-like materials (figure 2.2a and 2.2b):

The design variable  $x^e$  is the cross sectional area of element  $e$  and therefore  $\gamma^e$  is defined as the length  $l^e$  of the element. For manufacturing reasons we will introduce the penalizing term  $(l^{pref}/l^e)^\xi$ , which makes it possible to penalize solutions with long or short elements.  $l^{pref}$  is a preferred length of the elements, and elements longer or shorter than  $l^{pref}$  will be penalized by choosing  $\xi$  positive or negative. The density function for two dimensional truss-like materials can be written as

$$\rho = \sum_{e=1}^{NE} l^e (l^{pref}/l^e)^\xi x^e \quad (2.5)truss2d$$

For truss-like materials in three dimensions we will multiply by another penalizing term  $\mu^e$ , which makes it possible to penalize elements on the surface of the 3-d base cell. Choosing  $\mu^e$  smaller or greater than one for elements on the surfaces makes it possible to prefer one solution from another. By choosing  $\mu^e$  smaller than one, we get solutions with only interior elements and vice versa.

$$\rho = \sum_{e=1}^{NE} l^e (l^{pref}/l^e)^\xi \mu^e x^e \quad (2.5)truss3d$$

In the example section 2.3, different choices of penalty factors and their influence on the solutions will be discussed in more detail.

### Frame-like materials (figure 2.2c):

The design variable  $x^e$  represents the width of element  $e$  and therefore  $\gamma^e$  for this case is defined as the height  $h^e$  of element  $e$  times the length  $l^e$ . We will use the same penalization of long or short elements as for the truss-like materials such that the density function can be written as

$$\rho = \sum_{e=1}^{NE} h^e l^e (l^{pref}/l^e)^\xi x^e \quad (2.5)frame$$

### Continuum-like materials (figure 2.2d):

In this case, the design variable  $x^e$  represents the density of material in element  $e$ , where  $x^e$  is restricted to the interval  $]0, 1]$  and  $\gamma^e$  is the volume  $Y^e$  of element  $e$ . The design problem is likely to have solutions with areas of intermediate values of the design variable  $x^e$ . Such "grey" areas are undesirable because we want to make porous microstructures. As discussed in chapter three of this report (on general layout optimization of structures), solid/void solutions are obtained by introducing a penalty factor  $p$ , such that the modified material density can be written as

$$\rho = \sum_{e=1}^{NE} Y^e (x^e)^{1/p} \quad (2.5) continuum$$

By choosing  $p > 1$  we make intermediate values of  $x^e$  artificially "heavy" and thus unpreferable in the optimal solution.

### All material models

The four different forms of the modified density functions for the different microstructure discretizations are all contained in the general density expression (2.5).

Using the objective function (2.5) and the equality constraints (2.3) we can now state the general optimization problem as

$$\begin{aligned}
 & \text{Minimize : } \rho = \sum_{e=1}^{NE} \kappa^e \gamma^e (x^e)^{1/p} \\
 & \text{Subject to : } E_I^* - \sum_{e=1}^{NE} q_I^e x^e = 0 \quad , \quad I = 1, \dots, NC \\
 & \quad : 0 < x_{min} \leq x^e \leq x_{max} , \quad e = 1, \dots, NE \\
 & \quad \text{and : equilibrium equations}
 \end{aligned} \tag{2.6}$$

where  $x_{min}$  and  $x_{max}$  are lower and upper limits on the design variables respectively.

## 2.2 Solving the optimization problem

The optimization problem (2.6) can be solved by many different numerical optimization algorithms. However, the problem has many design variables but few global constraints and is therefore well suited to be solved by some of the efficient optimality criteria algorithms used in topology optimization. In defining the optimality criteria algorithm, the mutual influences from element to element is ignored which means that the design variables are updated independently in each iteration step. The method is widely used for large scale structural optimization problems, (more because of its computational efficiency than its mathematical rigour).

The optimality criteria algorithm described here includes multiple equality constraints such that the procedure must be divided in to an inner and an outer problem. The outer problem consists in the update of the design variables using a fixed-point type algorithm and the inner problem consists in determining the values of the multiple Lagrangian multipliers. The inner problem is solved by a standard Newton–Raphson procedure as proposed in Zhou and Rozvany, (1993).

The Lagrangian function for the optimization problem (2.6) can be written as

$$\begin{aligned} \mathcal{L} = & \sum_{e=1}^{NE} \kappa^e \gamma^e (x^e)^{1/p} + \sum_{I=1}^{NC} \nu_I \left( E_I^* - \sum_{e=1}^{NE} q_I^e x^e \right) + \\ & \sum_{e=1}^{NE} \alpha^e (-x^e + x_{min}) + \sum_{e=1}^{NE} \beta^e (x^e - x_{max}) \end{aligned} \quad (2.7)$$

where  $\nu_I$  are the  $NC$  Lagrangian multipliers for the  $NC$  equality constraints and  $\alpha^e$  and  $\beta^e$  are the  $NE$  Lagrangian multipliers for the  $NE$  lower and upper side constraints respectively. In (2.7) we have omitted the equilibrium equations as they do not have any influence on the updating scheme for the design variables. For the correct handling of equilibrium equations in the Lagrangian function, see chapter three. Here we will assume that they are fulfilled as the solutions of the finite element problem.

Stationarity of the Lagrangian function with respect to the design variables gives us the optimality criteria

$$\frac{\partial \mathcal{L}}{\partial x^e} = \frac{1}{p} \kappa^e \gamma^e (x^e)^{(1/p-1)} - \sum_{I=1}^{NC} \nu_I q_I^e - \alpha^e + \beta^e = 0 \quad , e = 1, \dots, NE \quad (2.8)$$

On the basis of (2.8), we can formulate an updating scheme for the design variable  $x^e$ . Assuming that the lower and upper side constraints are not active (i.e.  $\alpha^e = \beta^e = 0$ ), equation (2.8) can be written as

$$B_k^e(\nu) = \frac{\sum_{I=1}^{NC} \nu_I q_I^e}{\frac{1}{p} \kappa^e \gamma^e (x^e)^{(1/p-1)}} = 1 , e = 1, \dots, NE \quad (2.9)$$

Following Bendsøe, (1994), we can define the fixed point type updating scheme

$$x_{k+1}^e = x_k^e \left( B_k^e(\nu) \right)^\eta \quad (2.10)$$

where  $\eta$  is a damping factor and subscript  $k$  denotes the iteration number.

The updating scheme for the fixed point type algorithm is defined as

$$x_{k+1}^e = \begin{cases} \max \{(1-\varsigma) x_k^e, x_{min} \} & \text{if } x_k^e \left( B_k^e(\nu) \right)^\eta \leq \max \{(1-\varsigma) x_k^e, x_{min} \} \\ x_k^e \left( B_k^e(\nu) \right)^\eta & \text{if } \max \{(1-\varsigma) x_k^e, x_{min} \} \leq x_k^e \left( B_k^e(\nu) \right)^\eta \leq \min \{(1-\varsigma) x_k^e, x_{max} \} \\ \min \{(1 + \varsigma) x_k^e, x_{max} \} & \text{if } \min \{(1 + \varsigma) x_k^e, x_{max} \} \leq x_k^e \left( B_k^e(\nu) \right)^\eta \end{cases} \quad (2.11)$$

where  $\varsigma$  is a move limit.

Determination of the Lagrangian multipliers  $\nu_I$  has to be done iteratively in an inner loop. In order to get an implicit set of equations for the Lagrangian multipliers, we use that the equality constraints (2.3) should be satisfied for the new values of the design variables  $x_{k+1}^e$

$$E_I^* - \sum_{e=1}^{NE} q_I^e x_{k+1}^e = 0 , I = 1, \dots, NC \quad (2.12)$$

Substituting the updating formula (2.11) into the equality constraints (2.12), we get

$$\phi_I = E_I^* - \sum_{e \in R_{act}} q_I^e x_k^e \left( B_k^e(\nu) \right)^\eta - \sum_{e \in R_{pas}} q_I^e x_{k+1}^e = 0 , I = 1, \dots, NC \quad (2.13)$$

where  $\phi_I$  denotes the residual in obtaining the  $I$ 'th equality constraint,  $R_{act}$  denotes the group of elements governed by the center updating rule in (2.11) and  $R_{pas}$  denotes the group of elements

which are governed by the lower or upper side constraints  $x_{min}$  or  $x_{max}$ . To find the set of Lagrange multipliers that minimize the residuals  $\phi_I$ , we will use the standard Newton–Raphson iterative procedure. The recurrence formula is

$$\nu_{n+1} = \nu_n - (\nabla\phi)_n^{-1} \phi_n \quad (2.14)$$

where  $n$  is the iteration number of the Newton–Raphson algorithm and  $\nabla\phi$  is the  $NC \times NC$  Jacobian matrix. The individual elements of  $\nabla\phi$  are given by

$$\frac{\partial\phi_I}{\partial\nu_J} = - \sum_{e \in R_{act}} \eta q_I^e x_k^e \left( B_k^e(\nu_n) \right)^{(\eta-1)} \frac{\partial B_k^e(\nu)}{\partial\nu_J} \quad (2.15)$$

and

$$\frac{\partial B_k^e(\nu)}{\partial\nu_J} = \frac{q_J^e}{\frac{1}{p} \kappa^e \gamma^e (x^e)^{(1/p-1)}} \quad (2.16)$$

The Newton–Raphson procedure is iterated until satisfactorily accuracy in obtaining the equality constraints (2.12) is obtained, i.e., the inner loop is stopped when  $|\phi_I| < \delta$  for  $I=1, \dots, NC$ , where  $\delta$  is a small number.

The overall computational procedure is summarized in figure 2.3.

The above described computational procedure is also applicable to the design of materials with prescribed *thermoelastic* properties. The only change is, that the three extra equality constraints

$$\beta_{ij}^* - \sum_{e=1}^{NE} q_{ij}^e x^e = 0 \quad (2.17)$$

are added to the optimization problem (2.6). As the equality constraints (2.17) are in the same form as those for the elastic properties (2.1), the computational procedure is again given by figure 2.3, with the addition of three extra equality constraints such that  $NC=7$  in the two dimensional case.

Convergence of the optimization procedure is generally quite stable. For the two dimensional truss problems, 20–30 iterations are needed to converge (with six digits accuracy in the change in design variables). For the three dimensional truss and the frame–like microstructures, convergence is generally a little slower and for the continuum–like microstructures up to 100 iterations are needed. The actual convergence rate is dependent on the choice of move limit  $\varsigma$  and damping factor  $\eta$  in the updating scheme (2.11). For the truss and frame models, 0.02 and 0.8 respectively,

are good choices and for the continuum model 0.05 and 0.4 give stable convergence. Prescribing impossible elastic properties (e.g. elastic tensor non-positive definite) or prescribing elastic properties which are non-attainable by the chosen groundstructure, results in "jumping" of the design variables and lack of convergence, indicating that the operator should "relax" the prescribed elastic properties.

In the following sections, we will show how materials with a wide range of thermodynamically admissible properties can be designed by the proposed procedure. In the two dimensional examples we will assume plane stress state when we refer to the isotropic materials. In the figures, the elasticity tensor is written in a matrix form which is defined in appendix 2 together with definitions for different "families" of materials.

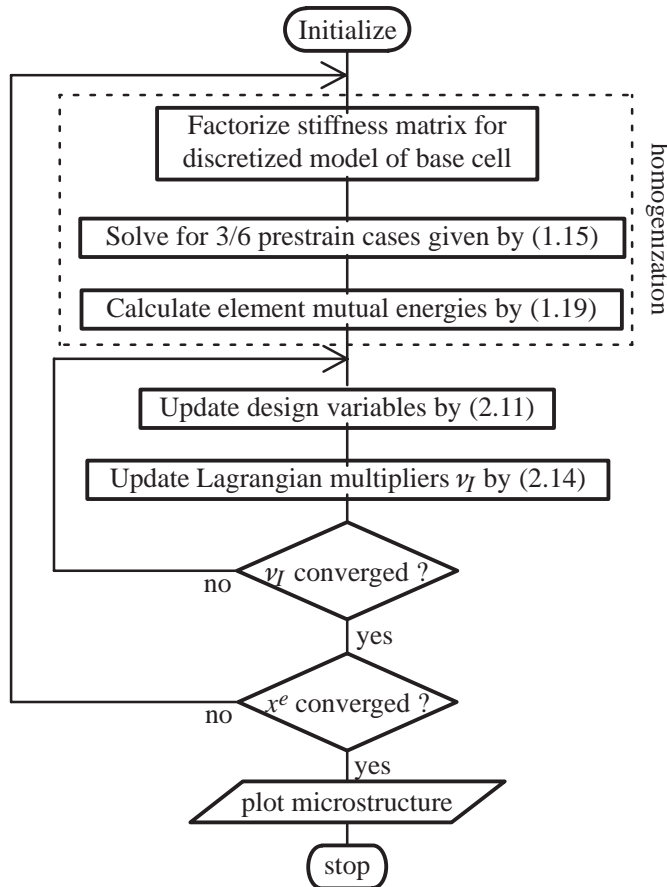


**Figure 2.3** Flowchart of the optimization algorithm

## 2.3 Truss–like materials

This section presents a number of examples obtained from groundstructures discretized by truss elements. It is shown that materials with a variety of properties, including materials with Poisson's ratios close to  $-1$  and  $0.5$  ( $-1$  and  $1$  in 2-d), can be constructed as truss modelled microstructures in two and three dimensions.

The presented results are limited to orthotropic materials with axis of symmetry coaligned with the coordinate system, although experiments show that all kinds of anisotropic and orthotropic materials with principal axes oriented in different directions can be constructed with the proposed algorithm.

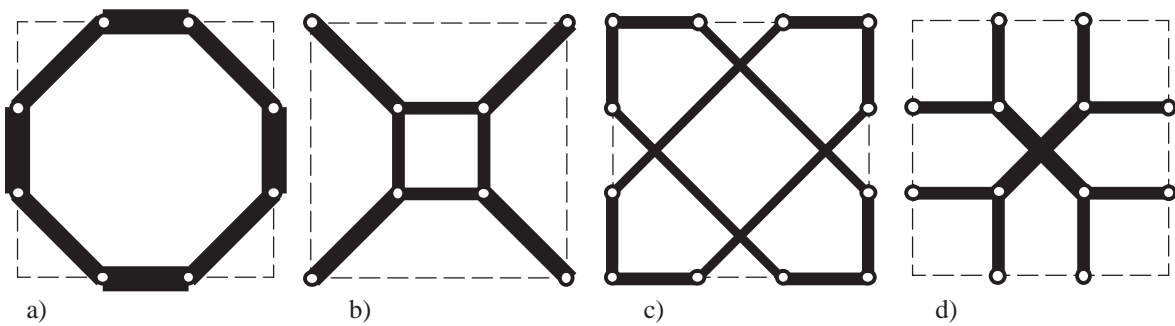
In the 2-d examples all microstructures are constructed from a 4 by 4 node full ground structure (known from topology optimization), with all nodes connected by bar elements, i.e. there are 120 potential bar members when overlapping is allowed (figure 2.2a). The groundstructure size of 4 by 4 nodes seems to be the ideal size of ground structure. Smaller ground structures do not have enough degrees of freedom to model complicated micro mechanical behaviour, and larger ground structures tend to result in more complicated topologies and are not so easily interpretable. In the 3-d examples a 4 by 4 by 4 ground structure (figure 2.2b) is chosen for the same reasons as in 2-d. Connecting all nodes by bars gives 2016 potential bar members.

The aim of the optimization procedure is to find out which of the potential members of the ground structure should vanish and to find the areas of the non-vanishing members which gives the desired elastic properties. As described in chapter one, vanishing members are not removed from the base cell but their areas are set to the minimum value  $x_{min}$ . By choosing  $x_{min}$  approximately  $10^7$  times smaller than the maximum member area, elements governed by the minimum constraint in (2.6) will have no structural significance, and they will not be shown in the examples in order to ensure simplicity of the graphics.

In all examples, Youngs modulus of the base material (the material the individual bars are made of) is normalized to unity. In order to ensure that the resulting truss–like microstructures are thin (have low density), the prescribed elastic properties  $E_{ijkl}^*$  are chosen so small that the resulting density is smaller than one. Using realistic elastic properties for the base material just requires linear scaling of the prescribed elastic properties due to the linearity of the design problem.

### Examples in two dimensions

In the first example we seek the material topology of a material with Poisson's ratio equal to 1. Optimizing a truss modelled base cell for the constitutive parameters obtained by inserting  $\nu=1$  in the elasticity tensor for an isotropic material in plane stress [see appendix 2, equation (A2.2)] and prescribing  $E_{1111}^*$  to be 0.05, results in several different solutions with the same overall density – four of them are shown in figure 2.4a–2.4d. The four different topologies are obtained by varying the penalty terms in (2.5)truss2d. For instance, 2.4a is obtained by penalizing long bars, and topology 2.4c by penalizing short bars. The two others were obtained by experimenting with different sizes of the move limits, but common to all results was a "switching" between the "basic" topologies such that move limits had to be made quite small to ensure final convergence. It is seen that the topologies are mechanisms as expected. In figure 2.5, periodic materials are constructed from the base cells in figure 2.4 and here it is easier to imagine the actual topologies of the materials.



$$(E^*) = 0.05 \begin{pmatrix} 1 & 1 & 0 \\ 1 & 1 & 0 \\ 0 & 0 & 0 \end{pmatrix}, \rho = 0.2$$

**Figure 2.4** Microstructures of materials with Poisson's ratio close to 1.0.

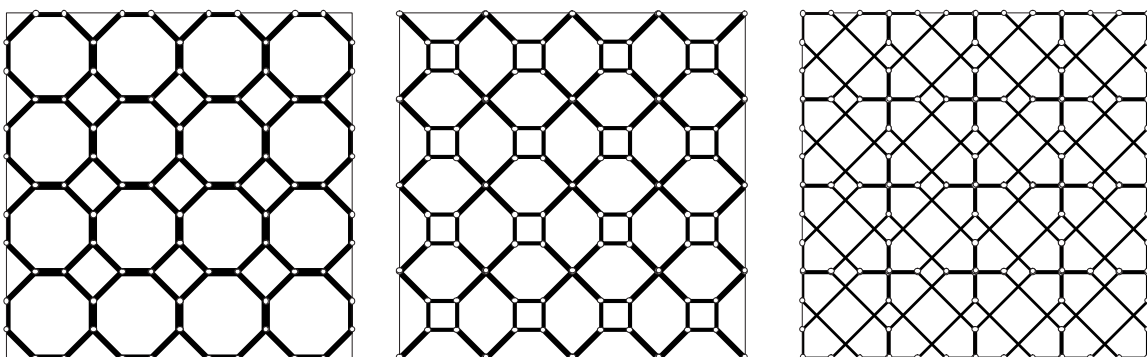


**Figure 2.5** Periodic materials with Poisson's ratio 1.0 constructed from the first three microstructures in figure 2.4.

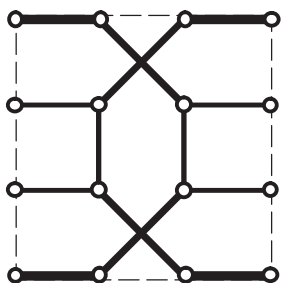
The microstructure in figure 2.4a can be interpreted as an octagonal honeycomb cell and can be compared with the original hexagonal honeycomb discussed in chapter one.

Figure 2.6 shows a honeycomb with less stiffness in the vertical direction and figure 2.7 shows a material where the only non-zero elastic parameter is  $E_{1111}^*$ . It is obvious, that the latter material only can take up loads in the horizontal direction and has zero shear stiffness.

Choosing an elastic tensor where  $E_{1122}^* < E_{1212}^*$ , the microstructures tend to be somewhat more complex than those previously shown. Figure 2.8 shows two topologies of truss-like anisotropic negative Poisson's ratio materials with  $E_{1111}^* = -E_{1122}^* = 0.05$  and  $E_{1212}^* = 0$ . The topologies have overlapping bars, so their shear displacement modes ( $\epsilon_{pq}^{*(12)}$  from equation (1.7)) are shown to illustrate the overlapping. The materials compress vertically subject to horizontal compression, but in shear, they will collapse in the mechanism-type motion shown in figure 2.8 (right).

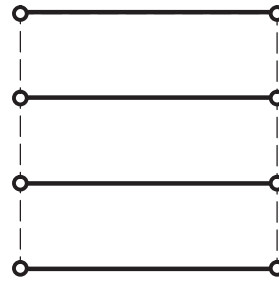
The previous example showed anisotropic materials with negative Poisson's ratio, where the shear stiffness  $E_{1212}^*$  was zero. The next examples will show "real" isotropic negative Poisson's ratio materials, i.e. negative Poisson's ratio materials with shear stiffness.

Requesting a material with Poisson's ratio close to  $-1$  the optimization algorithm returns only one simple solution (figure 2.9 left). As shown in the physical interpretation (figure 2.9 right) the base cell consists of two "stiff" quadratic frames (shown in black and grey) rotating about the center, such that expansion in one direction rotates the frames in opposite directions and thereby causes expansion perpendicular to the applied expansion. Subjected to shear, the frames will "lock" because of the periodicity conditions.



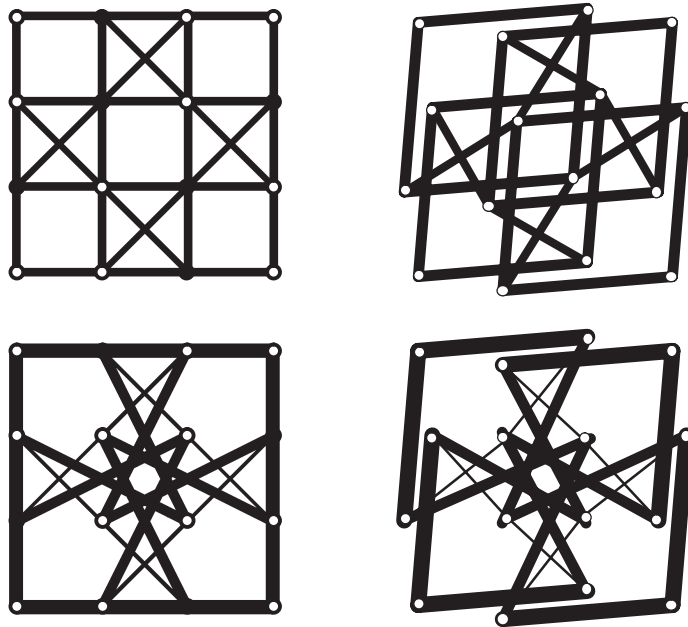
$$(E^*) = 0.05 \begin{pmatrix} 1 & 0.5 & 0 \\ 0.5 & 0.25 & 0 \\ 0 & 0 & 0 \end{pmatrix}, \rho = 0.113$$

**Figure 2.6** Honeycomb weakened in the vertical direction.



$$(E^*) = 0.05 \begin{pmatrix} 1 & 0 & 0 \\ 0 & 0 & 0 \\ 0 & 0 & 0 \end{pmatrix}, \rho = 0.05$$

**Figure 2.7** Rank 1 like material.



$$(E^*) = \begin{pmatrix} 1 & -1 & 0 \\ -1 & 1 & 0 \\ 0 & 0 & 0 \end{pmatrix}, \rho = 0.36 \text{ (top)} \text{ and } 0.45 \text{ (bottom)}$$

**Figure 2.8** Anisotropic negative Poisson's ratio materials.

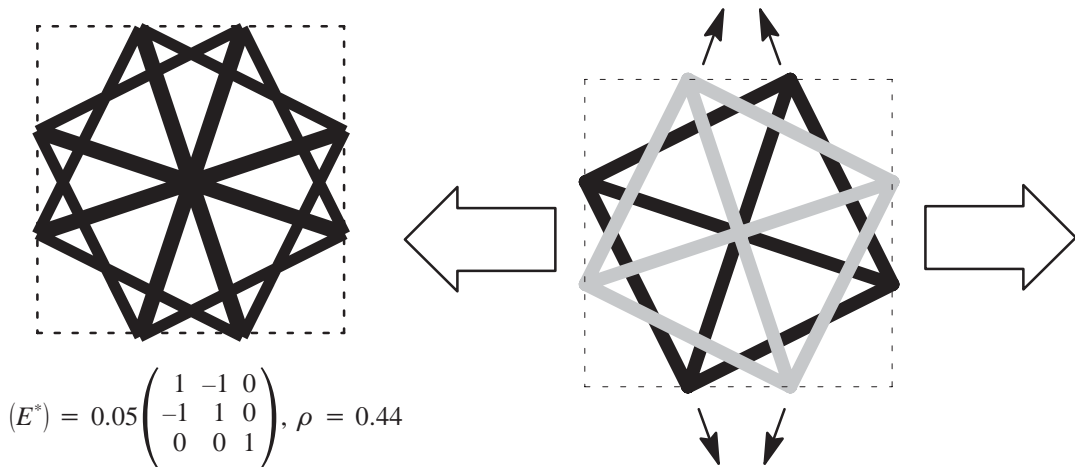


**Figure 2.9** 2-d base cell of an isotropic material with Poisson's ratio close to  $-1.0$  (left). The physical interpretation (right) shows that the material is composed of two stiff frames (shown in black and grey) free to rotate about their centers. When pulled horizontally (big arrows) the frames will rotate in the directions of the small arrows and thus expand vertically.

It was noted earlier, that a more complicated starting guess than the 4 by 4 node groundstructure does not give rise to simpler microstructures. Two examples of this are shown in figure 2.10, where the resulting microstructures for a Poisson's ratio 1 (figure 2.10 left) and  $-1$  (figure 2.10 right) material based on a 6 by 6 node groundstructure with 630 potential bar members are shown. The Poisson's ratio 1 microstructure (figure 2.10 left) can be compared with figure 2.4(c) – only differences are the coordinates of the nodal points. The Poisson's ratio  $-1$  microstructure

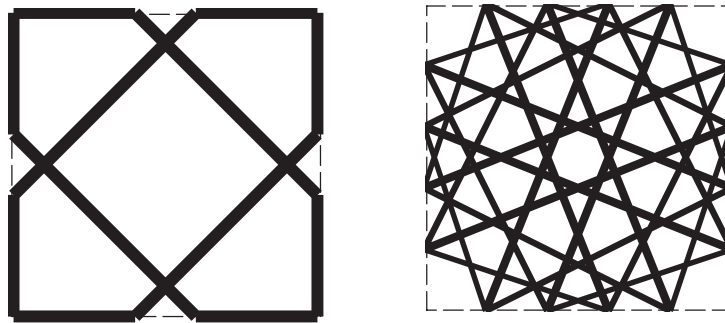


**Figure 2.10** Effect on choosing more complicated starting guesses. Poisson's ratio 1 (left) and -1 (right) microstructures are based on 6 by 6 node ground structures with 630 potential bar members.

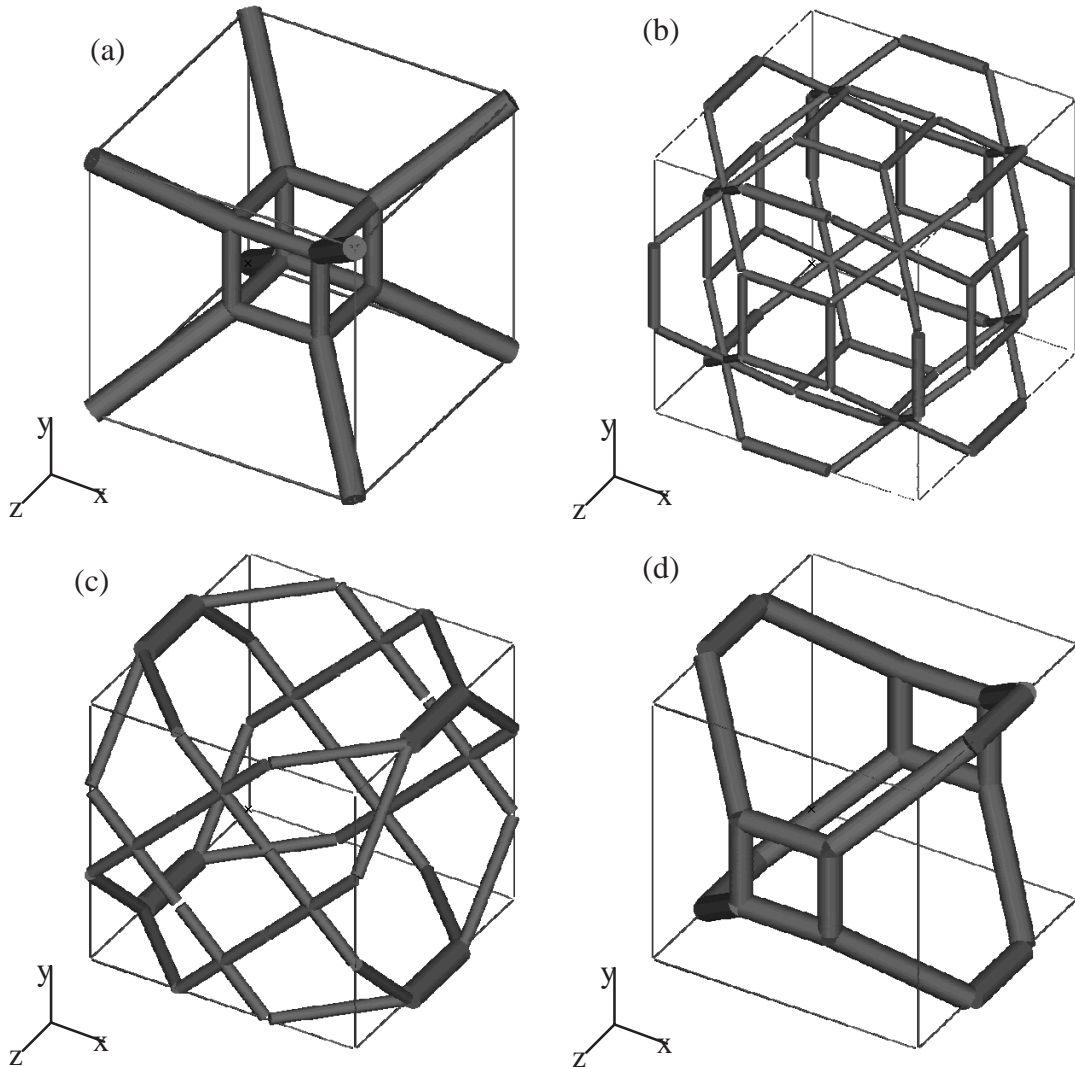
(figure 2.10 right) can be compared with figure 2.9, in this case we see, that starting with a more complicated groundstructure results in a more complicated though functionally similar solution.

### Examples in three dimensions

This section will show examples of 3-d microstructures with various material parameters, and their similarities with 2-d microstructures will be discussed.

Asking for a 3-d isotropic material with Poisson's ratio close to 0.5, the optimization algorithm returns several different topologies depending on choice of penalty factors, symmetry requirements and starting guesses. Four of the resulting microstructures which have equal structural weight are shown in figure 2.11a–d.

Figures 2.11a and 2.11b show Poisson's ratio 0.5 materials with full cubic symmetry. It is interesting to see that the microstructure in figure 2.11a corresponds to a 3-d version of the 2-d microstructure shown in figure 2.4b. Although figure 2.11b has an apparently more complicated microstructure this material too is composed of 2-d microstructures, namely a combination of those from figure 2.4a and b. Both figure 2.11a and b have bars in the interior of the base cells. It was tried to find a cubic symmetric Poisson's ratio 0.5 material with surface bars only by choosing the penalty factor  $\mu^e$  in (2.4) equal to 0.5, i.e. bars on the surfaces are made "cheaper" than interior bars. This approach does not result in any solution which was seen in lack of convergence of the optimization algorithm. In order to obtain a "surface" solution, requirements on symmetry are lessened, i.e. only symmetry about the three coordinate planes individually are required instead of the full cubic symmetry. This lessening of symmetry requirement results in the microstructure shown in figure 2.11c. This microstructure too is seen to be composed of 2-d microstructures, namely figure 2.4c in the xy-plane and figure 2.4a in the yz- and zx-planes. Lessening the symmetry requirements also results in another "interior" solution shown in figure 2.11d which actually is a simple version of figure 2.11b. We note that it is possible to construct isotropic materials which are not cubic symmetric in the microstructure.



$$(E^*) = .05 \begin{pmatrix} 1 & 1 & 1 & 0 & 0 & 0 \\ 1 & 1 & 1 & 0 & 0 & 0 \\ 1 & 1 & 1 & 0 & 0 & 0 \\ 0 & 0 & 0 & 0 & 0 & 0 \\ 0 & 0 & 0 & 0 & 0 & 0 \\ 0 & 0 & 0 & 0 & 0 & 0 \end{pmatrix}, \rho = 0.45$$

**Figure 2.11** 3-d base cells of isotropic materials with Poisson's ratio close to 0.5.

A base cell of a material with Poisson's ratio equal to zero is shown in figure 2.12. The solution is obtained by penalizing interior bars, thus the microstructure has only bars on the surface, but still it has a very complex microstructure.

Another interesting example in 3-d, is the tailoring of an isotropic Poisson's ratio -1.0 material. The first solution for this problem which is obtained without any penalty factors, results in a very complicated microstructure with a lot of crossing and overlying bars. The solution is structurally quite complicated and will not be shown here. Experiments with penalty factors ( $\mu^e = 0.5$ ,  $\xi = -1.0$  and  $l^{pref} = 0.5$ ) lead to a much nicer solution which is shown in figure 2.13. The microstruc-

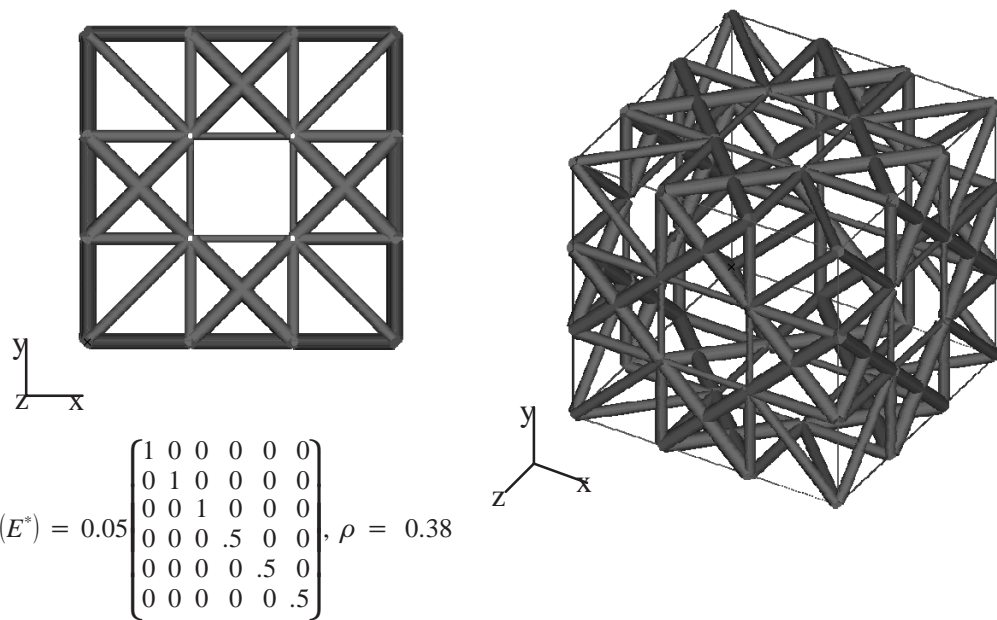


**Figure 2.12** 3-d base cell of an isotropic material with Poisson's ratio 0.

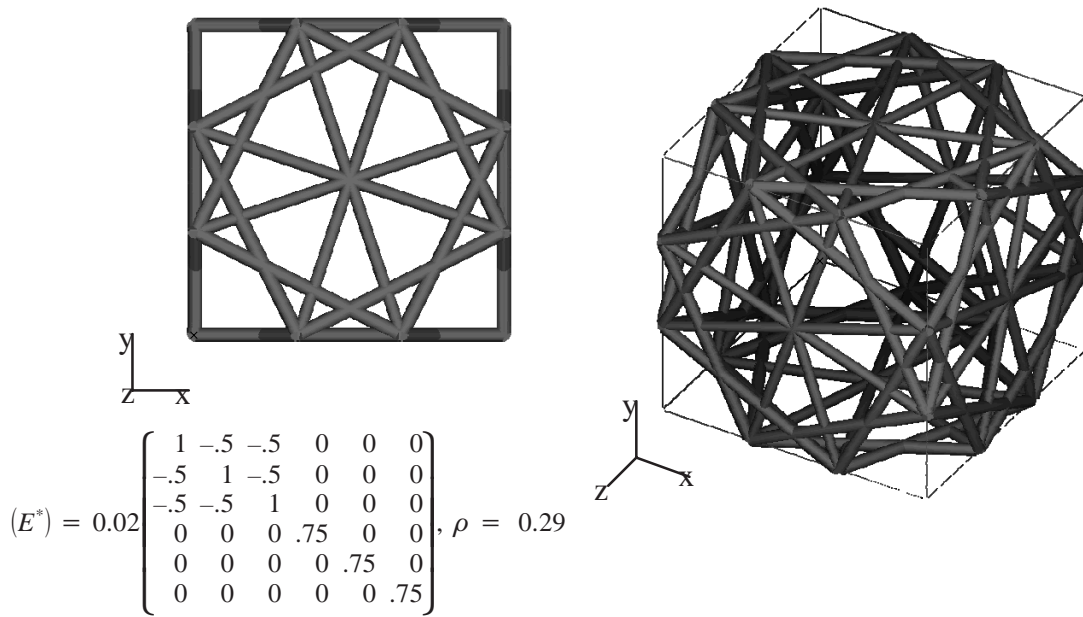


**Figure 2.13** 3-d base cell of an isotropic material with Poisson's ratio close to -1.0. The base cell is a cube where the six sides are built up by rotatable frames like in the two dimensional case (figure 2.9).

ture in figure 2.13 has only exterior bars, and is seen to be built up by rotatable frames like in the two dimensional case (figure 2.9).

The last example will show that it is also possible to tailor 3-d materials with different behaviour in different directions. Asking for Poisson's ratio -1.0 behaviour in the xy-plane and Poisson's ratio 0.5 behaviour in the yz- and zx-planes we get the 3-d microstructure shown in figure 2.14.

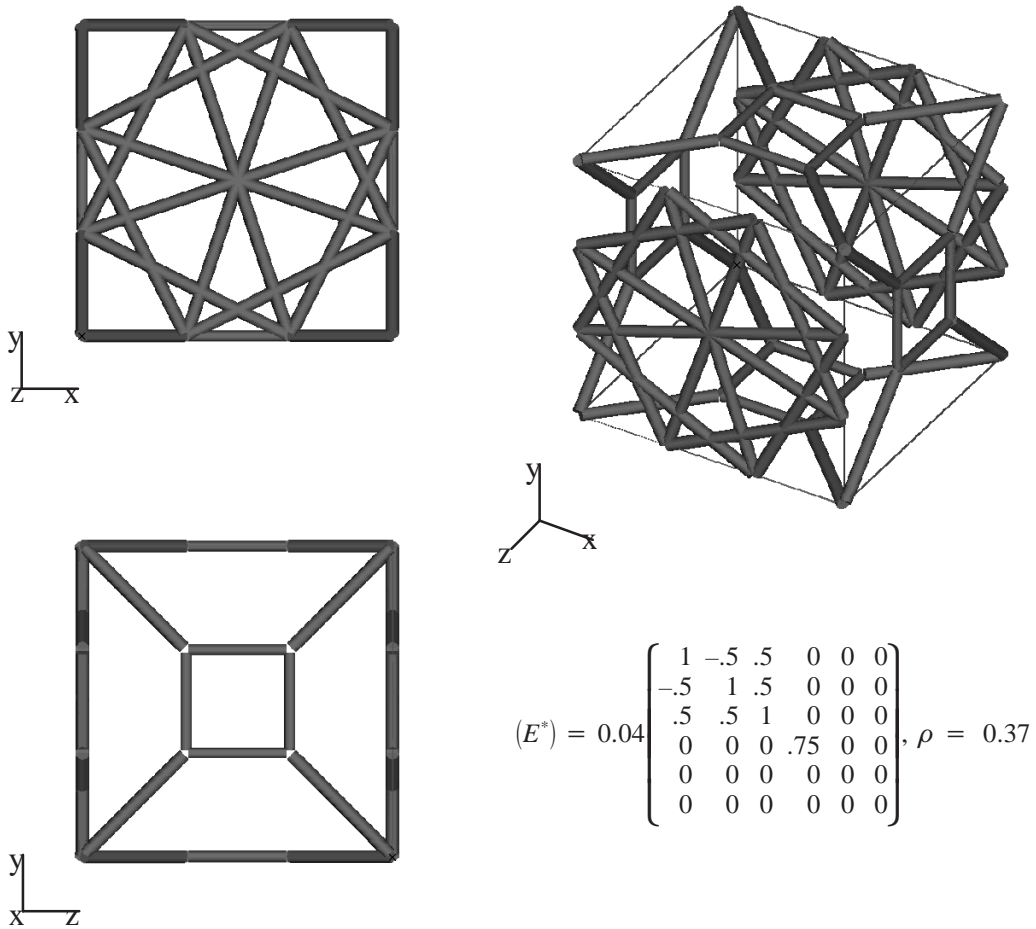


**Figure 2.14** 3-d base cell of an isotropic material with Poisson's ratio  $-1.0$  in the  $xy$ -plane and Poisson's ratio  $1.0$  behaviour in the  $yz$ - and  $zx$ -planes.

Examining figure 2.14, we notice that the microstructure is composed of the 2-d microstructures in figure 2.4(b) and figure 2.9. It can furthermore be seen, that the  $xy$ -plane with Poisson's ratio  $-1$  behaviour is not connected to the two other planes.

The 3-d microstructures in this section were obtained independently of the 2-d results and they all came from the 2016 bar ground structure (figure 2.2b). The results in this section can indicate that 3-d materials with arbitrary structural behaviour can be composed by "braiding" of 2-d microstructures into 3-d microstructures with small modifications. However, further investigation of this hypothesis is required.

## 2.4 Frame-like materials

This section shows that the topologies obtained by discretizing the groundstructure by frame elements resembles those obtained from the truss discretization, only difference is that the attainable elastic properties are "damped".

For the design of frame like materials, the design variables are given by the individual element widths and the height of each element is kept constant for all elements . The groundstructure with 120 possible beam elements, shown in figure 2.2c, is used as starting guess.

Design of the Poisson's ratio plus and minus 1 materials is used to illustrate the difference between discretizing the groundstructure by truss or frame elements. Table 2.1 shows attainable values of Poisson's ratios for varying beam thicknesses. The first row in the table shows the attainable Poisson's ratio for a truss modelled base cell. It is seen that the extreme values ( $\nu = 1$  and  $\nu = -1$ ) can not be obtained exactly, even for truss modelled materials. This lies in the fact that the elements governed by the minimum thickness constraint  $x_{min}$  prevent the base cell in becoming a true mechanism. The next rows in the table show the attainable values of Poisson's ratio for frame modelled microstructures of increasing thickness. It is seen that modelling the base cell from thick frame elements "damps" out extreme material behaviour as expected. Maximum beam thickness in the table is restricted to 20% of the base cell size. Allowing for thicker beams the microstructure should be thought of as a continuum with small holes.

Although not shown graphically, it should be noted that the material topologies for frame modelled base cells are apparently the same as for truss modelled base cells. This means that it is not so important to optimize the base cells using frame elements which, especially in 3-d, is a computationally more complicated task than the truss case (the number of degrees of freedom would be twice that of the truss case). Having optimized a truss modelled base cell, we will assume that the frame modelled microstructure can be constructed from the same topology, but it must be taken into account that the material parameters will be "damped" according to table 2.1.

Beam thickness in % of base cell dimension	$\nu = 1$ Attainable Poisson's ratio	$\nu = -1$ Attainable Poisson's ratio
0 (truss)	0.99996	-0.9998
1	0.9993	-0.997
2	0.997	-0.990
5	0.984	-0.94
10	0.94	-0.80
20	0.79	-0.63

**Table 2.1.** Attainable values of Poisson's ratio, from base cells modelled by frame elements with different thicknesses.

## 2.5 Continuum-like materials

This section demonstrates how a wide range of elastic properties can be obtained from ground-structures discretized by continuum type elements.

The microstructures shown in the following are all obtained from rectangular base cells discretized by four node bilinear elements. The design variables  $x^e$ , are the material densities in the individual elements with upper and lower bounds  $x_{max} = 1$  and  $x_{min} = 10^{-4}$ . The base material for all examples has Youngs modulus 0.91 and Poisson's ratio 0.3 such that a solid base cell will have  $E_{1111}=1.0$ . To obtain solid/void solutions, the penalty factor  $p$  in (2.5)*continuum* was varied between 2 and 5 depending on the problem. Very bad "checkerboard" patterns were seen in results from the preliminary tests of the algorithm. Consequently, early results published in Sigmund, (1994)<sup>1</sup>, only considered coarse design domains where the checkerboard problem was less prone to appear. In this chapter the checkerboard prevention scheme based on image processing techniques described in chapter 3 of this report, is used to obtain nice solutions for fine discretizations.

In usual topology optimization one takes a uniform distribution of material as a starting guess. This approach can not be taken here, because a uniform material distribution does not cause any microstructural variation and thus the overall strain fields  $\epsilon_{ij}$  are equal to the test strain fields  $\epsilon_{ij}^0$  in (1.5). Consequently, the values of the initial energies  $q_{ijkl}^e$  are constant. Therefore, we will use two different inhomogeneous starting guesses, for the first, the value of the design variable is proportional to its distance from the center of the base cell, and for the second, the values are chosen by a random process.

Generally many different solutions are found for the same prescribed elastic properties depending on the choice of starting guess, penalty factor and move limits. As for the truss- and frame-like discretizations many local minima exists, so the examples in this section are selected amongst many others mostly because they were the lightest found but also because they were the topologically simplest.

The EBE-PCG equation solver described in appendix 3 works very efficiently for the problems considered here. As an example, one FE-solution of a 60x60 element base cell might take one minute on an HP 735 workstation during the first design steps but later, during final convergence, the solution time is less than five seconds.

To test that the optimization algorithm gives reasonable results, we will try to "reinvent" the perfect honeycomb analyzed in chapter 1. Giving the design domain the same rectangular dimensions as specified in figure 1.7, and prescribing the elastic properties to the ones obtained from

---

the discretizations with 21x12 and 63x36 elements in table 1.1, we get the "optimal" microstructures shown in figure 2.15a and 2.15b. We see, that the optimized microstructures are very similar to the perfect honeycomb. Changing the design domain to a square cell discretized by 15x15 elements results in the topology shown in figure 2.15c. Now we get an "octagonal honeycomb" like the one obtained from the truss discretization in figure 2.4a. The density of the octagonal honeycomb is approximately the same as for the original honeycomb and therefore, manufacturability considerations must decide which of the topologies to choose.

Another testcase is the "reinvention" of the inverted honey comb from figure 1.9 and table 1.2. Using a 42x24 groundstructure as starting guess, the optimized topology is shown in figure 2.16. Again, the topology resembles the original in figure 1.9. Only difference is a "shifting" of the microstructure of half a period.

Changing the design domain to a square domain with 30x30 elements and imposing horizontal and vertical symmetry but prescribing the same elastic properties as in figure 2.16 resulted in the microstructure shown in figure 2.17a. The density of the quadratic groundstructure based material is 33% lower than the original inverted honeycomb but again, one might choose the

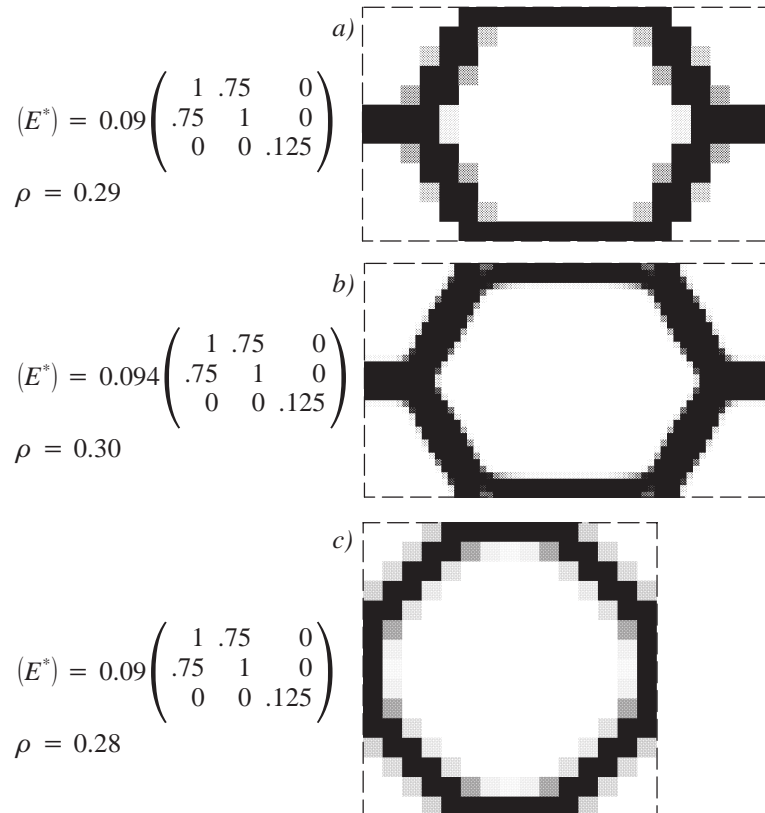


**Figure 2.15** "Reinvention" of the perfect honeycomb. Microstructures with Poisson's ratio equal to 0.75. Three different groundstructures: a) 21x12, b) 63x36 elements and c) 15x15 elements.

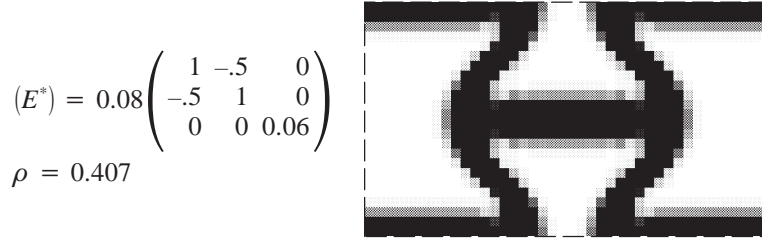


**Figure 2.16** "Reinvention" of the inverted honeycomb. Anisotropic microstructure obtained from groundstructures with 42x24 elements.

inverted honeycomb anyway for manufacturability reasons. The "optimal anisotropic negative Poisson's ratio material" in figure 2.17a can be extremized with Poisson's ratio equal to  $-0.7$  and  $-0.85$  as seen in figures 2.17b and c.

For frame like materials, the attainable properties were dependent on the density of material in the base cell; the same is the case for continuum like materials. The dependency is illustrated in figure 2.18. Prescribing  $E_{1111}^*$  to be 0.021, the highest attainable Poisson's ratio is 0.94, obtained with the microstructure shown in figure 2.18a. Again, we notice the similarity to the truss solution. Increasing the desired value of  $E_{1111}^*$  (figure 2.18b–2.18e) decreases the attainable Poisson's ratio until finally, we get to the solid base cell with  $E_{1111}^* = 1$  and  $\nu = 0.3$ . From this and other examples it appears that the attainable stiffness ratio between the effective properties and the properties of the base material defined as  $\max(E_{ijkl} / E)$  is low when we prescribe extreme elastics properties and we may conclude, that *we must accept low overall stiffness if we want materials with extreme values of Poisson's ratio*.

The anisotropic negative Poisson's ratio materials shown in figure 2.17 and the inverted honeycomb have very low shear stiffnesses. Almgren, (1985), suggests to modify the inverted honeycomb with struts and sliding hinges such that it gets a high shear stiffness. An interesting possibility to make a simple isotropic negative Poisson's ratio material by the present optimization algorithm, will therefore be to take the inverted honeycomb, say figure 1.9b as a starting guess, specify isotropic properties, and see if small structural modifications of the inverted honeycomb can lead to an isotropic solution. This showed out to be impossible; there was no convergence of the optimization algorithm.

Instead of starting out from the inverted honeycomb, it was tried to make an isotropic material with  $\nu = -0.7$  using a quadratic and fully symmetric 60x60 element groundstructure. The resulting topology is shown in figure 2.19 and looks very beautiful, but the micro-mechanical interpretation is difficult. The microstructure can be compared with the reentrant foams described in Lakes (1987). When stretched in one direction, the small bars and plates unfold and results in expansion in the opposite direction.

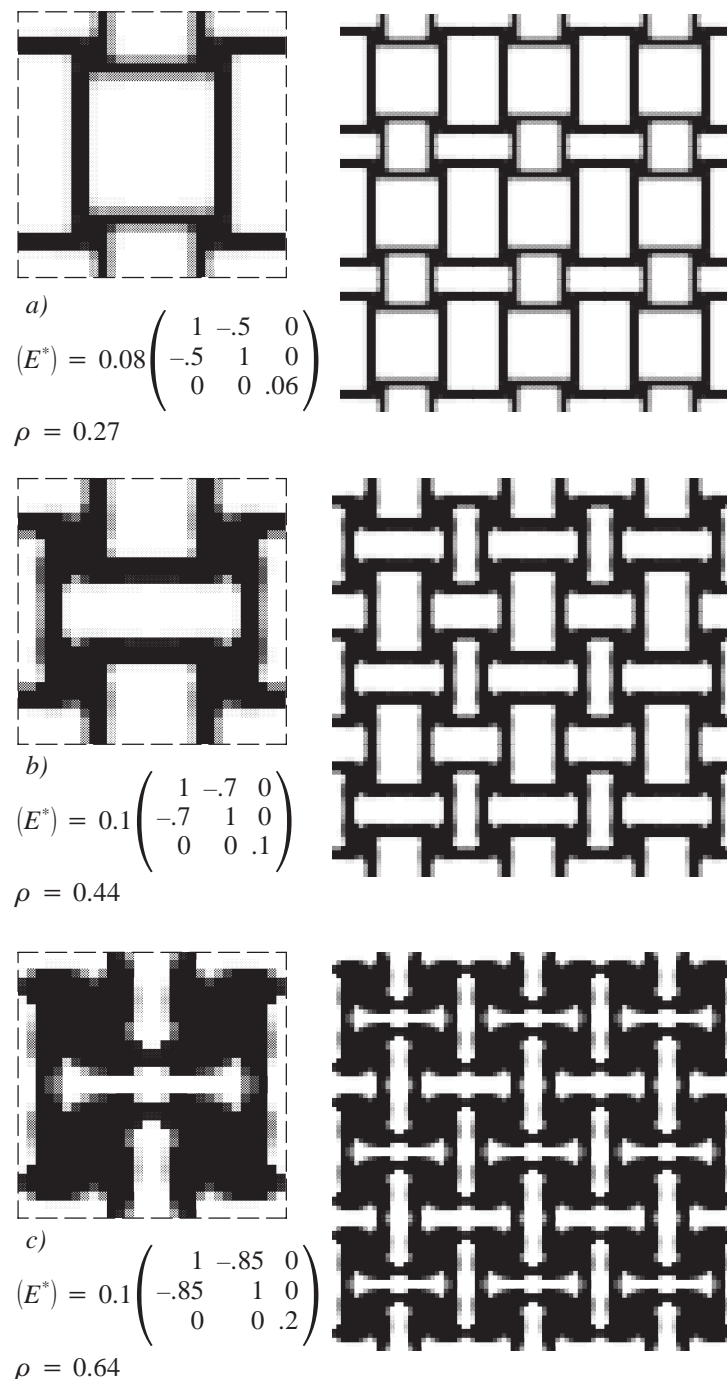


**Figure 2.17** Anisotropic "negative Poisson's ratio" material (low shear stiffness). Solutions obtained from groundstructures with 30x30 elements and horizontal and vertical symmetry enforcement.

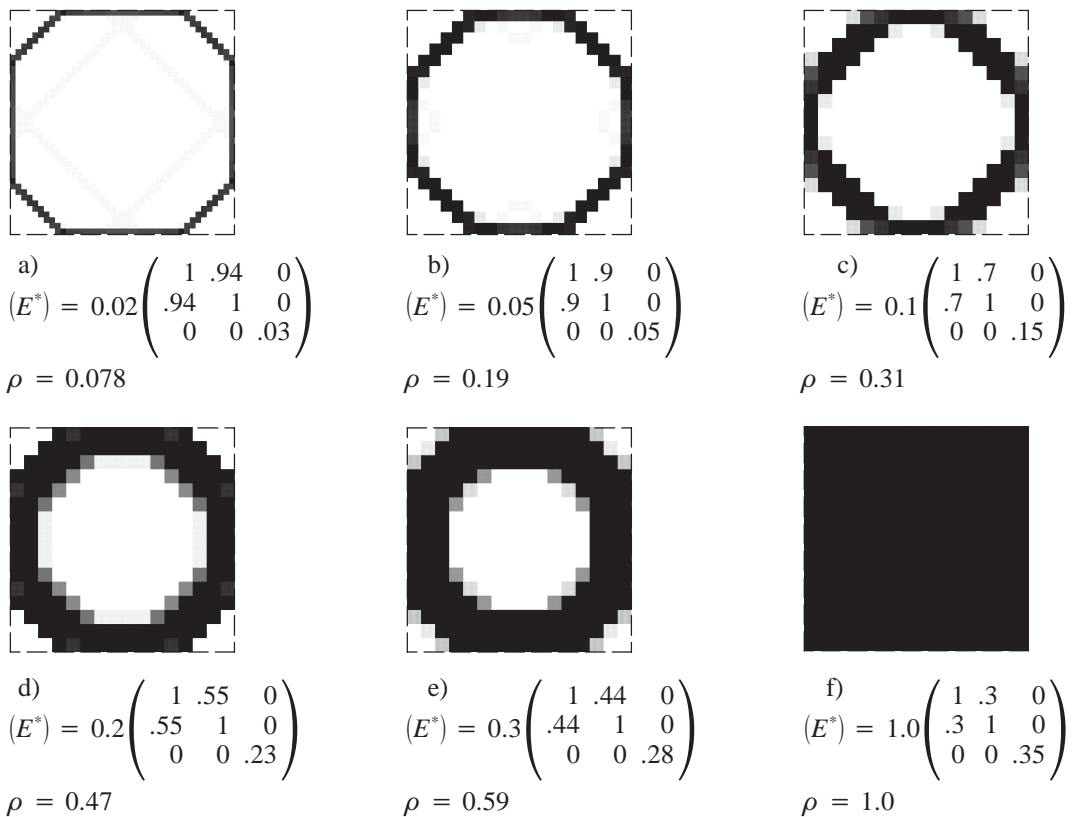


**Figure 2.18** Example of the dependence of the obtainable Poisson's ratio for various densities. Groundstructures are a) 40x40 elements, b) 20x20 elements and c) to f) 16x16 elements.

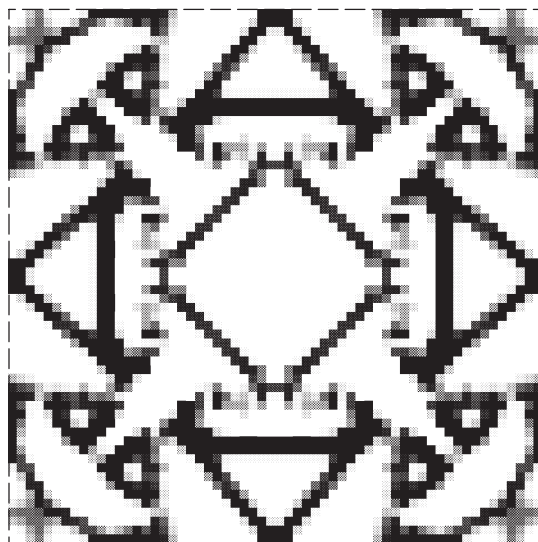


**Figure 2.19** Isotropic and symmetric microstructure with Poisson's ratio equal to  $-0.7$ . Groundstructure is 60x60 elements.

To get a simpler solution, the symmetry requirements were dropped and replaced by two extra equality constrains on the prescribed properties. Trying out different starting guesses and groundstructure sizes result in different more or less complicated solution. The simplest topology obtained is shown in figure 2.20a (left). By looking at the base cell alone it is difficult to see what is going on, therefore the base cell was repeated periodically in figure 2.20a (right). Now, the "mechanism" is seen clearly. Horizontal compression causes the triangles to "close" and thereby contract vertically.

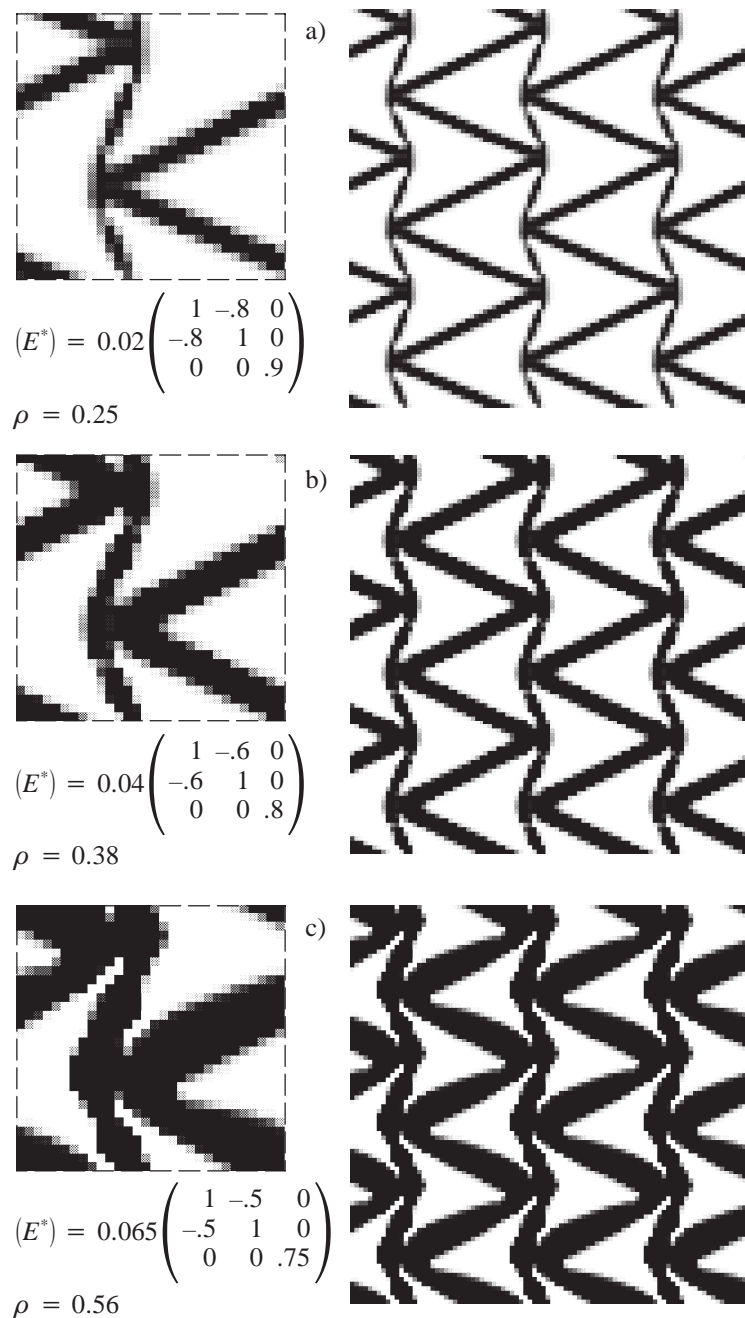


**Figure 2.20** Negative Poisson's ratio materials obtained from groundstructures with 30x30 elements and no symmetry enforcement.

The advantage of the continuum modelled negative Poisson's ratio material in figure 2.20 compared to the truss modelled "rotating frames" version in figure 2.9 is, that the continuum version has no sliding surfaces. The values of the stiffness and Poisson's ratio can be varied to a certain extent as seen in figure 2.20b–2.20c. It is interesting to note, that a microstructure neither has to be horizontally and vertically symmetric to be orthotropic, nor does it have to show 60 degrees symmetry to be isotropic.

The continuum modelled microstructure with Poisson's ratio  $-0.8$  in figure 2.20a can be interpreted as a rod and hinge model shown in figure 2.21 (left). The rod-and-hinge interpretation can be compared with the fish-bone like microstructures possessing Poisson's ratio  $-1$  proposed shown in figure 2.21 (right) by Milton, (1992). Milton assumed that his fish bone structure is built up from laminates of three different length scales and thereby proved mathematically that isotropic materials with negative Poisson's ratios exist within the framework of continuum elasticity. The fish bone structure of Milton belongs to the so-called ranked materials, which usually are considered as mathematical tools rather than being practical composites because of their widely differing length scales. The example in figure 2.20a and its possible interpretation in figure 2.21 indicates that the "mechanisms" of the extreme ranked material is reproduced in the one length scale microstructure proposed here.

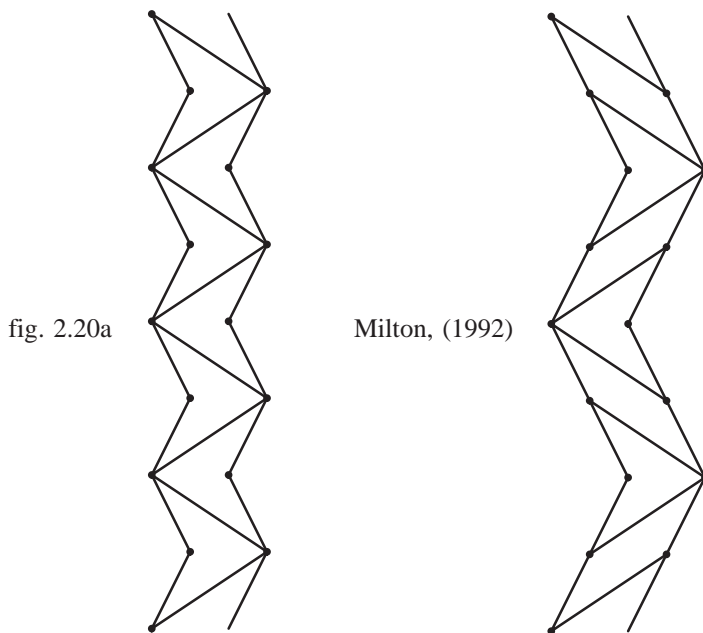


**Figure 2.21** Rod-and-hinge interpretation (left) of negative Poisson's ratio material from figure 2.20a compared with Rod-and-hinge interpretation of Milton's fish bone microstructure (right) with Poisson's ratio  $-1$  [Milton, (1992)].

For practical reasons, we might be interested in designing solid instead of porous microstructures. As an example, this could be done by embedding the considered microstructure in a soft matrix material. The matrix material has to be very soft compared with the base material in order not to damp out attainable properties too much. In fact, Cherkaev and Gibiansky, (1991), provide lower and upper bounds for the attainable values of Poisson's ratio for mixtures of two well ordered materials. They conclude that a stiffness ratio between the strong and the soft phase of more than 25 is necessary to achieve negative Poisson's ratio at all.

To study the influence on embedding one of the numerically developed microstructures in a soft matrix material, we will consider the Poisson's ratio  $-0.8$  microstructure in figure 2.20a. Simply embedding the microstructure in a matrix material with  $E_{1111}^M = x_m$  and Poisson's ratio  $0.3$ , can be done by specifying the lower bound on the design variables to be  $x_m$ . By numerical experiments, we found that the highest value of  $x_m$  which still gives a material with negative Poisson's ratio is  $0.014$  which means that the ratio between the strong and the soft phase should be more than  $71$  to get a negative Poisson's ratio for this particular numerical example. Examples of material combinations with high ratios could be steel/polystyrene ( $70$ ).

## 2.6 Continuum-like materials with prescribed thermoelastic properties

In this section, a simple example demonstrating the design of a material with prescribed thermoelastic properties is given.

The design of materials with prescribed thermal coefficients has large potentials in many engineering applications where temperature changes are large. Two well known examples are civil structures where temperature changes between summer and winter cause large structural expansion and space structures, where the temperature difference between the "sunny" and the "shady" side can be large and cause big structural distortions.

The design of a material with a prescribed thermal expansion tensor  $\alpha_{ij}^*$  can not be done alone by designing the microstructure based on one material – we have to consider a mixture of at least two materials with different thermal expansion coefficients  $\alpha_{ij}^1$  and  $\alpha_{ij}^2$ . The explanation of this comes from studying equation (1.12). We note that if we only have one material (or one material and void or one material with cracks),  $\alpha_{kl}$  is constant throughout the microstructure such that  $\alpha_{kl}$  can be put outside the integral in (1.12) and we get that  $\beta_{ij}^H = E_{ijkl}^H \alpha_{kl}$ .

To make a well posed example for design of materials with prescribed thermoelastic properties, we will consider the design problem sketched in figure 2.22. We are considering a mixture of two materials with different thermal expansion coefficients. The matrix phase has low thermal expansion coefficient  $\alpha_{11}^1 = \alpha_{22}^1 = 1$  and the square inclusion phase has high expansion coeffi-

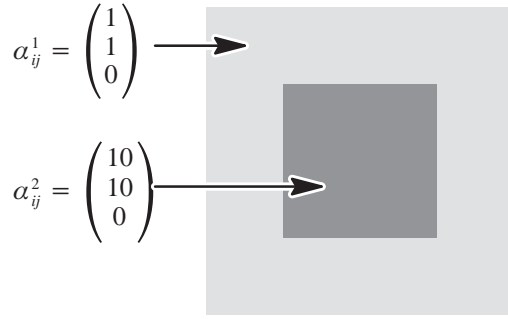


**Figure 2.22.** Initial base cell.

cient  $\alpha_{11}^2 = \alpha_{22}^2 = 10$ . The goal is to design elastically isotropic materials with Poisson's ratio 0.5 and various prescribed thermal expansion coefficients  $\alpha_{ij}^*$ . Having specified  $\alpha_{ij}^*$ , the prescribed thermal coefficient tensor  $\beta_{ij}^*$  used as constraint in the optimization problem is calculated as  $\beta_{ij}^* = E_{ijkl}^* \alpha_{kl}^*$ .

Prescribing a low overall thermal expansion coefficient  $\alpha_{11}^* = \alpha_{22}^* = 1.33$  we get the solution shown in figure 2.23a. It is seen that the solution resembles the octagonal honeycomb and that most of the material concentrates in the outer matrix phase with low expansion coefficient. Specifying a higher overall expansion coefficient results in material forming in the inclusion phase as seen in figure 2.23b and finally specifying a high overall expansion coefficient  $\alpha_{11}^* = \alpha_{22}^* = 3.66$  results in a "shifted" version of figure 2.23a as seen in figure 2.23c. We see that the microstructure tries to utilize the high expansion material in the square inclusion phase to make a high overall expansion coefficient. Finally, we will show that an elastically isotropic material can be designed with different thermal expansion coefficient in the horizontal and the vertical direction. Figure 2.23d shows a microstructure where  $\alpha_{11}^*$  and  $\alpha_{22}^*$  were prescribed to 5.33 and -0.66 respectively. It is seen, that the two horizontal bars in the high expansion inclusion phase will cause the material to expand heavily in the horizontal direction when heated, whereas only low expansion phase matrix material contributes to the vertical expansion.

The above example was quite basic and shall just be seen as a demonstration of which material properties it is possible to control. The high expansion inclusion phase can also be seen as a build-in actuator which could be controlled by an electric field (piezo electric actuator) instead of by temperature change, and the design goal could, for example, be to make a material with the largest possible expansion in a specified direction due to an electric input signal. Consequently, the author expects the method to be applicable (with minor modifications) to the design of smart or intelligent materials which can change their properties actively as a response to external stimuli.

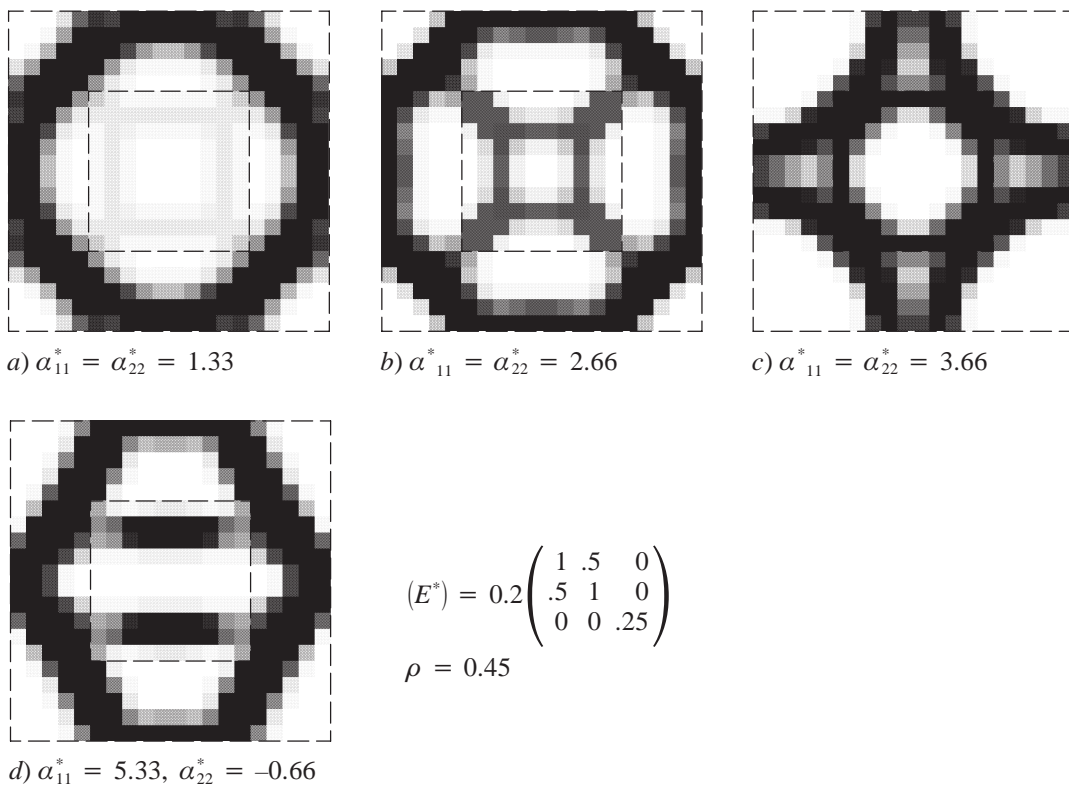


**Figure 2.23** Design of materials with prescribed thermoelastic properties. Groundstructure has 30x30 elements.

## 2.7 Practical considerations

In this section, we will discuss simple working models which were made to test that the numerically obtained results are practically realizable.

To test the function of the truss modelled two dimensional Poisson's ratio –1 material from figure 2.9, a lab model of the material consisting of an array of 4 by 4 connected base cells was constructed (figure 2.24). The model consists of two thin layers of celluloid, put on top of each other, and placed between two stiff transparent plates. Figure 2.25 shows the mechanical behaviour of the working model. Comparing the picture of the unstressed material (figure 2.25 left) with the stressed version (figure 2.25 right) the deformation mechanism is clearly seen.

The three dimensional truss modelled Poisson's ratio –1 material from figure 2.13 was also tested by a working model. A 15 by 15 by 15 cm. model of this microstructure was built in the lab, consisting of 72 plastic tubes connected by bent pieces of thin wire (figure 2.26). The test cube works nicely, which means that if compressed vertically, it will also compress in the two other directions. The negative Poisson's ratio behaviour of the base cell is, of course, limited to the point where the rotating square frames become parallel.

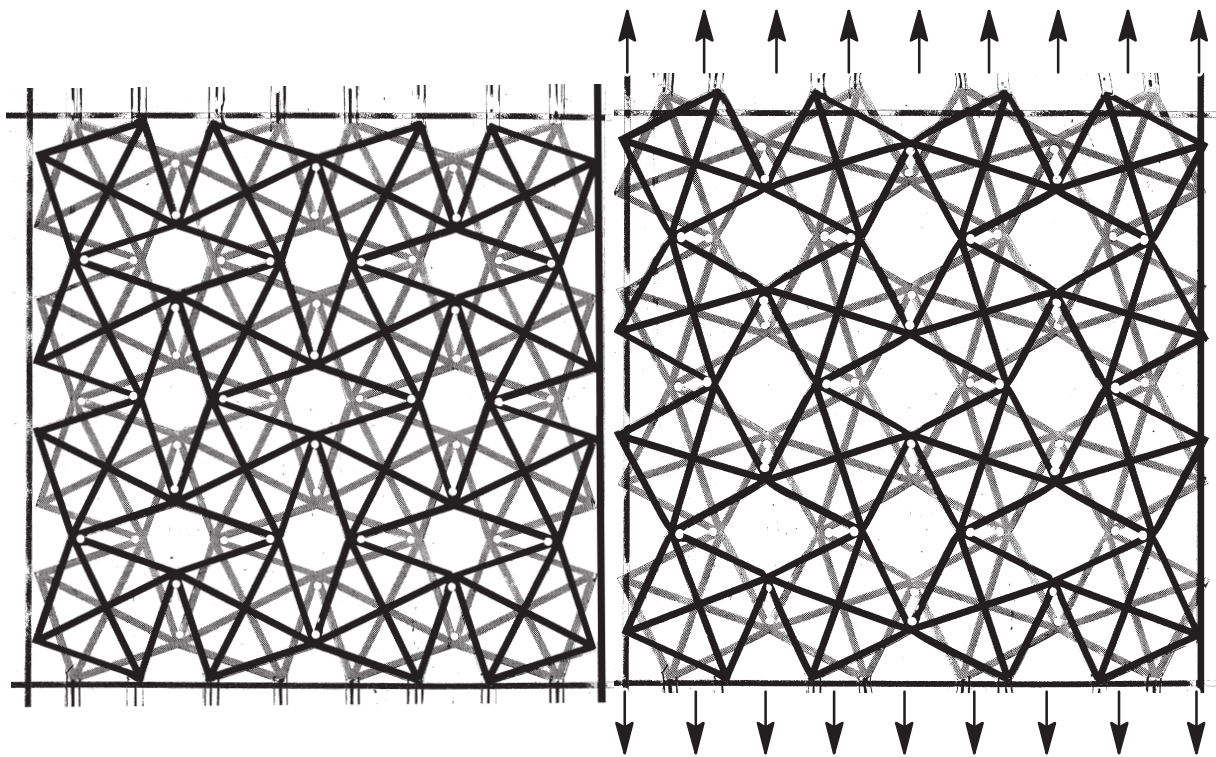


**Figure 2.25** Working model of the proposed negative Poisson's ratio material from figure 2.9. The undeformed material consisting of an array of 4 by 4 base cells is shown left. Expanded vertically we get the deformation pattern shown right.

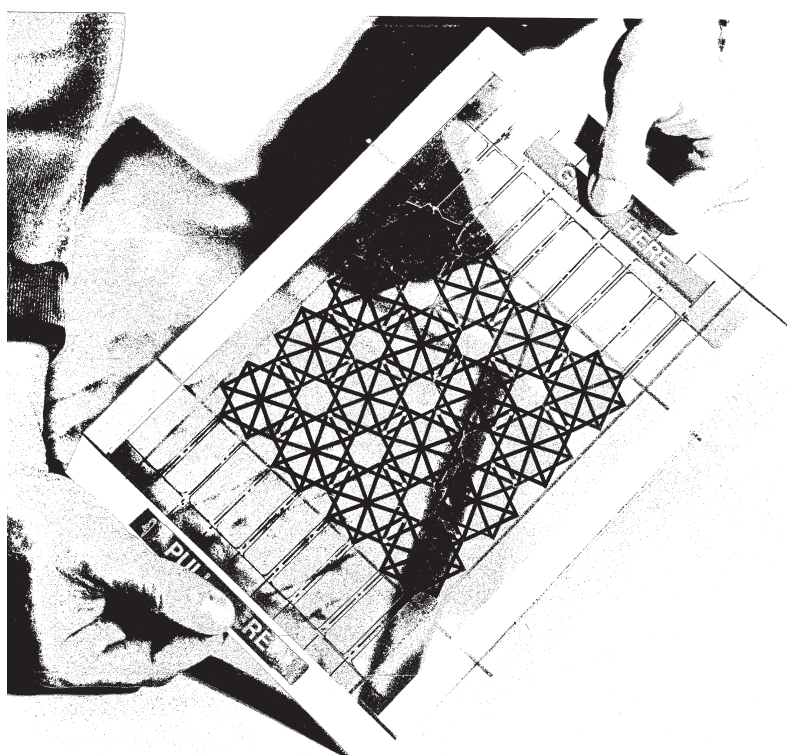


**Figure 2.24** Working model consisting of an array of 4 by 4 base cells of the proposed negative Poisson's ratio material from figure 2.9.

---

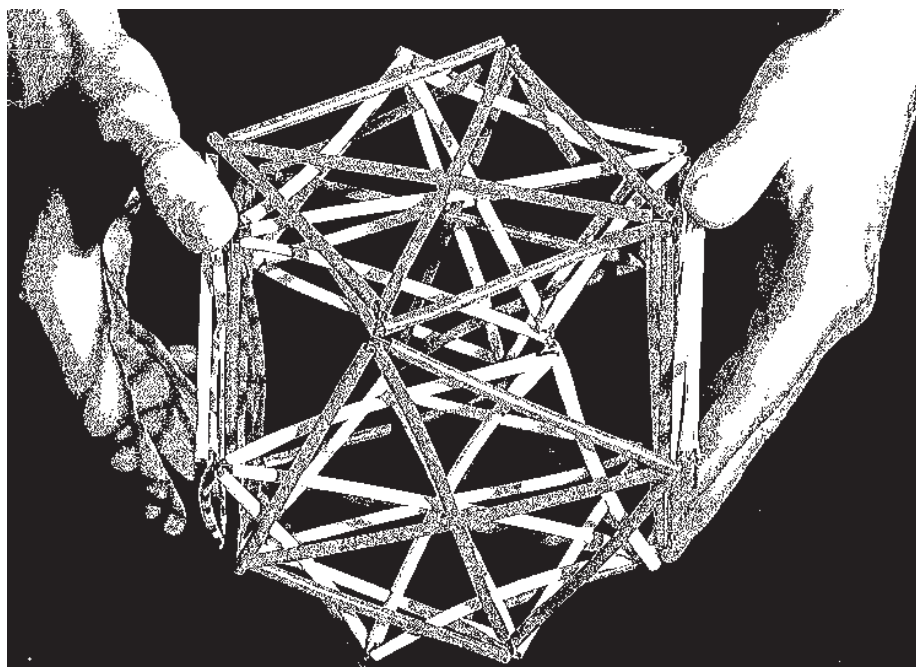


**Figure 2.26** Working model of the Poisson's ratio  $-1$  material from figure 2.13.

One might ask whether having two layers rotating on top of each other is essential for obtaining the isotropic negative Poisson's ratio material shown in figure 2.9 and ask if the much simpler one layer version in figure 2.27 could do the job. Comparing the modified microstructure in figure 2.27 with the continuum modelled microstructure from figure 2.17c, we get the answer. The two microstructures essentially have the same topology and because the continuum version (figure 2.17c) was computed to have low shear stiffness, we will expect the truss version to be anisotropic as well. We can therefore conclude that the two interconnected sliding layers in the original microstructure in figure 2.9 are essential for the isotropy of the truss like material.

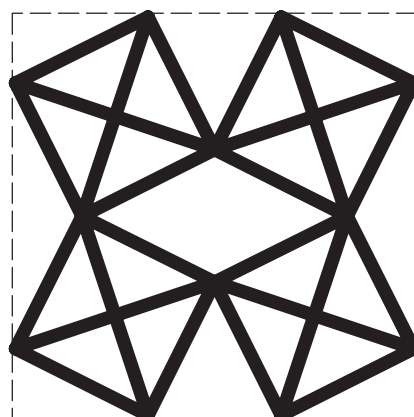


**Figure 2.27** One layer version of the Poisson's ratio  $-1$  microstructure from figure 2.9.

This conclusion is a serious drawback for the practical application of the truss modelled Poisson's ratio  $-1$  material. The sliding surfaces and the linking of the frames will be difficult to manufacture and may cause large microstructural stress concentrations.

The continuum modelled microstructures do not have the disadvantages of sliding surfaces and microscale links. Taking the Poisson's ratio  $-0.6$  material from figure 2.20b and post-processing it by taking the contour-line of density 0.5 as the border between solid and void, we get the microstructure seen in figure 2.28. Although it still has jagged edges due to the coarse discretization, we can clearly interpret the microstructure as a micro-frame like material with no sliding surfaces or micro-scale links. To remove the jagged edges, either more elements could be used in the groundstructure or, the microstructure could be taken into a shape optimization software to smooth boundaries and minimize stress concentrations.

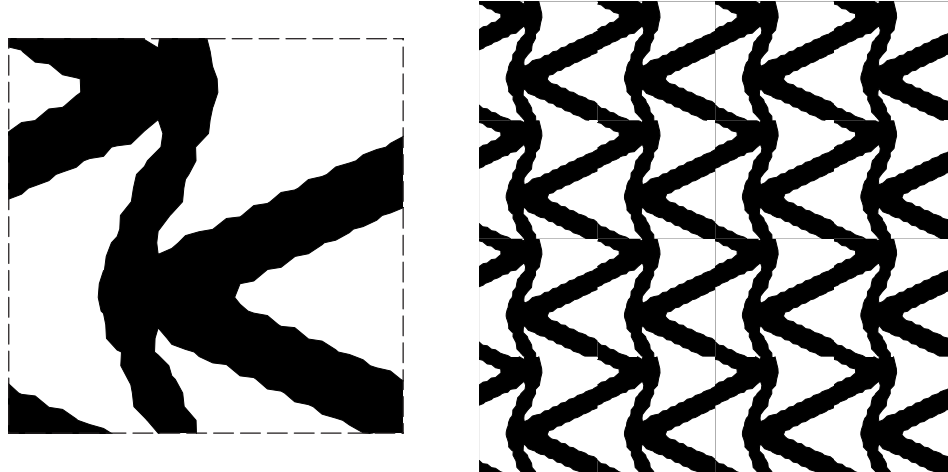


**Figure 2.28** Post-processed picture of microstructure with Poisson's ratio  $-0.6$  from figure 2.20b.

## 2.8 Summary and discussion

In this chapter we have proposed a numerical approach to the design of materials with prescribed thermoelastic properties. The method is based on algorithms and discretizations used in topology optimization of general structures. The material design problem is formulated as an optimization problem of minimizing weight of a base cell subject to equality constraints on the prescribed thermoelastic properties. The design domain is the topology of the representative base cell which has been discretized by truss, frame and continuum type finite elements to account for different material types. The groundstructure approach is used as a starting guess to the optimization procedure, which means that the best microstructure is sought within a fixed but very detailed discretization.

As demonstrated by many examples, the proposed numerically based design procedure can be used to tailor materials with a wide range of thermoelastic properties.

Using truss-like discretizations in two and three dimensions makes it possible to design materials with properties very close to the theoretical bounds (positive semi-definiteness of the elastic tensor) whereas using more practical frame elements damps out attainable properties. For the solutions in both the truss and the frame formulation, bars and beams are allowed to cross without (theoretical) interaction. This means that in practical realization of the microstructures, there will be parts sliding on top of each other which can cause difficulties in manufacturing or cause large stress concentrations. Both these problems are difficult to prevent in the truss and frame formulations.

More realistic microstructures are obtained by the continuum formulation because the discretization only has one layer and consequently does not allow sliding surfaces. Examples show that extreme elastic parameters can be obtained by the continuum formulation as well, however, experiments show that only low overall stiffness can be obtained if extreme elastic properties are prescribed. Further manufacturability constraints on the continuum like microstructures such as minimum size of holes or structural members can be imposed by using the mesh independency procedure developed in chapter 3 however, it must be taken into account that any topological constraint put on the microstructural geometry damps out the attainable elastic properties. As demonstrated in an example, the attainable properties are also damped when a porous microstructure is imbedded in a matrix material.

The possibility of designing materials with prescribed thermoelastic properties was demonstrated by a simple example using the continuum formulation. The obtained microstructure topologies showed "actuator" like elements which suggests that the present approach to material design can be used for design problems like optimal placement of actuators or sensors in design of smart materials or structures.

---

To test if the numerically obtained microstructures really work the predicted way, two very coarse models were built and both showed the expected (negative Poisson's ratio) behaviour. However, due to coarseness of the models, none of them allowed actual measurements of their elastic properties. Therefore, it would be interesting to make more realistic prototypes consisting of several base cells that could be tested by standard material testing methods. This is outside the scope of this thesis but in continuation of the work, prototypes of the proposed microstructures can be produced by the rapid prototyping or stereolithography technique. Briefly described, the method can produce prototypes of complicated three dimensional structures by layerwise hardening of liquid polymers or other base materials [e.g. overview in Ashley, (1994)<sup>2</sup>]. Commercially available rapid prototyping machinery can produce parts with resolutions down to a tenth of a millimeter but methods are developed which can produce geometries with resolution of a few micrometers [e.g. Ikuta *et al.* (1994)].

The microstructures obtained by the numerical method developed in this thesis shall not be seen as readily manufacturable solutions but rather as sources of inspiration to people involved in practical synthesis of novel microstructures.

### 3. The checkerboard and mesh-dependency problems in layout optimization

This chapter will present a method to prevent the formation of checkerboard patterns occurring in layout optimization of linear elastic structures and at the same time eliminate the mesh-dependency problem of optimal layouts.

In section 3.1, the layout problem expressed as a compliance minimization problem will be described, and the occurrence of checkerboard patterns for certain discretizations will be demonstrated. A checkerboard prevention scheme is proposed based on ideas borrowed from image processing techniques and therefore a brief introduction to image processing is given in section 3.2 and the application to structural layout problems is treated in section 3.3. Applying the proposed checkerboard prevention scheme to typical design examples a well known problem turns up, which is that optimal layouts are dependent on the finite element discretization. The checkerboard prevention scheme is therefore modified to obtain an algorithm that, although based on heuristics, produces efficient mesh-independent designs that satisfy manufacturability constraints such as exclusion of geometry change below a prescribed scale (section 3.4).

The general layout optimization problem is sketched in figure 3.1 and can be defined as follows. Find the distribution of material for a structure supported on its boundaries and subjected to a given loading condition, such that an objective function is optimized. The amount of material is constrained and the spatial distribution of material is limited to the design domain  $\Omega$ . The design domain can have holes (void regions) and regions with fixed solid material. As discussed in the introduction a structure can be discretized in a number of different ways and it can be modelled by full three dimensional analysis, plates with inplane or out of plane forces etc. In this chapter we will consider the layout optimization of continuous linear thin elastic plates (membranes) subject to inplane forces (plane stress) and discretized by four node quadrilateral finite elements.

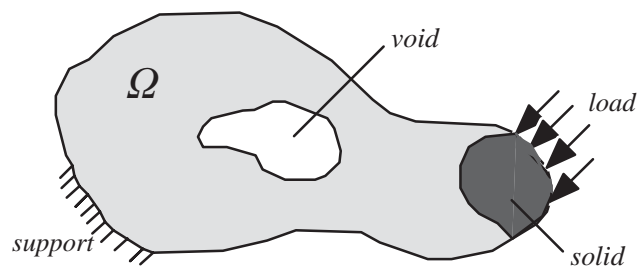


**Figure 3.1** The generalized layout optimization problem.

Practical layout optimization of continuum modelled plates can basically be divided into two different approaches. The first is the "Homogenization approach to topology optimization" introduced by Bendsøe and Kikuchi, (1988) and the second is the "Solid Isotropic Microstructures with Penalty" (SIMP) approach proposed in Bendsøe, (1989) and used in [Rozvany et al., \(1992\)](#). The penalization approach is also extensively used in biomechanics [see Huiskes and Hollister, (1993) and references herein]. Here we shall use a "mixture" of the two methods but the proposed prevention algorithm should be readily applicable to other formulations.

### 3.1 Design of structures by compliance optimization

Consider a linear elastic structure bounded on the domain  $\Omega$ , subject to surface tractions  $\{R\}$  and proper supports. Using standard finite element notation from Cook, Malkus and Plesha, (1988) the structure is discretized by  $NE$  finite elements. The compliance of the structure can be written as

$$W = \{D\}^T [S] \{D\} = \sum_{e=1}^{NE} \{d^e\}^T [s^e] \{d^e\} \quad (3.1)$$

where the global displacement vector  $\{D\}$  is the solution to the equilibrium problem

$$[S] \{D\} = \{R\} \quad (3.2)$$

and  $[S]$  is the global stiffness matrix of the discretized design domain  $\Omega$ . The global stiffness matrix is assembled from the local element stiffness matrices  $[s^e]$ , defined as  $[s^e] = \int_{V^e} [B^e]^T [E^e](\rho^e) [B^e] dv^e$  where  $[B^e]$  is the strain-displacement matrix,  $[E^e](\rho^e)$  is the constitutive matrix as a function of the density  $\rho^e$  and  $V^e$  is the volume of element  $e$ . Similarly the local displacement vectors  $\{d^e\}$  are the elements of the global displacement vector associated with element  $e$ .

The optimization problem is to minimize the compliance for a fixed amount of available material in the design domain. Assuming that the density of material in element  $e$  is  $\rho^e$ , the total volume of the structure can be written as

$$V = \sum_{e=1}^{NE} \rho^e V^e \quad (3.1)$$

In order to get a well posed problem, we will assume that the density in an element is bounded by  $0 < \rho_{min} \leq \rho^e \leq 1$ , where  $\rho_{min} \ll 1$  such that low-density regions have little influence on the overall structural behaviour.

---

We can now define the compliance optimization problem as

$$\begin{aligned}
 \text{minimize : } W &= \{D\}^T [S] \{D\} = \sum_{e=1}^{NE} \{d^e\}^T [s^e] \{d^e\} \\
 \text{subject to : } &\sum_{e=1}^{NE} \rho^e v^e - V \leq 0 \\
 &[S] \{D\} - \{R\} = \{0\} \\
 &0 < \rho_{min} \leq \rho^e \leq 1, e = 1, \dots, NE
 \end{aligned} \tag{3.2}$$

Remaining now is the problem of choosing a suitable material model for the density to stiffness relation at a point (element) in the structure.

The goal of the optimization algorithm is to find the optimal structure composed of solid and void regions. This problem is a 0–1 type optimization problem which is too large to be solved by any integer programming method even for a low number of elements. Furthermore the solution of the 0–1 problem does not converge towards a macroscopic solid–void layout when the mesh is refined. Instead, refining the mesh leads to chattering designs or solutions with an increasing number of small holes. This problem was first described in [Cheng and Olhoff, \(1981\)](#) for plates. To prevent these problems, a "relaxed" formulation is necessary [see [Allaire and Kohn, \(1993\)](#)<sup>1</sup> and references therein]. The relaxed formulation introduces a material microstructure consisting of so-called ranked materials made of microscopically oscillating material on differing length scales. Using homogenization methods to determine the effective properties of ranked materials and substituting the homogenized parameters into the "macroscopic" topology optimization problem, leads to the "homogenization approach to topology optimization" method introduced as a computational tool in the work of [Bendsøe and Kikuchi, \(1988\)](#). It can be shown [e.g. [Avellaneda, \(1987\)](#)], that solutions using ranked microstructures attain the lower bound on compliance for mixtures of two isotropic materials. Although proven optimal, the solutions obtained by using ranked materials have large "grey areas" of intermediate densities consisting of microporous regions. Aiming at producing structures with macroscopic voids more applicable to practical purposes, we have to consider "suboptimal" microstructures [e.g. [Bendsøe and Kikuchi 1988](#)], penalizations of intermediate densities [e.g. [Allaire and Kohn, \(1993\)](#)<sup>2</sup>, [Allaire and Francfort, \(1993\)](#), [Jog, \(1994\)](#)] or artificial microstructures [e.g. [Rozvany et al., \(1992\)](#), [Bendsøe, Díaz and Kikuchi, \(1993\)](#) and from biomechanics, [Mullender, Huiskes and Weihans, \(1994\)](#)].

Here we will use an artificial model for the stiffness to density relation, namely writing the constitutive matrix of element  $e$  as

$$[E^e](\rho^e) = (\rho^e)^p [E_0] = (\rho^e)^p \frac{E}{(1-\nu)^2} \begin{bmatrix} 1 & \nu & 0 \\ \nu & 1 & 0 \\ 0 & 0 & (1-\nu)/2 \end{bmatrix} \quad (3.3)$$

where  $E$  is the Young's modulus,  $\nu$  is the Poisson's ratio and  $[E_0]$  is the constitutive matrix for solid isotropic material. By choosing different values of the penalty factor  $p$ , "grey" regions or regions with intermediate values of  $\rho^e$  can be penalized. Figure 3.2 shows  $E_{1111}$  plotted versus  $\rho^e$  for different values of  $p$  compared with  $E_{1111}$  for a rank-2 material. The stiffness of a rank-2 material is not uniquely defined because it is optimized with respect to the given stress or strain field. The possible range of optimal stiffnesses for a rank-2 laminate with lamination directions aligned with the principal stress or strain directions are marked as a grey region in figure 3.2. Loosely interpreted the figure shows that the artificial material law (3.3) with penalty factor up to 1.5 should give solutions similar to solutions obtained by using rank 2 materials. Choosing a higher value for the penalty factor  $p$  will penalize intermediate densities and results in more distinct solutions.

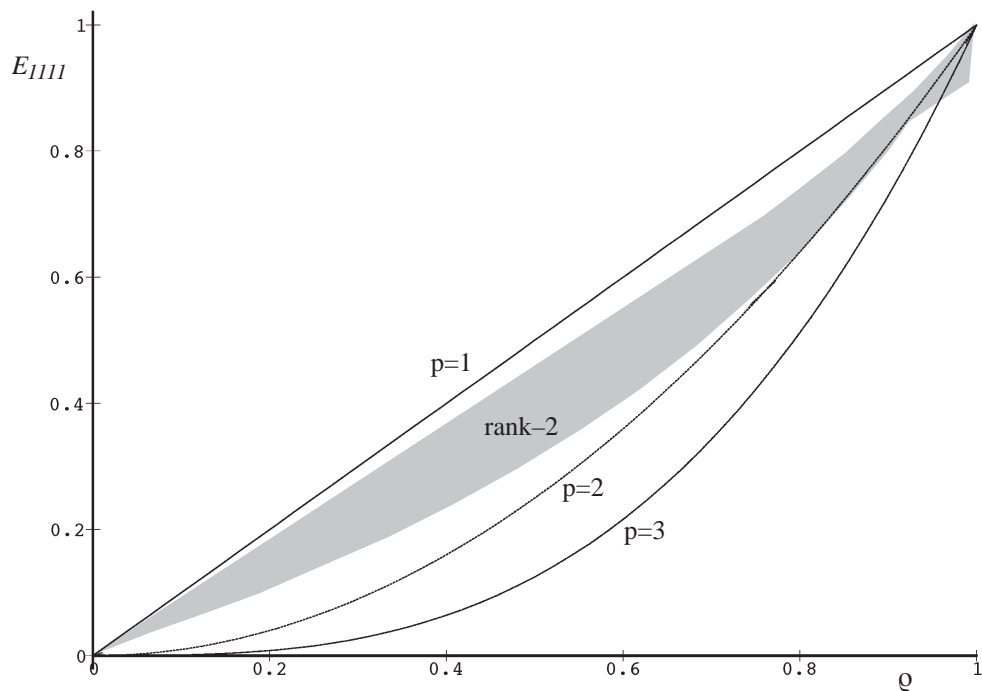


**Figure 3.2** Stiffness versus density for different penalty factors  $p$  compared with stiffness range of optimized rank-2 material (grey region).

Using the stiffness to density relation (3.3), the compliance optimization problem (3.2) can be written as

$$\begin{aligned}
 \text{minimize : } W &= \{D\}^T [S] \{D\} = \sum_{e=1}^{NE} \{d^e\}^T [s^e] \{d^e\} = \sum_{e=1}^{NE} (\rho^e)^p \{d^e\}^T [s_0^e] \{d^e\} \\
 \text{subject to : } &\sum_{e=1}^{NE} \rho^e v^e - V \leq 0 \\
 &[S] \{D\} - \{R\} = \{0\} \\
 &0 < \rho_{min} \leq \rho^e \leq 1, e = 1, \dots, NE \\
 \text{where : } [s^e] &= (\rho^e)^p [s_0^e], [s_0^e] = \int_{v^e} [B^e]^T [E_0] [B^e] dv^e, p \geq 1
 \end{aligned} \tag{3.4}$$

For convenience, we will define the element relative strain energies  $q^e$  as  $q^e = \{d^e\}^T [s_0^e] \{d^e\}$  such that the compliance can be written in the simple form

$$W = \sum_{e=1}^{NE} (\rho^e)^p q^e \tag{3.5}$$

To solve the optimization problem (3.4), we will use an optimality criteria based algorithm. Using the standard optimality criteria method for structural optimization [Bendsøe, (1994)], the Lagrangian function for (3.4) can be written

$$\begin{aligned}
 \mathcal{L} = & \{D\}^T [S] \{D\} + \lambda \left( \sum_{e=1}^{NE} \rho^e A^e - V \right) + \{\mu\}^T ([S] \{D\} - \{R\}) + \\
 & \sum_{e=1}^{NE} \alpha^e (-\rho^e + \rho_{min}) + \sum_{e=1}^{NE} \beta^e (\rho^e - 1)
 \end{aligned} \tag{3.6}$$

where  $\lambda, \alpha^e, \beta^e$  and  $\{\mu\}^T$  are the Lagrangian multipliers for the volume constraint, the lower and upper side constraints and the equilibrium equation respectively.

The necessary condition for optimality is stationarity of the Lagrangian function (3.6) with respect to the displacement vector and the design variables.

Stationarity with respect to the displacement vector gives

$$\frac{\partial \mathcal{L}}{\partial \{D\}} = 2\{D\}^T [S] + \{\mu\}^T [S] = \{0\} \Rightarrow \{\mu\} = -2\{D\} \tag{3.7}$$

Stationarity with respect to design variable  $\rho^e$  gives

$$\begin{aligned} \frac{\partial \mathcal{L}}{\partial \rho^e} = & 2\{D\}^T [S] \frac{\partial \{D\}}{\partial \rho^e} + \{D\}^T \frac{\partial [S]}{\partial \rho^e} \{D\} + \\ & \{\mu\}^T \left( \frac{\partial [S]}{\partial \rho^e} \{D\} + [S] \frac{\partial \{D\}}{\partial \rho^e} \right) + \lambda v^e - \alpha^e + \beta^e = 0, \quad e = 1, \dots, NE \end{aligned} \quad (3.8)$$

Substituting (3.7) into (3.8) we get

$$\begin{aligned} \frac{\partial \mathcal{L}}{\partial \rho^e} = & -\{D\}^T \frac{\partial [S]}{\partial \rho^e} \{D\} + \lambda v^e - \alpha^e + \beta^e = \\ & -\{d^e\}^T \frac{\partial [s^e]}{\partial \rho^e} \{d^e\} + \lambda v^e - \alpha^e + \beta^e = 0, \quad e = 1, \dots, NE \end{aligned} \quad (3.9)$$

and using that  $\partial [s^e]/\partial \rho^e = p (\rho^e)^{p-1} [s_0^e]$  we get

$$\frac{\partial \mathcal{L}}{\partial \rho^e} = -p (\rho^e)^{p-1} q^e + \lambda v^e - \alpha^e + \beta^e = 0, \quad e = 1, \dots, NE \quad (3.10)$$

For intermediate densities ( $\rho_{min} < \rho^e < 1$ ), the conditions (3.10) can be written

$$B_0 = \frac{p (\rho^e)^{p-1} q^e}{\lambda v^e} = 1, \quad e = 1, \dots, NE \quad (3.11)$$

The interpretation of (3.11) is that the sensitivities of a design change should be constant for all intermediate densities in the optimal solution.

Following Bendsøe, (1994), we can define the fix-point type update algorithm

$$\rho^e = \rho_0^e (B_0^e)^\eta, \quad e = 1, \dots, NE \quad (3.12)$$

where  $\eta$  is a damping factor and  $\rho_0^e$  is the value of the design variable from the previous iteration.

The updating scheme for the fixed point algorithm is defined as

$$\rho^e = \begin{cases} \max \{(1-\varsigma) \rho_0^e, \rho_{min}\} & \text{if } \rho_0^e B_0^\eta \leq \max \{(1-\varsigma) \rho_0^e, \rho_{min}\} \\ \rho_0^e B_0^\eta & \text{if } \max \{(1-\varsigma) \rho_0^e, \rho_{min}\} \leq \rho_0^e B_0^\eta \leq \min \{(1-\varsigma) \rho_0^e, 1\} \\ \min \{(1 + \varsigma) \rho_0^e, 1\} & \text{if } \min \{(1 + \varsigma) \rho_0^e, 1\} \leq \rho_0^e B_0^\eta \end{cases} \quad (3.13)$$

where  $\varsigma$  is a move limit.

As the new values of the design variables, defined by (3.12), are dependent on the Lagrangian multiplier  $\lambda$ , we have to perform an inner loop in the optimization algorithm to update the multiplier. The volume of the structure is a decreasing function of the multiplier and therefore we can use a bisection method for the inner loop.

A few words shall be devoted to the choice of penalty factor  $p$  in the stiffness to density relation (3.3). Choosing  $p=1$  we are back to the "thickness of a sheet" design problem which is a well posed problem. However, this problem generally results in solutions with large "grey" areas which we are trying to avoid. The higher we chose the value of  $p$ , the more distinct black and white (solid and void) structures we get. For  $p \approx 3$  we get solutions consisting almost entirely of solid and void regions.

A problem is, that different choices of  $p$  can lead to widely different topologies. In order to get solutions seemingly independent on the choice of penalty factor, we will make use of the so-called continuation approach used by Jog, (1994).

The idea of the continuation approach is to start with a low value  $p=p_0$ ; letting the subproblem converge; increase  $p$  by  $\Delta p$ ; converge, and continue this, till the desired value  $p=p_{max}$  has been reached. Although increasing the total number of required iterations considerably (up to 300), we do get more consistent and detailed solutions. Experiment with the values of  $p_0$ ,  $\Delta p$  and  $p_{max}$  have shown that 1.4, 0.1 and 3.0 respectively are good choices. The overall computational procedure is summarized in figure 3.3.

The optimization procedure was used to optimize the standard MBB-beam-example treated in Olhoff, Bendsøe and Rasmussen, (1992). The MBB-beam is a simply supported beam subject to a point load at the mid of the top edge as sketched in figure 3.4. Minimizing the compliance of the MBB-beam discretized by 72x24 4-node quadrilateral elements and constraining the amount of available material to 50% of the design domain resulted in the "optimal" layout shown in figure 3.5.

The resulting structure in figure 3.5 is seen to contain large regions with checkerboard patterns, where **checkerboard patterns** are defined as *regions with alternating void and solid elements ordered in a checkerboard like fashion*. The appearance of checkerboard patterns is a numerical problem due to poor modelling of the stiffness of a checkerboard by lower order finite elements and can not be interpreted as a kind of optimal porous microstructure. The actual stiffness of a checkerboard consisting of solid and void elements is zero due to the stress singularities at the corners of the solid regions as discussed in Berlyand and Kozlov, (1992).

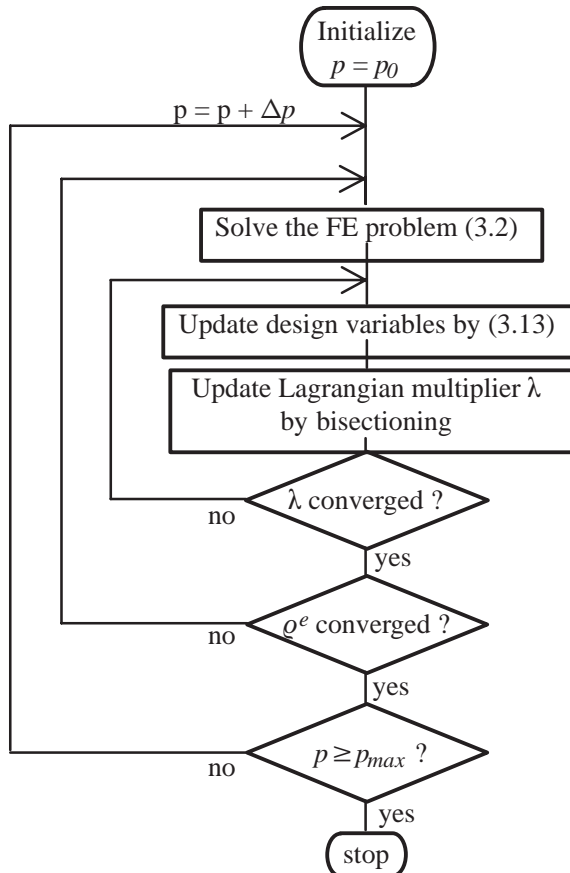


**Figure 3.3** Flowchart of the optimization algorithm

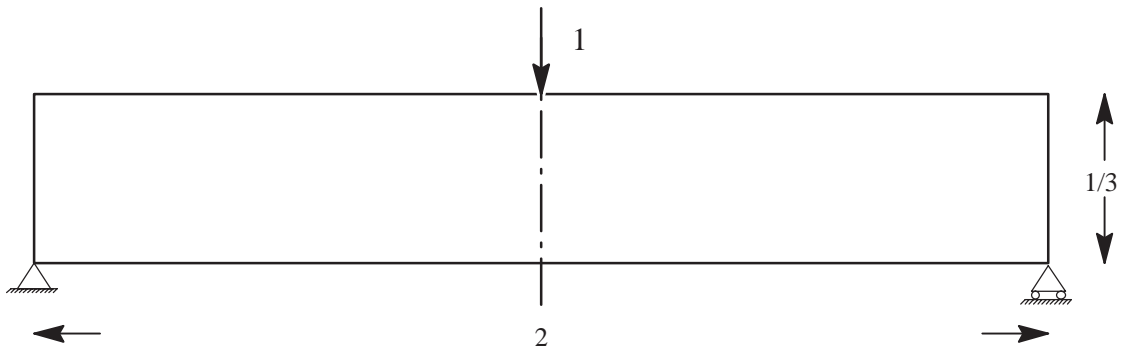


**Figure 3.4** Design domain of the MBB-beam.

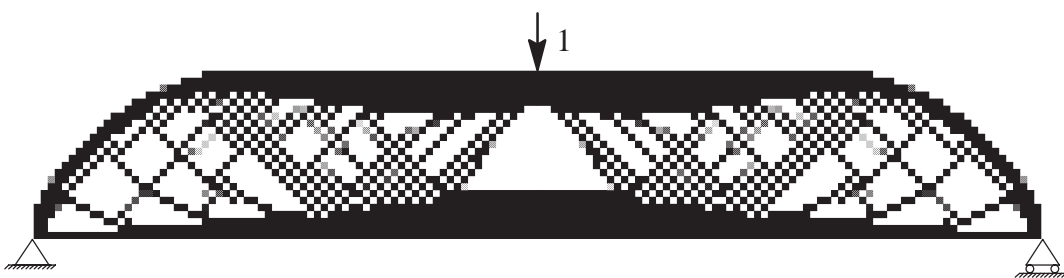


**Figure 3.5** Checkerboard patterns in layout optimization.

The checkerboard problem is discussed and the reason for its occurrence is explained extensively in Jog and Haber, (1994) and Díaz and Sigmund, (1994), the latter is supplied in appendix 1 of this report. The conclusion of the above mentioned papers is, that some precautions should be and can be taken to avoid checkerboards.

Different approaches to overcome the checkerboard problem has been described in literature. A very simple approach has been to ignore the presence of checkerboards during the design iteration procedure and then to interpret checkerboard regions as regions with intermediate uniform density during post-processing. Although this approach is simple to implement, it makes no sense to use it because the correct stiffness of the checkerboard pattern is zero [[Berlyand and Kozlov, \(1992\)](#)] and it can therefore not be interpreted as "grey". Another approach has been to discretize the design domain by 8– or 9–node elements [[Rodriques and Fernandes, \(1994\)](#) and [Jog, Haber and Bendsøe \(1994\)<sup>1</sup>](#)]. Although no checkerboards have been reported in practical problems using 8– or 9–node elements so far, [Jog and Haber, \(1994\)](#) and [Díaz and Sigmund, \(1994\)](#) show that checkerboards might appear in special cases, furthermore the use of 8– or 9–node elements suffers from the major drawback that computing time is increased by up to a factor of 16 and storage space by a factor of 4 (or more) compared to the same discretization using 4–node elements. In a recent paper by [Mullender, Huiskes and Wehnans, \(1994\)](#) a bone remodelling algorithm based on the assumption that bone growth at some point is dependent on loads at all other point in the bone structure was proposed. The algorithm is reported to prevent formation of checkerboards patterns and at the same time producing mesh–independent solutions. The algorithm proposed in this chapter can be compared to the algorithm proposed by [Mullender, Huiskes and Wehnans, \(1994\)](#) although the origins of the algorithms are widely different.

In order to maintain the use of lower order finite elements and at the same time prevent the formation of checkerboards, a prevention scheme was proposed by [Bendsøe, Díaz and Kikuchi, \(1993\)](#). The prevention scheme, which is applied after each design update, divides the design domain into patches of four elements (a kind of super elements) and modifies the cell parameters if checkerboards are detected in the patch. The prevention scheme does well in removing checkerboards but still, a considerable amount of checkerboards regions are observed in the resulting topologies. A reason for the methods lack in obtaining absolute checkerboard free solutions might lie in the fact that each patch of 4 elements does not overlap with the neighboring patches and thus checkerboards occurring "between" patches are not "detected" by the prevention scheme. An improved checkerboard prevention scheme is therefore needed.

---

Requirements to a good checkerboard prevention algorithm are the following:

- Checkerboard patterns must be removed entirely
- Computer time requirement must not be increased
- Must be simple to implement
- Must not destroy the stability of the optimization algorithm
- Must be applicable to any design domain

In the next sections, we will suggest a prevention scheme that tries to fulfill all the above mentioned criteria.

### **3.2 Checkerboard prevention scheme using image processing**

This section will give a brief introduction to noise-reduction techniques in digital image processing and their possible applications to the prevention of checkerboard patterns in layout optimization.

Digital image processing techniques are commonly used to process graphical data: good descriptions and many examples of applications are given in Pratt, (1991). A graphical image is digitized in to a finite number of pixels. The resolution, i.e. the number of pixels in the horizontal and vertical directions, is mostly determined by the quality of the recording device (camera) or the displaying device (monitor). Each pixel in a digital image represents a gray value and it is common to distinguish 256 levels of gray, thus the color of one pixel can be stored in eight bits or one byte. Here we will assume that the pixel values are continuous variables.

A common problem in image processing is noise coming from electrical sensor noise, transmission errors etc. Noise mostly appears as discrete isolated pixel variations, where pixels in error visually appear markedly different from their neighbors.

The discretized design domain in layout optimization can be seen as a digital image. Each element represents one pixel and the density in each element is represented by the gray scale: white is void and black is solid material. Checkerboard patterns can then be interpreted as unwanted noise in the layout optimized structure and thus one of the many powerful techniques developed for noise cleaning can be used as a checkerboard prevention scheme.

Pratt, (1991) describes linear and non-linear noise cleaning techniques. Non-linear techniques are reported to be superior to linear techniques but they can not be applied to layout optimization

---

because the smoothness of the design problem would be destroyed. We will therefore settle for the linear techniques.

Linear noise cleaning techniques can again be divided into two approaches: Fourier transformation based techniques and convolution based techniques.

Application of Fourier transformation based techniques immediately sound promising. The Fourier transform of an image provides insight into the different frequency components of an image. Cutting of high frequencies (low-pass filtering) and performing the inverse Fourier transformation will result in an image where high frequency components (checkerboards) are efficiently removed. The only, however grave, disadvantage of this method is that it only can be applied to regular rectangular meshes. Of course the design domain could be divided into regular subsections but this would require a complicated algorithm.

Convolution based techniques can also be used for linear noise cleaning. Properly executed, the convolution technique corresponds to the Fourier based techniques however, the former does not give the same intuitive insight into the nature of the noise cleaning filtering.

Following Pratt, (1991), the color (or density) of a pixel in the  $i$ 'th row and the  $j$ 'th column of an image is denoted  $F(i, j)$ . A spatially filtered output image  $G(i, j)$  is formed by a discrete convolution of the input image  $F(i, j)$  with an  $L \times L$  impulse response array  $H(i, j)$ . The convolution process is formulated as

$$G(i, j) = \sum_{m=1}^L \sum_{n=1}^L F(m, n) H(i-m + C, j-n + C) \quad (3.14)$$

where  $C=(L+1)/2$  and the limits of  $i$  and  $j$  are  $\max(1, i-C + 1) \leq m \leq \min(i + C-1, M)$  and  $\max(1, j-C + 1) \leq n \leq \min(j + C-1, N)$ , where  $M$  and  $N$  are the numbers of pixels in the vertical and horizontal directions of the picture respectively.

Choosing different impulse response matrices  $H$ , makes the convolution filter good for different purposes, two examples are edge crispening and image restoration. For noise cleaning purposes,  $H$  should be of low-pass form with only positive elements. Widely used is the 3x3 parametric low-pass filter whose impulse response matrix is defined as

$$H = \left(\frac{1}{b+2}\right)^2 \begin{bmatrix} 1 & b & 1 \\ b & b^2 & b \\ 1 & b & 1 \end{bmatrix} \quad (3.15)$$

where  $b \in [1, \infty[$ .

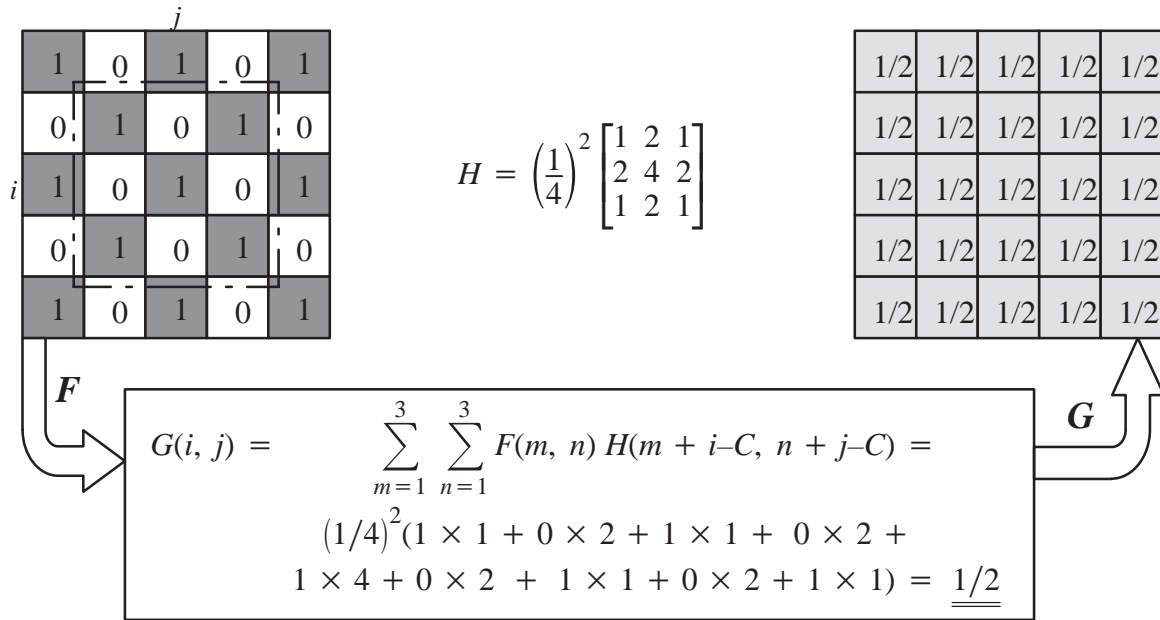


**Figure 3.6** Convolution of input image  $F$  with impulse response matrix  $H$  gives  $G$ . The filter parameter is set to  $b=2$ .

For  $b$  approaching infinity,  $G(i, j)$  approaches  $F(i, j)$  and thus no filtering is performed. For smaller values of  $b$  the output pixel value  $G(i, j)$  is a weighted average over the neighboring input values.

The convolution procedure is demonstrated by a small example sketched in figure 3.6. Consider the checkerboard pattern figure 3.6(left), where the numbers in each pixel denotes the density of the pixel. Performing the convolution (3.14) with  $b=2$  in (3.15), gives a uniform output pattern. Note that the average density of the image remains constant under the convolution.

The linear low-pass convolution procedure reduces checkerboard noise efficiently, is easy to implement, is applicable to any design domain and is therefore ideally suited for our purposes.

### 3.3 Implementation of the checkerboard prevention scheme

In this section, the linear convolution noise cleaning method will be applied to layout optimization of structures.

The simplest way to perform the noise cleaning procedure is to take the resulting layout from the optimization algorithm (i.e. figure 3.5) and postprocess it by the convolution procedure. This approach would convert checkerboard regions into "grey" regions which also are unpreferable in the final design. Therefore the noise cleaning must be performed as a part of the optimization algorithm.

Applying the convolution procedure after each iteration in the optimization algorithm was tested and resulted in checkerboard free final designs however, applying the noise cleaning after each optimization step is a rather empirical approach and certainly destroys the optimality conditions in (3.9). The conclusion is that the noise cleaning process must be integrated in the optimization problem – how to do this is described in the following.

The element relative strain energies  $q^e$  are modified as

$$\bar{q}^e = \frac{1}{(\rho^e)^p} \sum_{f=1}^9 H^f q^f (\rho^f)^p \quad (3.16)$$

where  $H^f$  is the impulse response matrix defined in (3.15) written in vector form and the summation is taken over the nine elements in the neighborhood of element  $e$ . The modified element relative strain energies  $\bar{q}^e$  can be interpreted as the weighted average of strain energies in element  $e$  and its eight direct neighbors.

A problem in the summation of (3.16) arises when element  $e$  is situated on the boundary of the design domain and therefore has less than eight neighbors. One possibility to avoid this problem is to assume that the non-existing elements have  $q^f=0$  but this tends to suppress formation of material at the boundaries.

Instead we will only perform the summation over the  $n_H$  *existing* neighboring elements of  $e$ . We will therefore introduce a new filter vector  $H_*^f$  which is equal to  $H^f$  defined in (3.15) *without* the scaling factor  $1/(b+2)^2$ . The modified relative strain energies (3.16) can then be written as

$$\bar{q}^e = \frac{1}{(\rho^e)^p \sum_{i=1}^{n_H} H_*^i} \sum_{f=1}^{n_H} H_*^f q^f (\rho^f)^p \quad (3.17)$$

where  $n_H \leq 9$ . For  $n_H = 9$ , (3.17) corresponds to (3.16).

The optimality criteria for the modified problem is defined as

$$\frac{\partial \mathcal{J}}{\partial \rho^e} = -p (\rho^e)^{p-1} \bar{q}^e + \lambda v^e - \alpha^e + \beta^e = 0, \quad e = 1, \dots, NE \quad (3.18)$$

and it is seen that the only change in (3.18) compared to the original optimality criteria (3.10), is the exchange of the relative strain energies  $q^e$  with the modified or averaged ones  $\bar{q}^e$ . The modification is rather heuristic and the actual objective function or Lagrangian with minimum defined by (3.18) is not known for the time being however, numerical evidence shows that imple-

mentation of the modified stationarity condition (3.18) in an iterative process, generates structures with decreasing compliance where checkerboard patterns are removed. For the filter factor  $b$  approaching infinity the modified stationarity condition (3.18) approaches the original one (3.10). Further explanation of the modified objective function will be subject to future research.

The overall computational procedure corresponds to the original procedure (figure 3.3), except for the substitution of the element relative strain energies  $q^e$  in (3.10) with the weighted averages  $\bar{q}^e$  computed by (3.17).

Physically an infinite value of  $b$  corresponds to specifying an infinite "cut-off" frequency of the low-pass filter. Decreasing  $b$  corresponds to lowering the cut-off frequency and thereby filtering out rapidly varying densities. When the filter factor is chosen below a certain value  $b_{check}$ , all checkerboard patterns are filtered out. To find a critical value of  $b_{check}$ , we will apply the convolution filter to the previously considered MBB-beam design problem.

Figure 3.7 shows the optimal layouts of the MBB beam discretized by  $120 \times 40 = 4800$  elements, where different filter parameter values  $b$  were used for the convolution filter. The filtered designs can be compared with the unfiltered design at the top of the figure. It is seen that the filter value  $b=100$  hardly removes any checkerboards. For decreasing values of  $b$ , the checkerboard areas get smaller and for  $b=15$ , they are entirely removed. Decreasing  $b$  further results in thicker bars of the structure. It can be concluded that the value of the filter parameter  $b$  in (3.16) should be 15 (or 12 to be on the safe side), to get the most efficient solutions without checkerboards. The critical value of  $b_{check}$  might change for other formulations (other elements or material models) and should be determined by experiments as done here.

A few words shall be devoted to the practical application of the checkerboard prevention scheme and its applicability to other design formulations or problems.

Finding the neighbors defined by the filter window is very simple in the case where the design domain is discretized as a regular mesh in a rectangular domain. In the case of more complicated geometries and irregular meshes another approach must be taken. In preprocessing the design problem, we will make a call to a subroutine which produces a list of neighbors of each element. The subroutine must consist of a search loop where the (eight) neighboring elements to the considered element must be found. The search might be computationally expensive but as the subroutine only has to be called once in the beginning of procedure, the problem is not considered of major concern.

The method is directly applicable to the "homogenization approach to layout optimization", where the design variables are densities and orientation of the ranked material in each element.

---

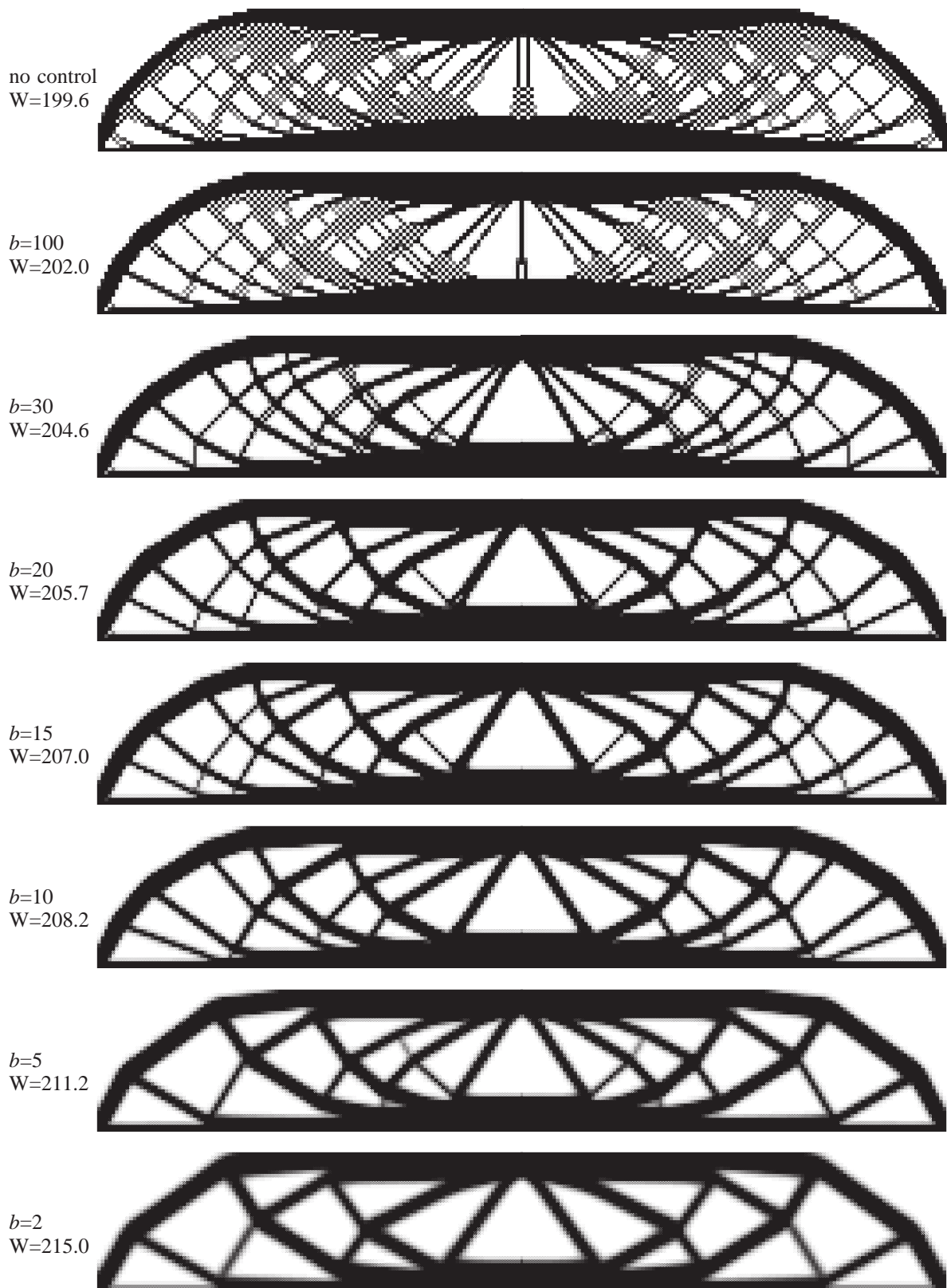


**Figure 3.7** Influence of filter factor  $b$  on the optimal layout of the MBB-beam defined in figure 3.4. The ground structure (half of the beam) consists of  $120 \times 40 = 4800$  4-node elements and the volume is restricted to 50% of the design domain.

The element relative strain energies are modified as described above and the lamination angles can be determined the usual way.

Discretizing the structure by triangular elements would require a modification of the impulse response matrix  $H$  in (3.15), which would have to be reduced to four elements (only direct neighbors). Experiment would have to be performed to find the right weighting factors.

The described procedure can easily be extended to three dimensions by adding a third dimension to the impulse response matrix. Assuming a discretization by 8-node brick elements, the impulse response matrix  $H$  will contain 27 factors.

### 3.4 Elimination of mesh-dependency

Applying the checkerboard prevention scheme proposed in the last section to the MBB-beam example discretized by  $210 \times 70 = 14700$  elements, we get the optimal topology shown in figure 3.8.

Comparing figure 3.8 with the optimal topology using 4800 elements and filter factor 15 (figure 3.7), we notice that the solution has become more detailed. In other words, the solution becomes more chattering when the mesh is refined. The mesh-dependency is explained by the ill-posedness of the penalized problem discussed earlier. For practical reasons we are interested in "coarse" solutions with a few large holes and we must therefore find a method to "fix" the topology no matter how fine the mesh-discretization is made. Eventually mesh-refinement shall only result in smoother and better descriptions of the boundaries between solid and void regions in the optimal layout.

An approach to eliminate the problem of mesh dependency and at the same time ensuring a unique solution is the perimeter control method proposed by Jog, Haber and Bendsøe, (1994)<sup>2</sup>. The formulation of the perimeter control method ensures a well-posed problem by combining a constraint on the global perimeter of the structure with penalization on intermediate density values. Implementation of the method involves adding a (non-linear) constraint in the optimality

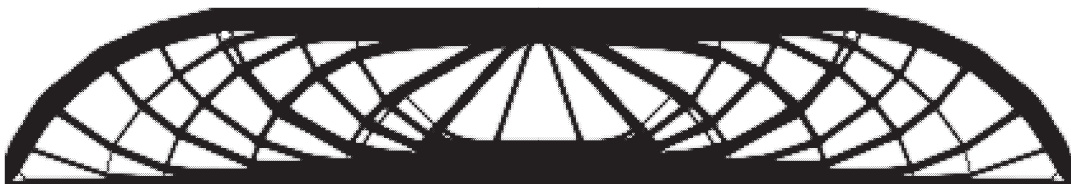


**Figure 3.8** MBB-beam example discretized by  $210 \times 70 = 14700$  elements and filter factor  $b=15$ .  
 $W=203.4$ .

---

criteria and a critical choice of penalty factors and therefore, convergence is reported to be rather unstable.

To get a robust procedure which requires no interaction of the engineer and ensures mesh-independency of the solution, a modification of the checkerboard prevention algorithm described in the last section is proposed in the following.

From figure 3.7 can be observed that low values of the filter factor  $b$  give more manufacturable designs. Mesh-independent designs could therefore be obtained by specifying lower values of  $b$  for finer meshes. However, this approach is rather empirical and it is difficult to assign a filter factor to a given mesh. We will therefore modify the checkerboard convolution filter such that the filter area is independent on the mesh size.

For the checkerboard prevention algorithm, the size of the convolution filter  $H_*^i$  was fixed to 3x3 elements. Extending the filter size to the elements within a radius  $r_{min}$  of element  $e$ , we can define a convolution filter

$$\hat{H}^f = v^f [r_{min} - \text{dist}(e,f)] , \{f \in NE \mid \text{dist}(e,f) \leq r_{min}\} \quad (3.19)$$

where the operator  $\text{dist}(e,f)$  is defined as the distance between the center of element  $e$  and the center of element  $f$ , and  $v^f$  is the volume of element  $f$ .

If  $n_r$  denotes the number of elements which have centers within the radius  $r_{min}$  of element  $e$ , the modified relative strain energies can be written in parallel to (3.17) as

$$\hat{q}^e = \frac{1}{(\rho^e)^p \sum_{i=1}^{n_r} \hat{H}^i} \sum_{f=1}^{n_r} \hat{H}^f q^f (\rho^f)^p \quad (3.20)$$

The weights of the filter can be seen as a cone with bottom radius  $r_{min}$  and volume one.

To clarify what happens to the strain energies when the filter is applied, we will consider two simple (one dimensional examples). Without any filtering a bar in a layout can have the thickness of only one element as sketched in figure 3.9a. The coordinate system shows the unfiltered strain energies  $q^e(\rho^e)^p$  as a function of the elements in a column of a layout. Applying the filter with  $r_{min}$  equal to three times the element size results in the modified strain energies  $\hat{q}^e(\rho^e)^p$  shown in figure 3.9b. The sums of the unfiltered and filtered strain energies are equal but the strain energy distribution is changed to a cone like shape clearly seen for the fine mesh in figure 3.9c. The base radius of the cone is  $r_{min}$ .

Figure 3.10 shows the filter effect on a double impulse which physically can represent two thin bars. In figure 3.10a, the distance between the two bars is  $r_{min}$ . The effect of filtering with filter size  $r_{min}$  is shown in figure 3.10b and we notice, that the two bars have been merged to one but the sum of the strain energies (=compliance) is preserved. It can be concluded that *applying the filter introduces a length scale  $r_{min}$  underneath which structural variation is not allowed.*

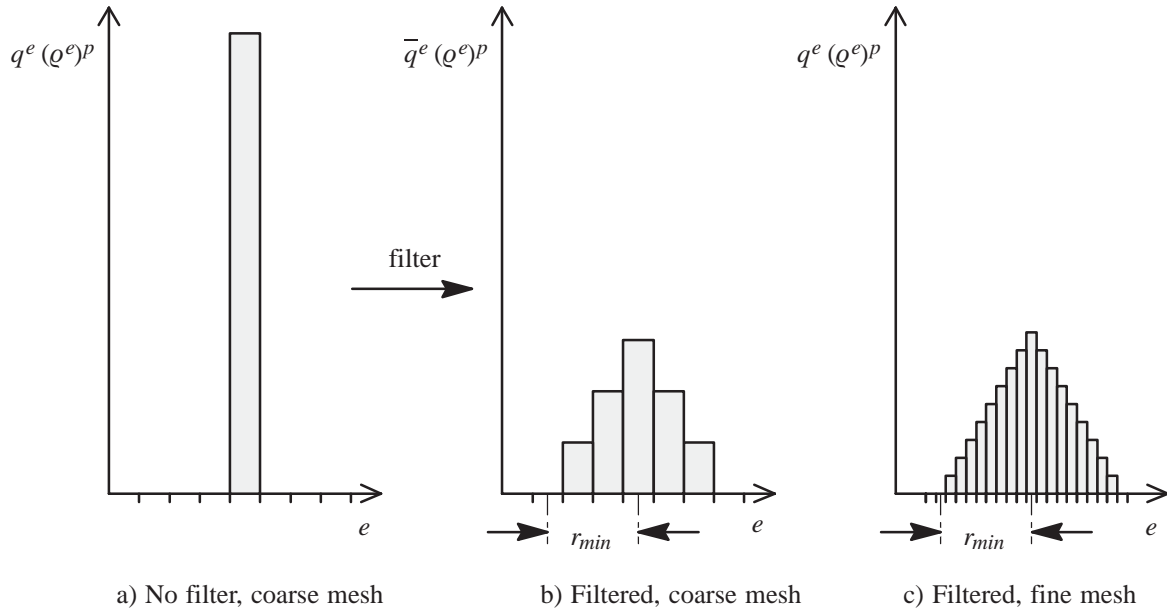


**Figure 3.9** Change of impulse after filtering with the mesh-independency filter.

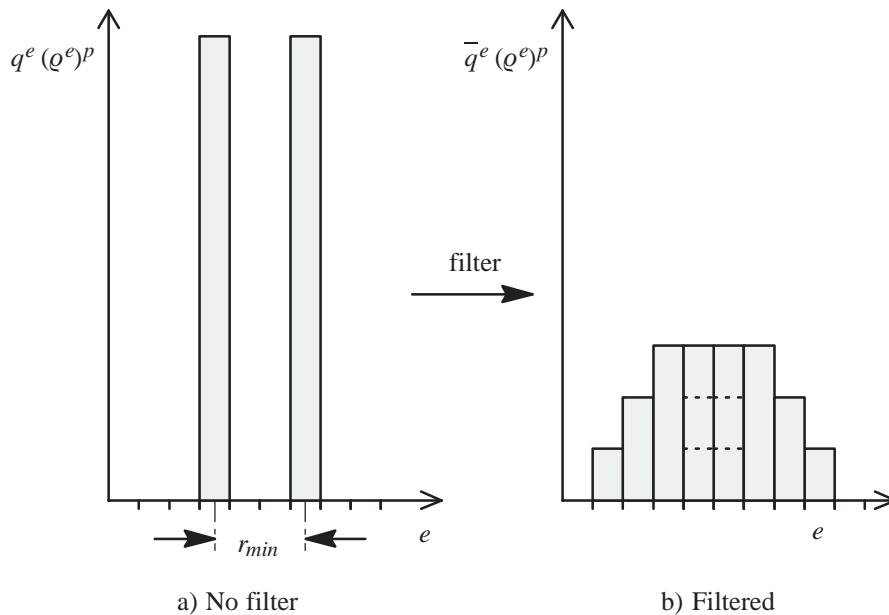


**Figure 3.10** Change of double impulse after filtering with the mesh-independency filter.

The modified optimality criteria for the mesh–independency algorithm is written as

$$\frac{\partial \mathcal{L}}{\partial \rho^e} = -p (\rho^e)^{p-1} \hat{q}^e + \lambda v^e - \alpha^e + \beta^e = 0, \quad e = 1, \dots, NE \quad (3.21)$$

As for the checkerboard scheme defined earlier it must be emphasized that the modification is based on heuristics but numerical evidence shows that implementation of the procedure in an iterative process generates structures with decreasing compliance.

The present *mesh–independency algorithm* can be seen as a "mix" of compliance optimization and image processing which gives good results. *By filtering the strain energies with the extended impulse response matrix  $\hat{H}^f$ , we have introduced a length scale  $r_{min}$ , underneath which structural variation is not allowed.*

We can also say, that we have separated the design variables from the finite element discretization. Keeping the value of  $r_{min}$  fixed, independent on mesh refinements, means that the allowed variation of the density is mesh–independent and we will therefore expect to get mesh–independent optimal layouts. The boundaries between solid and void regions will be monotonously varying grey scales of width approximately equal to  $r_{min}$ .

Choosing  $r_{min}$  to be 1.1 times the element size makes the modified filter very similar to the checkerboard filter (3.15) with filter factor  $b=15$ . Therefore,  *$r_{min}$  should always be chosen greater or equal to 1.1 times the maximum element size to prevent formation of checkerboards.*

The modified impulse response filter (3.19) was applied to the MBB–beam example. Figure 3.11 shows the optimal topologies obtained for  $r_{min}=0.04$  and varying numbers of elements. It is seen in the figure that topologically similar structures are obtained independent on the grid refinement.

Figure 3.12 shows three different topologies obtained from a fixed discretization of 120x40 elements and varying values of  $r_{min}$ . It is seen from the figure, that the complexity of the topologies can be controlled by the choice of  $r_{min}$  and that the smallest bars in the topologies are of approximately the same size as  $r_{min}$ .

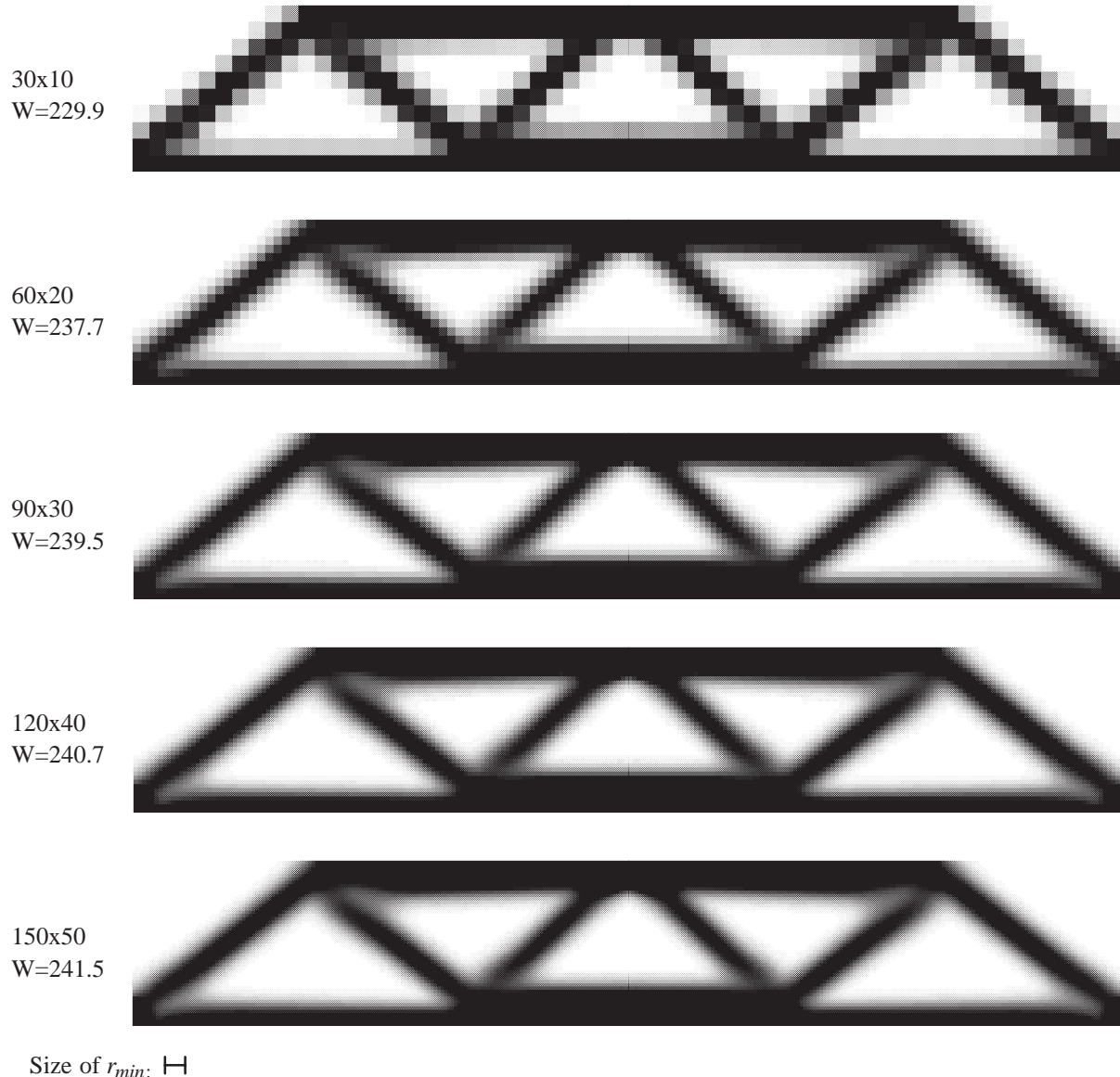


**Figure 3.11** Elimination of the mesh-dependency problem by application of the modified convolution filter with  $r_{min}=0.04$ . Mesh discretizations ranging from 30x10 to 150x50. The design problem is defined in figure 3.4.

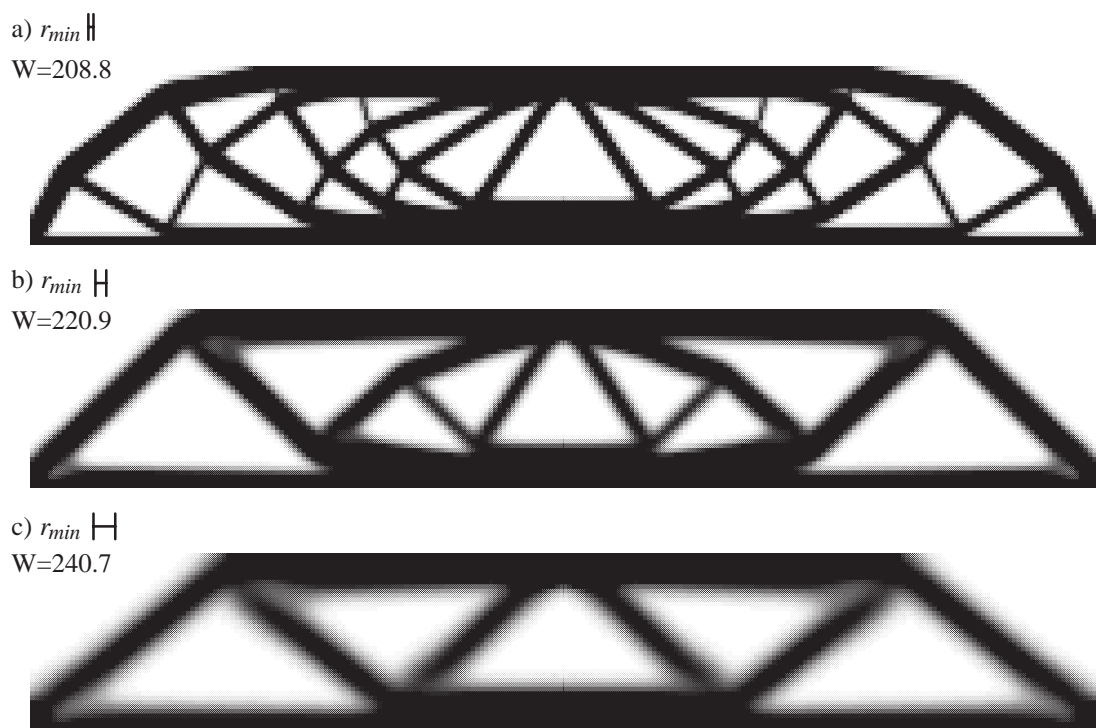


**Figure 3.12** Dependency of optimal topology on filter size. Groundstructure has 120x40 elements and a)  $r_{min}=0.01$ , b)  $r_{min}=0.02$  and c)  $r_{min}=0.04$ .

Another example is shown in figure 3.13. In this example the topology of a "bicycle wheel" is optimized. The figure shows the optimal layouts for different mesh sizes obtained with and without the modified convolution filter.

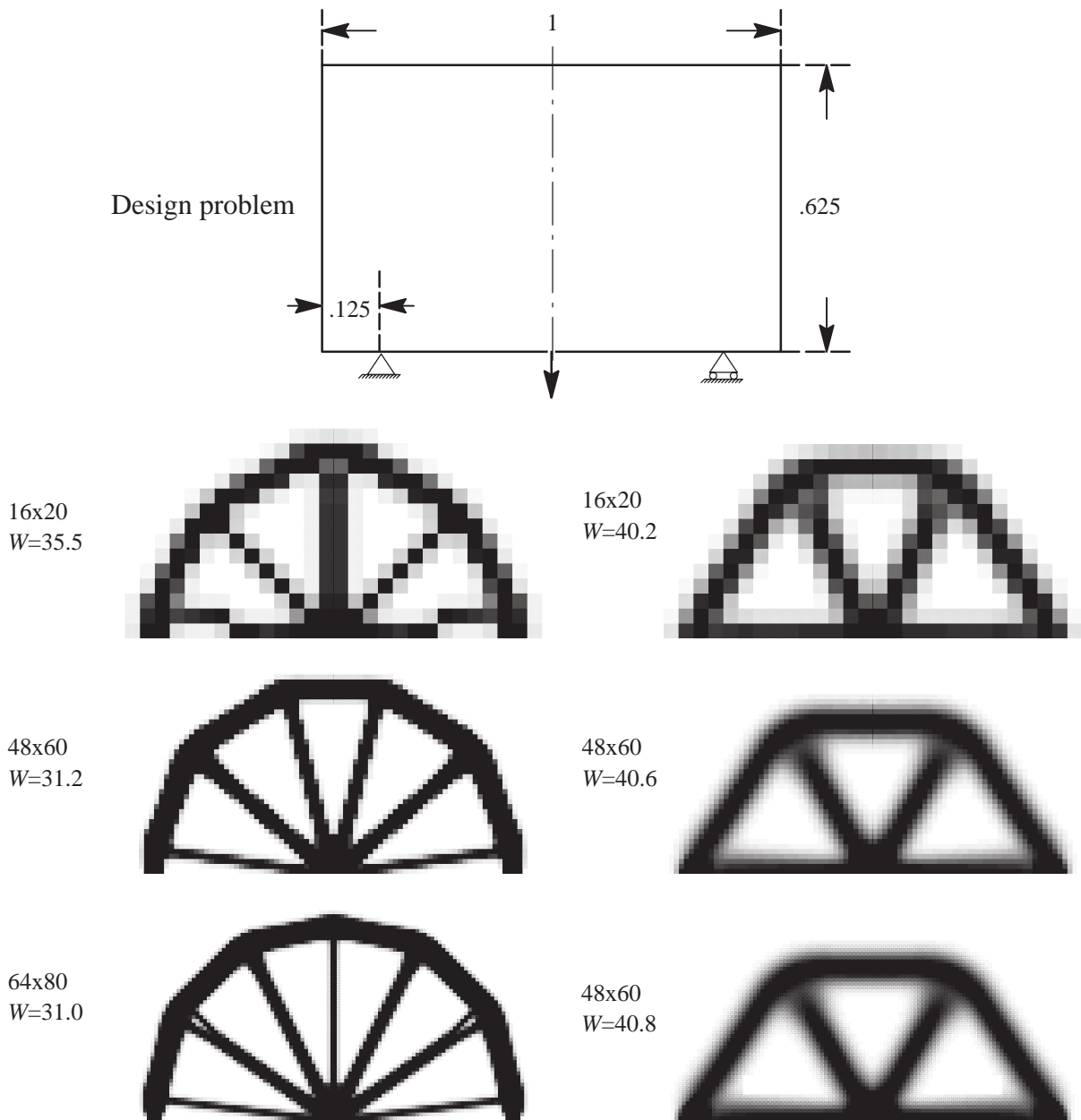


**Figure 3.13** The Bicycle Wheel example with volume fraction 20%. The three solutions left shows mesh-dependency of optimal layout (original checkerboard filter,  $b=15$ ). The three solutions right are generated using the mesh-independency algorithm with  $r_{min}=0.04$  and shows topologically similar solution for different meshes.

Many test examples used in literature (and here) are very idealized in the sense that groundstructures are symmetric, rectangular, discretized by quadratic elements and loads are applied either horizontally or vertically. "Real life" problems have complex geometries and non-symmetric loadings and therefore algorithms which work well on "laboratory problems" might fail to work on more complicated problems. Consequently, A. R. Díaz (in private communication) has suggested a standard "worst case" test example shown in figure 3.14(upper right). The "worst case" design problem is a variation of the well known short cantilever problem in figure 3.14(upper left). The challenge in the "worst case" problem has three sources. First, the original problem has been rotated, second, the individual elements are rectangular not quadratic such that element-to-element symmetry of the solution is hindered and third, the starting guess is non-uniform varying from zero density at the left edge to full density at the right edge. Ideally, solving the original and the modified problem using a topology optimization algorithm should result in two similar (symmetric) topologies because we are seeking mesh-independent solutions.

The "worst case" example was used to test the proposed checkerboard and mesh-independency algorithms. As a reference topology we have figure 3.14a which was produced by the mesh-independency algorithm with  $r_{min}=0.035$  (1.2 times maximum element size). The solution to the worst case problem using the checkerboard prevention scheme is seen in figure 3.14b. It is seen that there are no checkerboards but the topology is unsymmetric which could be expected because the checkerboard filter has become unsymmetric due to the rectangular elements. Solving the problem with the mesh-independency algorithm with  $r_{min}=0.035$  results in the topology in figure 3.14c which is seen to be symmetric and similar to the topology of the original problem in figure 3.14a. To demonstrate the importance of using the continuation method (gradual increase of penalty factor  $p$ ), the worst case problem was solved by the mesh-independency algorithm but fixing the penalty factor  $p$  to 3 from the first iteration. The resulting topology (figure 3.14d) is seen to be very unsymmetric.

From this example, it can be concluded that the proposed mesh-independency algorithm must be preferred to the checkerboard prevention scheme because the former produces mesh-independent and checkerboard free designs.

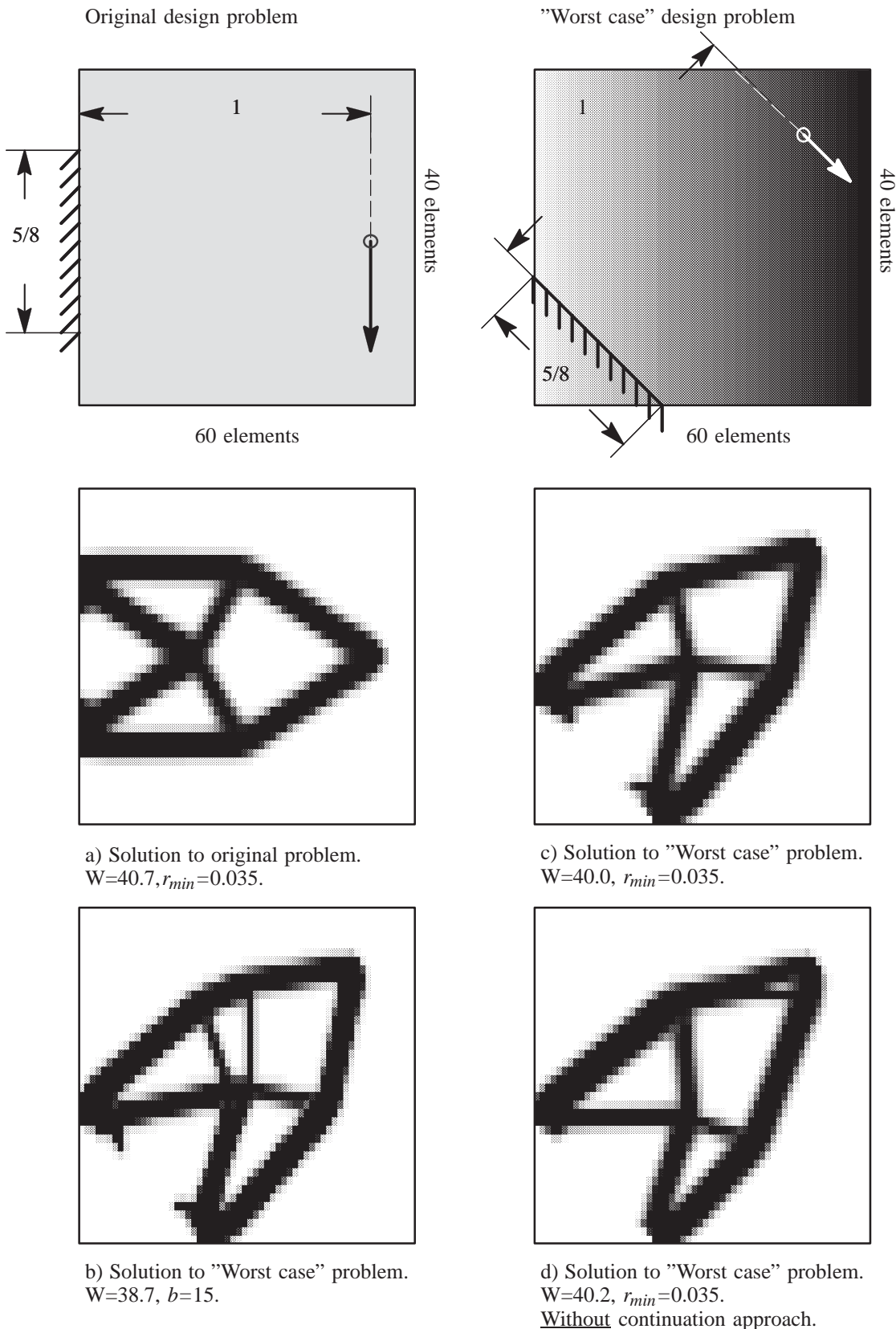


**Figure 3.14** "Realistic" design problem, shows difference in optimal topologies obtained by: b) checkerboard control, c) mesh-independency control and d) mesh-independency control without continuation approach. All groundstructures have  $60 \times 40 = 2400$  elements and volume fraction are 25%.

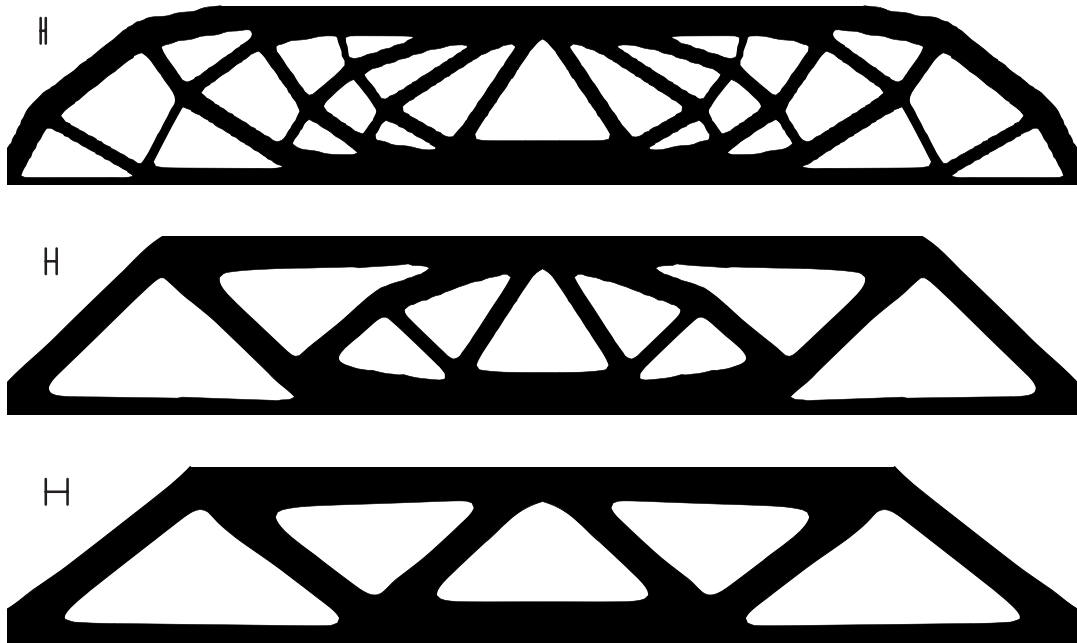


**Figure 3.15** Contour plots of the above 0.5 density level of the the MBB-example in figure 3.12a–c.

The optimal topologies obtained by the mesh-independency filter do not need much post-processing. A contour plotting program (here we have used the software MATHEMATICA) can threshold the density values  $\rho > 0.5$  as shown in figure 3.15. The resulting boundaries between solid and void are seen to be smooth but should still be analyzed for stress concentrations by some general FE-program or shape optimization software.

A fundamental difference exists between the *mesh-independency algorithm* proposed here and the *perimeter control algorithm* proposed in Jog, Haber and Bendsøe, (1994)<sup>2</sup>. In the latter approach, a constraint on the overall perimeter is imposed which means that we do get mesh-independent solutions but in principle nothing prevents a particular bar in becoming thinner and thinner with mesh refinement. The approach presented here prevents bars or holes that are smaller than  $r_{min}$  in being formed, and therefore the method both eliminates mesh-dependency and keeps characteristic sizes constant with mesh refinement. This does not mean that one method should be preferred from the other but it means, that layouts obtained from the two methods can not be directly compared.

### 3.5 Summary

In this chapter, we have proposed a computationally simple procedure to prevent two well known problems in layout optimization, namely, the problem of checkerboard–like patterns occurring in optimal designs due to bad finite element discretizations and the problem of mesh–dependency of optimal solutions due to non–existence of solutions to the penalized problem.

The prevention scheme is based on noise cleaning methods from the field of image processing. The scheme can be seen as a low–pass filter which prevents rapid oscillation of the densities of a structure. The cut–off frequency is independent on the discretization and we thereby obtain an algorithm where the operator can control characteristic sizes such as minimum bar or hole sizes.

Several numerical examples show that the proposed method gives efficient checkerboard–free and mesh–independent designs, readily applicable to manufacturing and with the possibility of controlling characteristic sizes such as minimum diameter of holes and minimum thickness of bars.

Although based on heuristics, the numerical experiments are encouraging and current effort therefore tries to put the procedure into a mathematical framework.

## Conclusions

In the present thesis, a numerical method for design of linear elastic materials with prescribed thermoelastic properties has been proposed. The design problem is formulated as a topology optimization problem where the objective function is to minimize weight pr. unit volume and the design degrees of freedoms are geometrical properties of the periodic material microstructures represented by base cells.

To analyze effective properties of a base cell discretized by finite elements, a numerical homogenization procedure is developed and applied to truss-, frame- and continuum-like discretizations of microstructures. Great savings in computer time and storage requirements can be obtained by taking advantage of sparse and iterative methods in solving the associated finite element problem.

The truss-, frame- and continuum-like discretizations are used as groundstructures or starting guesses for the optimization problem, which means that the optimal microstructure for prescribed elastic properties is sought within a fixed but very detailed discretization.

As demonstrated by many examples, the proposed numerically based design procedure can be used to tailor materials with a wide range of thermoelastic properties.

Using truss-like discretizations in two and three dimensions makes it possible to design materials with properties very close to the theoretical bounds (positive semi-definiteness of the elastic tensor) whereas using more practical frame elements damps out attainable properties. Both the truss and the frame formulations allow bars and beams to cross without interaction. This means that practical realization of the microstructures will be difficult due to crossing members and sliding surfaces.

More realistic microstructures are obtained by the continuum formulation. Examples show that extreme elastic parameters can be obtained by the continuum formulation as well, however, experiments show that only low overall stiffness can be obtained if extreme elastic properties are prescribed. Generally it can be said that any topological constraint imposed on the microstructural geometry damps out the attainable elastic properties. As demonstrated in an example, the attainable properties are also damped when one of the proposed porous microstructures is imbedded in a softer matrix material.

Isotropic materials with negative Poisson's ratios are obtained from all three discretization types but the continuum topology is preferred due to the above mentioned manufacturability constraints.

---

The possibility of designing materials with prescribed thermoelastic properties is demonstrated by a simple example using the continuum discretization.

The numerically predicted material properties are tested by two working models of truss like microstructures with negative Poisson's ratios and showed the expected behaviour. Unfortunately, due to simplicity and coarseness of the models, none of them allowed actual measurements of their elastic properties.

The microstructures obtained by the numerical method developed in this thesis shall not be seen as readily manufacturable solutions but rather as sources of inspiration to people involved in practical synthesis of novel microstructures.

Two well known problems in general topology optimization of structures, namely the checkerboard problem and the mesh-dependency problem were encountered in design of the continuum-like microstructures. The checkerboard problem refers to the formation of regions in optimized topologies with alternating solid and void elements ordered in a checkerboard like fashion. The reason for the occurrence of checkerboards is discussed in Díaz and Sigmund, (1994), supplied in appendix 1, and can simply be explained by poor numerical modelling of the stiffness of checkerboards by lower order finite elements. The mesh dependency problem refers to the non-convergence of solutions with mesh refinement. A procedure to eliminate both problems based on ideas borrowed from image processing has been developed. Although based on heuristics, the proposed procedure shows promising results when applied to topology optimization of continuum structures.

As a continuation of the work presented in this thesis, following subjects are suggested:

- More realistic prototypes of the proposed materials can be produced by the rapid prototyping technique. Actual properties of the prototype materials can be tested by standard mechanical test procedures and can be compared with the theoretically predicted values.
  - Contact to researchers involved in practical synthesis of novel microstructures can be established. In connection with this, the idealized modelling of microstructures used in this work might have to be extended to handle non-linearities or other problems encountered in the practical implementation.
  - The optimal microstructural topologies for the example with prescribed thermoelastic properties showed "actuator" like elements which suggests that the present approach to material design can be used for design problems like optimal placement or configuration of actuators or sensors in the design of smart materials.
-

- Although the suggested procedure to prevent the checkerboard and mesh–dependency problems is based on heuristics, the numerical results are encouraging and efforts invested in formulating the procedure in a mathematical framework seem rewarding.

## List of publications

### Lyngby, January 1993 – December 1994.

Díaz, A.R. and *Sigmund, O.* (1995). Checkerboard patterns in layout optimization, *Structural Optimization*, **10**(1), pp. 40–45.

*Sigmund, O.* (1994)<sup>1</sup>. Materials with prescribed constitutive parameters: an inverse homogenization problem, *Int. J. Solids Struct.*, **31**(17), pp. 2313–2329.

*Sigmund, O.* (1995)<sup>2</sup>. Tailoring materials with prescribed elastic properties". *Mech. Materials*. 20, pp. 351–368.

*Sigmund, O.* (1995)<sup>3</sup>. Tailoring materials for specific needs. *J. of Intelligent Structures and Materials*. 5, pp. 736–742.

### Work published in Essen, October 1991 – December 1992.

Rozvany, G.I.N., Lewinski, T, Sigmund, O., Gerdes, D. and Birker, T. (1993). Optimal topology of trusses or perforated deep beams with rotational restraints at both ends. *J. Struct. Optim.*, **5**, pp. 268–270.

Rozvany, G.I.N., Sigmund, O., and Birker, T. (1993). Optimal design of composite and fibre-reinforced plates. In *Optimization with Advanced Materials*, (ed. Pedersen, P.), Elsevier, Amsterdam, pp. 293–309.

Rozvany, G.I.N., Sigmund, O., Lewinski, T, Gerdes, D., and Birker, T. (1993). Exact optimal layouts for non-self-adjoint problems. *J. Struct. Optim.*, **5**, pp. 204–206.

Rozvany, G.I.N., Sigmund, O., Zhou, M. and Birker, T. (1993). Iterative discretized methods for layout optimization and generalized shape optimization. In *Structural Optimization 1993*, Proceedings (ed. Herskovits, J.), Rio de Janeiro, Brazil, pp. 139–151.

Rozvany, G.I.N., Zhou, M., Birker, T. and Sigmund, O. (1993). Topology optimization using iterative Continuum-type Optimality Criteria (COC) methods for discretized systems. In *Topology optimization of structures*, (eds. Bendsøe, M.P.; Mota Soares, C.A.), Kluwer, Dordrecht, pp. 273–286.

Rozvany, G.I.N., Zhou, M., Lewinski, T. and Sigmund, O. (1993). Optimal layout theory: new classes of exact solutions for trusses including several load conditions and non-self-adjoint problems. In *Structural Optimization 1993*, Proceedings (ed. Herskovits, J.), Rio de Janeiro, Brazil, pp. 37–46.

Rozvany, G.I.N., Zhou, M. and Sigmund, O. (1994). Topology optimization in structural design. In *Advances in Design Optimization*, (ed. Adali, H.), Chapman and Hall, London, UK, pp. 340–399.

Sigmund, O., Zhou, M. and Rozvany, G.I.N. (1993). Layout optimization of large FE systems by new optimality criteria methods: applications to beam systems. In *Concurrent Engineering Tools and Technologies for Mechanical Systems Design*, (ed. Haug, E.J.), Springer Verlag, New York, pp. 803–819.

---

## References

- Aboudi, J. (1991). *Mechanics of Composite Materials*. Elsevier Science Publishers B.V.
- Allaire, G. and Francfort, G.A. (1993). A numerical algorithm for topology shape optimization. In *Topology optimization of structures*, (eds. Bendsøe, M.P.; Mota Soares, C.A.), Kluwer, Dordrecht, pp. 239–248.
- Allaire, G. and Kohn, R.V. (1993)<sup>1</sup>. Optimal design for minimum weight and compliance in plane stress using extremal microstructures. *European J. Mech. A*, **12**, pp. 839–878
- Allaire, G. and Kohn, R.V. (1993)<sup>2</sup>. Topology optimization and optimal shape design using homogenization. In *Topology optimization of structures*, (eds. Bendsøe, M.P.; Mota Soares, C.A.), Kluwer, Dordrecht, pp. 207–218.
- Almgren, R.F. (1985). An isotropic three-dimensional structure with Poisson's ratio = -1. *J. Elasticity*, **15**, pp. 427–430.
- Ashby, M.F (1991). Materials and shape, *Acta. Metall. mater.*, **39**(6), pp. 1025–1039.
- Ashby, M.F and Jones, D.R.H. (1986). *Engineering Materials 2*, Pergamemnon Press.
- Ashley, S. (1994)<sup>1</sup>. Small-scale structure yields big property payoffs. *Mech. Engng.*, February, pp. 52–57.
- Ashley, S. (1994)<sup>2</sup>. Prototyping with advanced tools. *Mech. Engng.*, June, pp. 48–55.
- Autio, M., Laitinen, M. and Pramila, A. (1993). Systematic creation of composite structures with prescribed thermomechanical properties. *Comp. Eng.* **3**(3), pp. 249–259.
- Avellaneda, M. (1987). Optimal bound and microgeometries for elastic two-phase composites. *SIAM J. App. Math.*, **47**, pp. 1216–1228.
- Bakhvalov, N. and Panasenko, G. (1989). *Homogenization: averaging processes in periodic media*. Kluwer Academic Publishers, Dordrecht.
- Bendsøe, M.P. (1989). Optimal shape design as a material distribution problem. *Struct. Optim.*, **1**, pp. 193–202.
- Bendsøe, M.P. (1994). *Methods for the Optimization of Structural Topology, Shape and Material*. Springer.
- Bendsøe, M.P., Díaz, A.R. and Kikuchi, N. (1993). Topology and generalized layout optimization of elastic structures. In *Topology optimization of structures*, (eds. Bendsøe, M.P.; Mota Soares, C.A.), Kluwer, Dordrecht, pp. 159–206.
- Bendsøe, M.P., Díaz, A.R., Lipton, R. and Taylor, J.E. (1993)<sup>2</sup>. Optimal design of material properties and material distribution for multiple loading conditions. To appear in *Int. J. Num. Meth. Engng.* **38**(7), pp. 1149–1170.

- Bendsøe, M.P., Guedes, J.M., Haber, R.B., Pedersen, P. and Taylor, J.E. (1994)<sup>1</sup>. An analytical model to predict optimal material properties in the context of optimal structural design. *J. Appl. Mech.*, **61**(4), pp. 930–937.
- Bendsøe, M.P. and Kikuchi, N. (1988). Generating optimal topologies in structural design using a homogenization method. *Comp. Meth. Appl. Mechs. Engng.*, **71**, pp. 197–224.
- Benssousan, A., Lions, J.L. and Papanicolau, G. (1978). *Asymptotic analysis for periodic structures*. North Holland, Amsterdam.
- Berlyand, L.V. and Kozlov, S.M. (1992). Asymptotics of homogenized moduli for the elastic chess–board composite. *Arch. Rational Mech. Anal.*, **118**, pp. 95–112.
- Bourgat, J.F. (1977). Numerical experiments of the homogenization method for operators with periodic coefficients. *Lecture Notes in Mathematics* **704**, Springer Verlag, Berlin, pp. 330–356.
- Caddock, B.D. and Evans, K.E. (1989). Microporous materials with negative Poisson’s ratios: I. Microstructure and mechanical properties. *J. Phys. D: Appl. Phys.*, **22**, pp. 1877–1882.
- Cheng, G. and Olhoff, N. (1981). An investigation concerning optimal design of solid elastic plates. *Int. J. Solids Struct.*, **16**, pp. 305–323.
- Cherkaev, A.V. and Gibiansky, L.V. (1993). Coupled estimates for the bulk and shear moduli of a two-dimensional isotropic elastic composite. *J. Mech. Phys. Solids* **41**(5), pp. 937–980.
- Choi, J.B. and Lakes, R.S. (1991). Design of fastener based on negative Poisson’s ratio foam. *Cellular Polymers*, **10**(3), pp. 205–212.
- Cioranescu, D. and Saint Jean Paulin, J. (1986). Reinforced and honey–comb structures, *J. Math. Pures et Appl.* **65**, pp. 403–422.
- Cook, R.D., Malkus, D.S., Plesha, M.E. (1989). *Concepts and Applications of Finite Element Analysis*. John Wiley & Sons.
- Díaz, A.R. and Kikuchi, N. (1992). Solutions to shape and topology eigenvalue optimization problems using a homogenization method. *Int. J. Num. Meth. Engng.*, **35**, pp. 1487–1502.
- Díaz, A.R., Lipton, R. and Soto, C.A. (1994). A new formulation of the problem of optimum reinforcement of Reissner–Mindlin Plates, *Preprint*, Dept. of Mech. Engng., Michigan State University, East Lansing, USA.
- Díaz, A.R. and Sigmund, O. (1994). Checkerboard patterns in layout optimization. (Submitted).
- Dvorak, J. (1993). Optimization of composite materials. *Master’s Thesis*, Faculty of Mathematics and Physics, Charles University, Prague, Czech Republic.
- Evans, K. E. (1989). Tensile network microstructures exhibiting negative Poisson’s ratios. *J. Phys. D: Appl. Phys.*, **22**, pp. 1870–1876.
- Evans, K. (1990). Tailoring the negative Poisson’s ratio. *Chemistry & Industri*, **15**, October .

- Ferencz, R.M. (1989). Element–by–element preconditioning techniques for large–scale, vectorized finite element analysis in nonlinear solid and structural mechanics. *Ph.D.–thesis*, Stanford University.
- Gibson, C.S. and Ashby, M.F. (1988). *Cellular Solids*. Pergamemnon, Oxford.
- Greenbaum, A., Greengard, L. and McFadden, G.B. (1993). Laplace's equation and the dirichlet–neumann map in multiply connected domains. *J. Comp. Phys.*, **105**, pp. 267–278.
- Guedes, J.M. and Kikuchi, N. (1991). Preprocessing and postprocessing for materials based on the homogenization method with adaptive finite element methods. *Comp. Meth. Appl. Mech. Eng.* **83**, pp. 143–198.
- Guedes, J.M., Neves, M.M. and Orlando, J. (1994). *Users manual for the program PREMAT2D, Vers. 2.1*. Report Instituto Superior Technico, Cemul, Portugal.
- Hollister, S.R. and Riemer, B.A. (1993). Digital image based finite element analysis for bone microstructure using conjugate gradient and Gaussian filter techniques. *SPIE Vol. 2035 Math. Meth. in Medical Imaging II*, pp. 95–106.
- Huiskes, R. and Hollister, S.J. (1993). From structure to process, from organ to cell: recent developments of FE–analysis in orthopaedic biomechanics. *J. Biomech. Engng.*, **115**, pp. 520–527.
- Ikuta, K., Hirowatari, K. and Ogata, T. (1994). Ultra high resolution stereo lithography for three dimensional micro fabrication. In Proc. *5'th Int. Conf. on Rapid Prototyping*, June 12–15, Dayton, Ohio.
- Jog, C. (1994). Variable–topology shape optimization of linear elastic structures. *Ph.D.–thesis*, Dept. of Theoretical and Applied Mechanics, Univ. of Illinois at Urbana–Champaign, USA.
- Jog, C. and Haber, R.B. (1994). Stability of finite element models for distributed–parameter optimization and topology design. *TAM–report No. 758*, Dept. of Theoretical and Applied Mechanics, Univ. of Illinois at Urbana–Champaign, USA.
- Jog, C., Haber, R.B. and Bendsøe, M.P. (1994)<sup>1</sup>. Topology optimization with optimized, self–adaptive materials. *Int. J. Num. Meth. Engng.*, **37**, pp. 1323–1350.
- Jog, C., Haber, R.B. and Bendsøe, M.P. (1994)<sup>2</sup>. Variable–topology shape optimization with a constraint on the perimeter. In Proc. *20'th ASME Design Automation Conference*, Minneapolis, Mn., Sept. 11–14, ASME publ. DE–Vol. 69–2, 261–272.
- Kohn, R.V. and Strang, G. (1986). Optimal design and relaxation of variational problems. *Comm. Pure Appl. Math.*, **39**, pp. 1–25, 139–182, 353–377 (Part I–III).
- Kolpakov, A.G. (1985). Determination of the avarage characteristics of elastic frameworks. *PMM J. appl. Math. Mech. U.S.S.R.* **49**, pp. 739–745.
- Lakes, R. (1987). Foam Structures with Negative Poisson's Ratio. *Science* **235**(Feb.), p. 1038.

- Lakes, R. (1993)<sup>1</sup>. Design considerations for materials with negative Poisson's ratios. *J. Mech. Design*, **115**, pp. 696–700.
- Lakes, R. (1993)<sup>2</sup>. Materials with structural hierarchy, review article. *Nature* **361**(Feb.), pp. 511–515.
- Lakes, R. and Elms, K. (1993). Indentability of conventional and negative Poisson's ratio foams. *J. Comp. Mat.*, **27**(12), pp. 1193–1202.
- Kostar, T.D. and Chou, T.-W. (1994). Microstructural design of advanced multi-step three-dimensional braided preforms. *J. Comp. Mater.*, **28**(13), pp. 1180–1201.
- Michell, A.G.M. (1904). The limit of economy of material in frame structures. *Philosophical Magazine*, Series 6, **8**, 589–597.
- Milton, G.W. (1992). Composite materials with Poisson's ratios close to –1. *J. Mech. Phys. Solids*, **40**(5), pp. 1105–1137.
- Milton, G.W. and Cherkaev, A.V. (1993). Materials with elastic tensors that range over the entire set compatible with thermodynamics. Presented at the *Joint ASCE–ASME–SES Mett'N*, June 1993, University of Virginia, Charlottesville, Virginia, USA.
- Moore, J.S. (1993). Odd solid predictions. *Nature*, **365**, p. 690.
- Moulinec, H. and Suquet, P. (1994). A fast numerical method to compute the linear and nonlinear mechanical properties of composites. *C. R. Acad. Sci. Paris, t. 318, Serie II*, pp. 1417–1423.
- Mullender, M.G., Huiskes, R. and Weinhans, H. (1994). A Physiological approach to the simulation of bone remodelling as a self-organizational control process. *J. Biomech.*, **11**, pp. 1389–1394.
- Nemat-Nasser, S. and Hori M. (1993). *Micromechanics*. Elsevier, Amsterdam.
- Nkansah, M.A., Evans, K.E. and Hutchinson, I.J. (1994). Modelling the mechanical properties of an auxetic molecular network. *Modelling Simul. Mater. Sci. Eng.*, **2**, pp. 337–352.
- Olhoff, N. Bendsøe, M.P. and Rasmussen, J. (1992). On CAD–integrated structural topology and design optimization. *Comp. Meth. Appl. Mechs. Engng.*, **89**, pp. 259–279.
- Sanchez-Palencia, E. (1980). Non-homogeneous Media and Vibration Theory. *Lecture Notes in Physics* **127**, Springer Verlag, Berlin.
- Pedersen, P. (1970). On the minimum mass layout of trusses. *AGARD conf. proc. No. 36, Symposium on Structural Optimization*, AGARD–CP–36–70.
- Pratt, W.K. (1991). *Digital Image Processing*. John Wiley and Sons, New York.
- Press, W.H., Teukolsky, S.A., Vetterling, W.T. and Flannery, B.P. (1992). *Numerical Recipes in Fortran*, Cambridge University Press.

- Ringertz, U. (1988). A mathematical programming approach to structural optimization. *Research Report No. 88-24*, Dept. of Leightweight Structures, The Royal Institute of Technology, Stockholm, Sweeden.
- Ringertz, U. (1993). On finding the optimal distribution of material properties. *Struct. Optim.*, **5**, pp. 265–267.
- Rodriques, H.C. and Fernandes, P. (1995). A material based model for topology optimization of thermoelastic structures. *Int. J. Num. Meth. Engng.*, **38**(12), pp. 1951–1965.
- Rothenburg, L., Berlin, A.A. and Bathurst, J. (1991). Microstructures of isotropic materials with negative Poisson's ratio. *Nature*, **354**, pp. 470–472.
- Rozvany, G.I.N., Zhou, M., Birker, T. and Sigmund, O. (1992). Topology optimization using iterative continuum type Optimality Criteria (COC) methods for discretized systems. In *Topology Design of Structures*, (ed. Bendsøe, M.P. and Soares, C.A.), Springer, pp. 273–286.
- Rozvany, G.I.N., Zhou, M. and Sigmund, O. (1994). Topology optimization in structural design. In *Advances in Design Optimization*, (ed. Adali, H.), Chapman and Hall, London, UK, pp. 340–399.
- Sanchez-Palencia, E. (1980). Non-homogeneous media and vibration theory. *Lecture Notes in Physics*, **127**, Springer Verlag, Berlin.
- Sankaranarayanan, S., Haftka, R.T. and Kapania, R.K. (1993). Truss topology optimization with stress and displacement constraints. In *Topology Design of Structures*, (ed. Bendsøe, M.P. and Soares, C.A.), Springer, pp. 71–78.
- Sigmund, O. (1994)<sup>1</sup>. Materials with prescribed constitutive parameters: an inverse homogenization problem, *Int. J. Solids Structures*, **31**, pp. 2313–2329.
- Sigmund, O. (1994)<sup>2</sup>. Tailoring Materials with Prescribed Elastic Properties, to appear in *Mech. Materials*. **20**, pp. 351–368.
- Walker, K.P., Freed, A.D. and Jordan, E.H. (1991). Microstress analysis of periodic composites. *Comp. Engng.*, **1**(1), pp.29–40.
- Weihans, H., Huiskes, R. and Grootenboer, H.J. (1992). The behaviour of adaptive bone-remodeling simulation models. *J. Biomech.*, **25**(12), pp. 1425–1441.
- Zhou, M. and Rozvany, G.I.N. (1993). DCOC: an optimality criteria method for large systems, Part I: Theory, *Struct. Optim.*, **5**, pp. 12–25.

# **Appendix 1**

## **Checkerboard patterns in layout optimization**

Alejandro R. Díaz

Department of Mechanical Engineering  
Michigan State University  
East Lansing, MI 48824  
USA

Ole Sigmund

Department of Solid Mechanics  
Technical University of Denmark  
DK-2800 Lyngby  
Denmark

### **Abstract**

Effective properties of arrangements of strong and weak materials in a checkerboard fashion are computed. Kinematic constraints are imposed so that the microscale deformation is consistent with typical finite element approximations. It is shown that when four-node quadrilateral elements are involved, these constraints result in a numerically induced, artificially high stiffness. This can account for the formation of checkerboard patterns in continuous layout optimization problems of compliance minimization.

Comment to pdf–version, July, 1998: This paper is left out but has appeared as:

Díaz, A.R. and Sigmund, O. (1994). Checkerboard patterns in layout optimization, *Structural Optimization*, **10**, 40–45

## Appendix 2

### Notations for the constitutive tensor

Reference to the constitutive tensor will be given in the standard engineering notation.

For two dimensional orthotropic materials the constitutive tensor is written in matrix form as

$$(E)_{ort}^{2-d} = \begin{pmatrix} E_{1111} & E_{1122} & 0 \\ E_{1122} & E_{2222} & 0 \\ 0 & 0 & E_{1212} \end{pmatrix} \quad (\text{A2.1})$$

and for isotropic materials assuming plane stress state as

$$(E)_{iso, pl. stress}^{2-d} = \frac{E}{1-\nu^2} \begin{pmatrix} 1 & \nu & 0 \\ \nu & 1 & 0 \\ 0 & 0 & \frac{1-\nu}{2} \end{pmatrix} \quad (\text{A2.2})$$

For three dimensional orthotropic materials, the constitutive tensor is written in matrix form as

$$(E)_{ort}^{3-d} = \begin{pmatrix} E_{1111} & E_{1122} & E_{1133} & 0 & 0 & 0 \\ E_{1122} & E_{2222} & E_{2233} & 0 & 0 & 0 \\ E_{1133} & E_{2233} & E_{3333} & 0 & 0 & 0 \\ 0 & 0 & 0 & E_{1212} & 0 & 0 \\ 0 & 0 & 0 & 0 & E_{1313} & 0 \\ 0 & 0 & 0 & 0 & 0 & E_{2323} \end{pmatrix} \quad (\text{A2.3})$$

Limiting the properties of the three dimensional materials further by assuming isotropy in each plane of symmetry, and assuming that the moduli in the three principal directions are equal ( $E_{1111} = E_{2222} = E_{3333}$ ), we get

$$(E)_{ort, iso}^{3-d} = E \begin{bmatrix} \frac{1-\nu_{23}^2}{\Delta} & \frac{\nu_{12} + \nu_{13}\nu_{23}}{\Delta} & \frac{\nu_{13} + \nu_{12}\nu_{23}}{\Delta} & 0 & 0 & 0 \\ \frac{\nu_{12} + \nu_{13}\nu_{23}}{\Delta} & \frac{1-\nu_{13}^2}{\Delta} & \frac{\nu_{23} + \nu_{12}\nu_{13}}{\Delta} & 1 & 0 & 0 \\ \frac{\nu_{13} + \nu_{12}\nu_{23}}{\Delta} & \frac{\nu_{23} + \nu_{12}\nu_{13}}{\Delta} & \frac{1-\nu_{12}^2}{\Delta} & 0 & 0 & 0 \\ 0 & 0 & 0 & \frac{1}{2(1+\nu_{12})} & 0 & 0 \\ 0 & 0 & 0 & 0 & \frac{1}{2(1+\nu_{13})} & 0 \\ 0 & 0 & 0 & 0 & 0 & \frac{1}{2(1+\nu_{23})} \end{bmatrix} \quad (\text{A2.4})$$

where

$$\Delta = 1 - \nu_{12}^2 - \nu_{23}^2 - \nu_{13}^2 - 2 \nu_{12} \nu_{23} \nu_{13}$$

and  $\nu_{ij}$  are the Poisson's ratios in the  $ij$ -plane.

Assuming full isotropy ( $\nu_{12} = \nu_{23} = \nu_{13} = \nu$ ) we have

$$(E)_{iso}^{3-d} = E \frac{1-\nu}{(1+\nu)(1-2\nu)} \begin{pmatrix} 1 & \frac{\nu}{1-\nu} & \frac{\nu}{1-\nu} & 0 & 0 & 0 \\ \frac{\nu}{1-\nu} & 1 & \frac{\nu}{1-\nu} & 0 & 0 & 0 \\ \frac{\nu}{1-\nu} & \frac{\nu}{1-\nu} & 1 & 0 & 0 & 0 \\ 0 & 0 & 0 & \frac{1-2\nu}{2(1-\nu)} & 0 & 0 \\ 0 & 0 & 0 & 0 & \frac{1-2\nu}{2(1-\nu)} & 0 \\ 0 & 0 & 0 & 0 & 0 & \frac{1-2\nu}{2(1-\nu)} \end{pmatrix} \quad (\text{A2.5})$$

## Appendix 3

### The Element–by–Element Preconditioned Conjugate Gradient Method

This appendix is more or less a repetition of the description of the EBE–PCG method introduced in section 1.4 but some details on the computational implementation are emphasized.

The Conjugate Gradient method solves the  $N \times N$  linear system

$$[S]\{D\} = \{R\} \quad (\text{A1.1})$$

by minimizing the function

$$f(\{D\}) = \frac{1}{2}\{D\}^T [S]\{D\} - \{R\}^T \{D\} \quad (\text{A1.2})$$

which corresponds to the minimization of potential energy in the linear elastic elastic body. The function  $f$  (potential energy) has a stationary point when the gradient

$$\nabla f = [S]\{D\} - \{R\} \quad (\text{A1.3})$$

is zero which correspond to (1.22).

The minimization is performed as an iterative procedure computing the search direction  $\{p\}_k$  and improved minimizer  $\{D\}_k$ . At each step  $k$  in the iteration a factor  $\alpha$  is determined such that  $f(\{D\}_k + \alpha \{p\}_k)$  is minimized; the new minimizer  $\{D\}_{k+1}$  is then set equal to the new point  $\{D\}_k + \alpha \{p\}_k$ .

Choosing the search direction  $\{p\}_k$  as the direction of greatest descent, namely he negative of the current residual vector  $\{r\}_k = [S]\{D\}_k - \{R\}_k$  we have defined the *Method of Steepest Descent*. The convergence of this method can be very slow and therefore the search direction should be made  $[S]$ –conjugate, i.e.

$$\{p\}_i^T [S] \{p\}_j = 0, \quad j < i \quad (\text{A1.4})$$

By making the search vector  $[S]$ –conjugate, the procedure is guarantied to converge to the exact solution in at most  $N$  iterations.

The convergence of the conjugate gradient algorithm is dependent of the square of the condition number (ratio between highest and lowest eigenvalue of the stiffness matrix  $[S]$ ). Convergence can therefore be speeded up by preconditioning the system. Many different choices of preconditioners have been discussed in literature but Hollister and Riemer, (1993) report good results by simply taking the diagonal of the stiffness matrix as the preconditioner  $[L]=\text{diag}([S])$ . The com-

putational procedure of the PCG–method is summarized in figure 1.1.

- 1)  $\{r\}_0 = \{R\} - [S]\{D\}_0$
- 2)  $\{z\}_0 = \{r\}_0^T [L]^{-1}$
- 3)  $\{p\}_0 = \{z\}_0$
- 4)  $\gamma = \{r\}_0^T \{z\}_0$
- 5)  $k = 0$
- 6)  $\{v\}_k = [S]\{p\}_k$
- 7)  $\alpha = \gamma / (\{p\}_k^T \{v\}_k)$
- 8)  $\{D\}_{k+1} = \{D\}_k + \alpha \{p\}_k$
- 9)  $\{r\}_{k+1} = \{r\}_k - \alpha \{v\}_k$
- 10) *if*  $|\{r\}_{k+1}| < \delta$  *then STOP*
- 11)  $\{z\}_{k+1} = \{r\}_{k+1}^T [L]^{-1}$
- 12)  $\gamma' = \gamma$
- 13)  $\gamma = \{r\}_{k+1}^T \{z\}_{k+1}$
- 14)  $\beta = \gamma / \gamma'$
- 15)  $\{p\}_{k+1} = \{z\}_{k+1} + \beta \{p\}_k$
- 16)  $k = k + 1$
- 17) *goto 6*

**Figure 1.1.** Computational procedure for the Element–By–Element Preconditioned Conjugate Gradient method.

The computationally most time consuming step of this procedure is step 6, the multiplication of the global stiffness matrix  $[S]$  and the search direction vector  $\{p\}_k$ . However, this multiplication can be done on the element level as

$$\{v\}_k = \sum_{e=1}^{NE} [s^e] \{p^e\}_k \quad (\text{A1.5})$$

using the appropriate assembly procedure from local to global coordinates. As seen in equation (A1.5), the global stiffness matrix never has to be assembled – this feature makes the requirement to storage space very small in the EBE–PCG procedure.

In practice we do not require the procedure to converge exactly and we can therefore stop the algorithm when the norm of the residual vector gets below a stopping criteria  $\delta$ . In fact  $\delta$  can be chosen very gross when the EBE–PCG algorithm is used as a part of an iterative optimization procedure. Only in the final iterations of the optimization procedure we require an exact solution and then  $\delta$  can be made smaller for final convergence.

## Appendix 4

### Continuum equivalence of bar elements and equivalent nodal loads

Modelling a truss member as a 2-node continuum element is done the following way. The shape functions  $N_i$  for a bar element with a linear axial displacement field are given as

$$N_1 = \frac{L-t}{L} \text{ and } N_2 = \frac{t}{L} \quad A(3.1)$$

where  $L$  is bar length and  $0 \leq t \leq L$ . The bar is rotated the angle  $\alpha$  with respect to the global coordinate system. The shape functions  $N_i$  are therefore functions of  $\alpha$  and the derivatives of  $N_i$  with respect to horizontal and vertical coordinates  $x_1$  and  $x_2$  are

$$\frac{\partial N_1}{\partial x_1} = -\frac{c}{L}, \quad \frac{\partial N_1}{\partial x_2} = -\frac{s}{L}, \quad \frac{\partial N_2}{\partial x_1} = \frac{c}{L} \text{ and } \frac{\partial N_2}{\partial x_2} = \frac{s}{L} \quad A(3.2)$$

where  $c$  and  $s$  is  $\cos(\alpha)$  and  $\sin(\alpha)$  respectively.

Following the matrix notation of [Cook et al., \(1989\)](#), the strain-displacement matrix  $[B]$  can be written as

$$[B] = \frac{1}{L} \begin{bmatrix} -c & 0 & c & 0 \\ 0 & -s & 0 & s \\ -s & -c & s & c \end{bmatrix} \quad A(3.3)$$

The constitutive matrix for a bar modelled as a 2-node continuum in a local coordinate system aligned with the bar is

$$[E'] = \begin{bmatrix} E & 0 & 0 \\ 0 & 0 & 0 \\ 0 & 0 & 0 \end{bmatrix} \quad A(3.4)$$

which of course corresponds to a material with only stiffness in one direction and no shear stiffness. Now the 2-node continuum element can be treated the usual way known from plane FE-problems [e.g. [Cook et al., \(1989\)](#)] and we get the stress-strain relation

$$\{\sigma\} = [T]^T [E'] [T] \{\epsilon\} \quad A(3.5)$$

where  $\{\sigma\}$  and  $\{\epsilon\}$  are the 3x1 stress and strain vectors respectively and  $[T]$  is a transformation matrix given as

$$[T] = \begin{bmatrix} c^2 & s^2 & cs \\ s^2 & c^2 & -cs \\ -2cs & 2cs & c^2 - s^2 \end{bmatrix} \quad A(3.6)$$


---

To calculate the equivalent nodal load vector  $\{r_e\}$  for elements subject to the prestrainfield  $\{\epsilon_0\}$  we have the following relation

$$\begin{matrix} \{r_e\} = \int_{Y^e} [B]^T [T]^T [E'] [T] \{ \epsilon_0 \} dY^e \\ 4x1 \quad 4x3 \quad 3x1 \end{matrix} \quad A(3.7)$$